POLITECNICO DI TORINO

Collegio di Ingegneria Chimica e dei Materiali

Corso di Laurea Magistrale
in Ingegneria dei Materiali per l'Industria 4.0

Tesi di Laurea Magistrale

Study of PLA-containing Blends. The Effect of Aging

Relatori

Prof. Alberto Frache

Correlatrice

Prof.ssa Rossella Arrigo

Candidato

Abdul Kader Adra

July 2026

INDEX

1 Introduction:

1.1 Overview

Conventional petroleum-based plastics are indispensable in modern society; however, their persistence in the environment has raised significant sustainability concerns. For 96.6% of Italians, plastic is fundamental in at least one of its many uses that can range from packaging, technology, textiles, and even hygiene among many others as well [1]. Worldwide production of plastics continues to soar (reaching 430.9 Mt [2] with the increasing population and the resulting increase of products, adding strain to the manufacturing industry. Plastic appears as a great solution for these markets due to the reduced cost, and the lower energy demand required in production. Furthermore, their low weight opens a variety of different uses from domestic to heavy industrial, and the high adaptability offers great advantages in terms of variety and personalisation (especially useful for applications such as packaging). The majority of the plastic produced to this day still is fossil based (almost 90%) as seen in the figure below.

Fig. 1: Chart showing the polymers being produced and the fossil based, circular, and bio-based split [3]

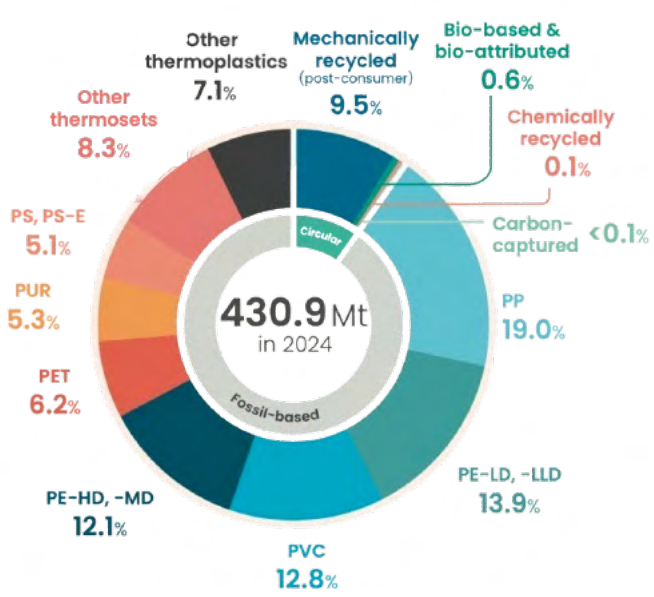

This causes problems for European manufacturers, as the evermore constricting EU regulations that are being made to combat climate change asks for the inclusion of more recycled and bio-based plastics, as well as the restrictions being imposed on single use plastics. This has resulted in a decline in the competitiveness of European plastics manufacturing as global production increases by 16.3% in 2024 comparing to 2018 (from 370.6 Mt to 430.9 Mt) while the European production decreased by 12.4% in the same period. Fig. 2 shows a continuously increasing global production, despite European production decreasing, and Europe becoming a net importer rather than exporter. While this has spurred and incentivised many manufacturers towards recycling and bio-based plastics the lack of turnover risks stagnation.

Despite the increase in circular solutions, almost 90% of the plastic produced in 2024 was still from fossils. The Fig. 2 below shows an increase in the percentage of mechanically recycled plastics from 8.7% in 2023 to 9.5% in 2024. Chemically recycled and bio – based production are still below 1%, highlighting the difficulties in achieving environmentally friendly results. One of the main challenges of mechanical recycling is cross – contamination, where blends or different streams of materials can get mixed up causing complications further down the line.

Fig. 2: Histogram of the evolution of the world's plastic production

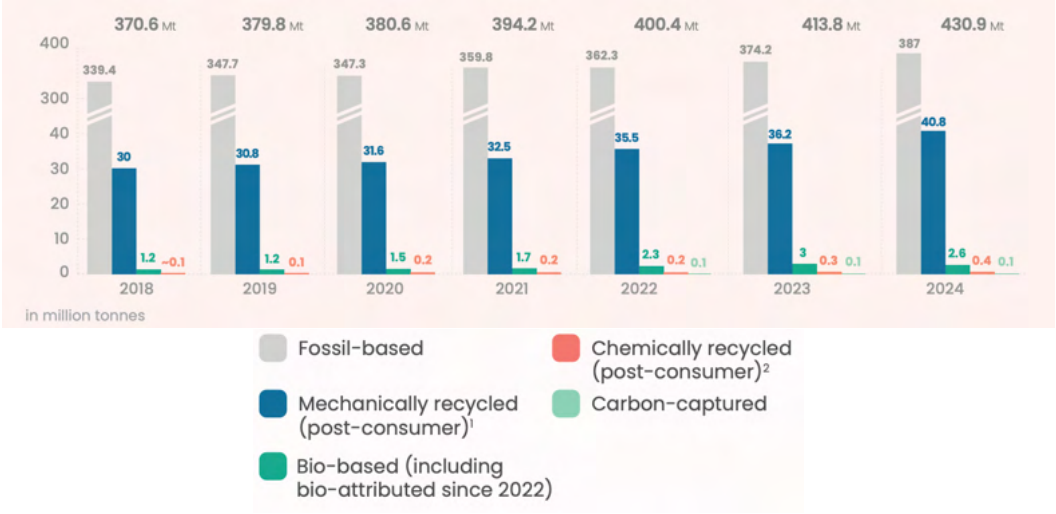

1.2 Scope of the thesis

Taking all this into consideration the scope of this work was to explore the possibility of creating new material that is not fully fossil – based, and able to compete with its purely fossil counterparts on both the aesthetic point of view and mainly on the mechanical front even with aging. The material is produced via a twin-screw extruder with a flat head attachment to create a film. This thesis will focus on both PMMA / PLA blends and PET / PLA blends, in the following weight percentages 100/0, 80/20, 60/40, and 50/50. To accelerate the aging process, the blends were then put into the QUV machine (will be developed in the following chapter) where they were subject to UV radiation and condensation. This thesis will also take into consideration all the aspects of material preparation, and blend preparation.

1.3 Blends

Polymeric blends are a mixture of 2 or more polymers, in which each component is present in a minimum percentage of 2%. The development and production of said blends is in response to the increasing demand of material with optimised mechanical, chemical, and functional properties. Contrary to traditional mixtures, polymeric mixtures involve interactions between macromolecules. The extent of the compatibility between the component of the blend, is often given by the miscibility. This in turn depends on thermodynamic and kinetic factors, including but not limited to Gibbs free energy. According to Gibbs to obtain a homogenous blend, the enthalpic contribution must be negative to favour the interaction between the polymer chains.

If the interactions are not sufficient, phase separation occurs. While blends can be amorphous, crystalline, or semi – crystalline miscibility, takes place in the amorphous region.

The study and optimisation of blends such as PMMA / PLA and PET / PLA requires a multifaceted approach:

- Thermal analysis is essential to understand the conditions of miscibility, and interaction between polymers.

- Rheology allows a for a valuation of the material behaviour during the processing phase.

- The morphology on the other hand gives information on phase distribution, and microstructure of the blends.

Variations in the processing phase and the use of compatibilizers could influence the properties of the blend. However, for the PMMA / PLA and PET / PLA blends explored in this research compatibilizers were not used, and variations to the processing parameters were not explored. This was a choice made to simplify later analysis, and better simulate possible future integration with pre – existing large-scale productions.

2 Materials & Methods:

In this chapter the materials used will be introduced alongside the methods adopted to produce the film blends, as well as the tests to obtain our results which will be discussed in the next chapter.

2.1 Materials:

2.1.1 PMMA (Polymethyl Methacrylate):

PMMA (Polymethyl Methacrylate) is another very well-known transparent plastic, despite not being as widely produced. When produced as a film, it can offer high transparency and good resistance to UV (Ultra Violet) radiation. The two most common methods for PMA synthesis are:

- Suspension polymerisation: It works by suspending MMA droplets in an aqueous medium and heated to 85°C, a stabiliser such as polyvinyl alcohol is used to prevent the droplets from aggregating, while benzoyl peroxide often acts as an initiator.
- Emulsion polymerisation: It works by emulsifying MMA in water using surfactants such as sodium oleate, then a water-soluble initiator such as potassium persulphate drives the reaction producing PMMA particles. Conversion of the emulsified monomer into a stable dispersion of polymers is by free – radical propagation mechanism.

Transparent PMMA has various applications in different industries, such as in displays, durable labels, decorative and functional panels, optical filters, coatings and smooth surfaces, biomedical packaging etc. It can also just be generally used as a replacement for glass (glass windows, panels, skylights, etc.). [4], [5], [6], [7]

The specific one used in this study is PLEXIGLAS® 8N by Röhm. This material is extremely brittle making some of the material management later more difficult. It is also characterised by its transparency. The relevant data as communicated by the manufacturers (Röhm) is shown in the table below.

Fig . 3: Properties of PMMA as reported in the technical data sheet [8]

	Parameter	Unit	Standard	PLEXIGLAS® 8N
Mechanical Properties				
Tensile Modulus	1 mm/min	MPa	ISO 527	3300
Stress @ Break	5 mm/min	MPa	ISO 527	77
Strain @ Break	5 mm/min	%	ISO 527	5.5
Charpy Impact Strength	23°C	kJ/m²	ISO 179/1eU	20
Thermal Properties				
Vicat Softening Temperature	B / 50	°C	ISO 306	108
Glass Transition Temperature		°C	ISO 11357	117
Temp. of Deflection under Load	0.45 MPa	°C	ISO 75	103
Temp. of Deflection under Load	1.8 MPa	°C	ISO 75	98
Coeff. of Linear Therm. Expansion	0 - 50°C	E-5 /°K	ISO 11359	8
Classes of construction product			DIN EN 13501-1	E
Flammability UL 94	1.5 mm	Class	IEC 60695-11-10	HB
Rheological Properties				
Melt Volume Rate, MVR	230°C / 3.8kg	cm³/10min	ISO 1133	3
Optical Properties	d=3 mm			
Luminous transmittance	D65	%	ISO 13468-2	92
Haze			ASTM D1003	< 0.5
Refractive Index	589nm/23°C		ISO 489	1.49
Other Properties				
Density		g/cm³	ISO 1183	1.19
Recommended Processing Conditions				
Predrying Temperature		°C		max. 98
Predrying Time in Desiccant-Type Drier		h		2 - 3
Melt Temperature		°C		220 - 260
Mold Temperature (Injection Molding)		°C		60 - 90

2.1.2 PET (Polyethylene Terephthalate):

PET (Polyethylene Terephthalate) is a polyester synthesised from terephthalic acid monomer units. The monomer can be synthesised either by an esterification reaction oxidising para-xylene in an acetic acid medium and ethylene glycol, or by a transesterification reaction between dimethyl-terephthalate and ethylene glycol with antimony as a catalyst. Polymerisation is done through a polycondensation reaction of the monomer in vacuum at temperatures as high as 300 °C, this process is shown in Fig. 4. As we can see from Fig. 1 above, one of the most commonly produced plastics is PET constituting 6.2% of the total plastics produced. Some of the most common applications of PET films are in industrial films, photosensitive materials, electrical insulation, packaging decoration, screen protection, optical grade mirror surface protection, etc. The wide range of application is due to the high physical and chemical stability as well as its transparency. [9], [10], [11]

Fig. 4: Chemical reactions in PET manufacturing

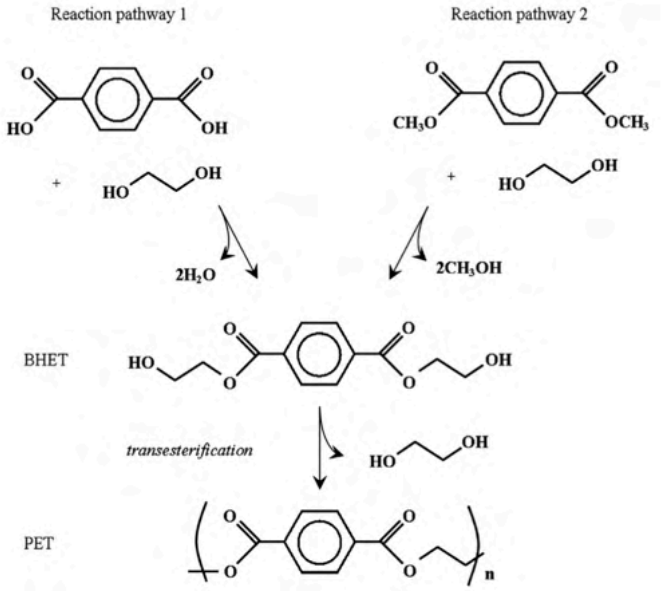

The specific one used in this study is Eastlon PET CB-602AB (Bio PET) by FKuR. It is another transparent polymer, although not as brittle as the PMMA it is still quite fragile, just more manageable. The relevant data as communicated by the manufacturers (FKuR) is shown in the table below.

Fig . 5: Properties of PET as reported in the technical data sheet [12]

Physical properties			
Intrinsic viscosity (IV)	75 - 79	[ml/g]	FENC Method
DEG Content	1.1 - 1.5	[%]	FENC Method
Melting temperature	240 - 260	[°C]	ISO 3146-C
Acid number	25 - 45	[meq/kg]	FENC Method
Water content	< 0.4	[%]	FENC Method
Density	1.3 - 1.4	[g/cm³]	ISO 1183
Bulk density	820 - 920	[kg/m³]	ISO 60

2.1.3 PLA (Polylactic acid):

Among the most promising polymers that are being used for bio-based plastics is PLA (Poly Lactic Acid), that is mainly due to its sustainability and low carbon footprint, because it is derived from renewable resources. PLA also possesses superior properties with respect to other biopolymers. However, biopolymers tend to have a shorter lifetime compared to their fossil counterparts. PLA films have many different applications in packaging, agricultural film, labels and stickers, lamination films, single use products (such as cups and utensils), etc. More applications are shown in Fig. 6 below.

PLA can be produced on a large scale, starting from the monomer lactic acid through two main processes. The processes being direct polycondensation, and ROP (Ring Opening Polymerization). Direct polycondensation has fewer manufacturing steps, lower costs, and easier to manipulate thus easier to commercialise. ROP on the other hand, is more useful when high molecular weight products are required. [12], [13], [14]

Fig. 6: different applications of PLA divided into their respective sectors [15]

Use of PLA in different sectors.

Name of industry	Use	Advantages	Disadvantages
Pharmaceutical industry	Control drug carriers Tablets Intravascular Surgical sutures	Improves the replenishing of fluids	Can change the shape of red blood cells
Cosmetic industry	Moisturizers Exfoliating agent Lightening agent Anti-aging Anti-acne	Improves antibacterial activity Used for hydration and lightening of skin Alpha–hydroxy acid removes dead cells	Cause skin irritation
Plastic	PLLA PDLA PDLLA	Used in polymerization, dehydration, reduction. decarboxylation and self-esterification processes.	Low molecular weight
Agriculture	Vegetation nets Mulch films Seeding pots	Biodegradability Ecological nature Hydrophobic nature	More acidic No nutrient Change the pH of soil
Textile	Sanitary napkins Household wipes Disposable garments UV-resistant fabrics Upholstery	Biodegradability Great durability Fire resistance Phytosanitary effect	Low recyclability
Transportation	Impacts shields of car Components of car doors Engine covers Instrument panels	Plasticization to increase ductility High tensile strength High stiffness	Low thermal stability Low toughness Brittle behavior Low impact resistance
Electronics	Porous membrane in water purification and air filtration system	Dielectric properties	High melt flow rate
Food Packaging	Cups Overwraps Containers Bottles Compostable bags	Biodegradability Easy processing	Low heat resistance Low recyclability Compostable but not fast enough
Orthopedics	Sutures Screws Pins, plates Scaffolds	Resorbability Easy processing	Low mechanical properties Low biocompatibility

The specific one used in this study is Ingeo™ Biopolymer 4032D by NatureWorks. As with the other 2 materials this is another brittle fragile material. The relevant data as communicated by the manufacturers (NatureWorks) is shown in the table below.

Fig . 7: Properties of PLA as reported in the technical data sheet [16]

Typical Material & Application Properties (1, 2, 3)			
Film Properties		**Ingeo 4032D**	**ASTM Method**
Density		1.24 g/cc	D1505
Tensile Strength	MD TD	15 kpsi 21 kpsi	D882 D882
Tensile Modulus	MD TD	500 kpsi 550 kpsi	D882 D882
Elongation at Break	MD TD	180% 100%	D882 D882
Elmendorf Tear	MD TD	17 g/mil 14 g/mil	D1922 D1922
Spencer Impact		2.5 joules	
Transmission Rates	Oxygen Carbon Dioxide Water Vapor	675 cc-mil/m^2-24hr-atm 2,850 cc-mil/m^2-24hr-atm 375 g-mil/m^2-24hr-atm	D1434 Internal F1249
Optical Characteristics	Haze Gloss, 20°	2.1% 90	D1003 D1003
Thermal Characteristics	Melting Point	155-170°C	D3418

(1) Typical properties; not to be construed as specifications.
(2) All properties measured on 1.0 mil film.
(3) Typical values for a film oriented 3.5x in MD and 5x in TD.

Processing Temperature Profile (1)		
Melt Temperature	410 ± 15°F	210 ± 8°C
Feed Throat	113°F	45°C
Feed Temp.	355°F	180°C
Compression Section	375°F	190°C
Metering Section	390°F	200°C
Nozzle	390°F	200°C
Mold	390°F	200°C
Screw Speed	20-100 rpm	
Back Pressure	140-160°F	60-70°C
Mold Shrinkage	160-175°F	

2.2 Instruments and Method:

2.2.1 Thermo Fisherscientific™ twin screw extruder model process 11 with flat head attachment and hopper/ dispenser:

Products obtained via extrusion can be rigid or flexible, however, they usually have an infinite length along one direction. An extruder will usually also be accompanied by a collection instrument. The extruder used in this study was of the intermeshing corotating type. These extruders are superior to the single screw extruders in that they offer better mixing as the corotation applies more shear, and they can be self – cleaning.

In processes such as filming, which was used in this thesis, the stretching speed applied after the extrusion can have a big influence on the final morphology. The study by N. Chapleau and Garcia-Masabet et al, shows in Fig. 8 below that an increase in stretching at higher temperatures progressively changes the morphology of the particles from: spherical to ellipsoidal, then elongated structures, to finally a micro fibrous structure. [17]

Fig. 8: Relation between the type of flow and induced morphology in different zones of an extrusion die [18]

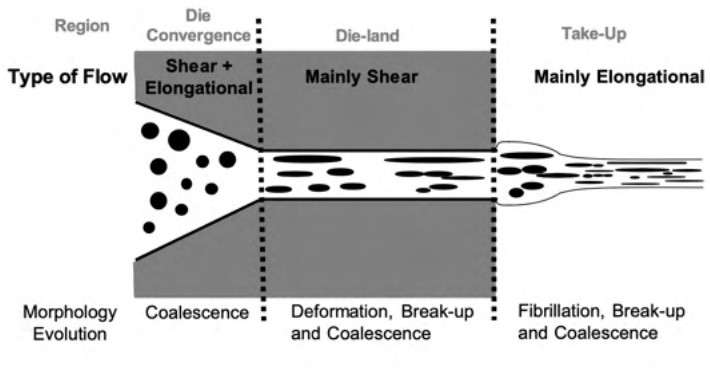

Film extrusion was performed using a co-rotating twin screw extruder equipped with a volumetric feeder and a calendering system. The feeder dispensing rate could be adjusted by varying the rotational speed (rpm). Extruder operating conditions, including barrel temperature profile and screw, were controlled through the integrated touchscreen interface, which also displayed torque and die pressure during processing.

The extruder had a screw diameter of 11 mm, a screw length-to-diameter ratio (L/D) of 40, and consisted of eight heating zones. The maximum operating temperature was 350 ℃. A flat film die (shown in Fig. 9) was mounted at the extruder exit and heated to the same processing temperature as the barrel.

Fig. 9: Flat head attachment 25 mm wide, and 1mm thick [19]

The screw configuration included conveying, feeding, and kneading (or mastication) elements, as illustrated in Fig. 10. The abbreviations at the bottom of each section in the diagram are defined as follows:

- **FS**: For transportation elements. [20]
- **PS**: For feeding elements, with deeper flights and larger pitch with respect to normal transport elements imparting less or no pressure on the polymer.
- **F30, F60, F90**: For kneading, mixing, or mastication, the number indicates the angle at which the mixing is done. Higher angles result in more shear and thus mixing.
- **EXT**: For the exit

Fig. 10: a) The screws in top view, b) The diagram of the screws

a)

b)

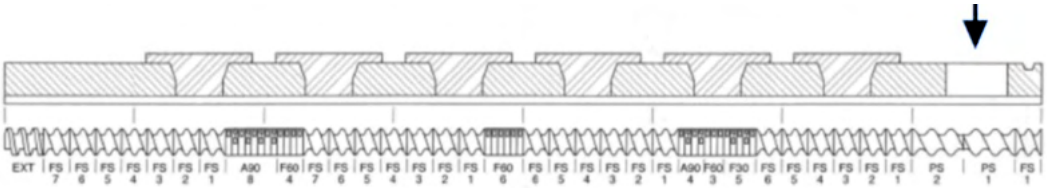

Prior to extrusion, all polymer pellets were dried at 60 °C for 6 h to minimise moisture content. After drying, the pellets were stored under vacuum at 30 °C until use. The dryer and extruder are shown in Fig. 11.

Fig. 11: Twin screw extruder and dispenser on top (left), dryer (right)

Screw extruder

Dryer

PMMA/PLA and PET/PLA blends were prepared in mass ratios of:

- 100/0
- 80/20
- 60/40
- 50/50

The pellets were mechanically mixed inside bags before loading into the hopper to promote homogenous distribution of the components.

The feeder throughput was calibrated for each composition by measuring the mass flow rate over one minute and converting the result to g/h. The target throughput for PMMA/PLA blends was 400 g/h. However, PET/PLA blends were processed at 300 g/h due to the elevated torque generated during extrusion.

Extrusion Temperatures and Screw Rotation Speeds were set as shown in the below table:

Table 1. *Extrusion temperature & Screw rotation speed*

	PMMA/PLA	**PET/PLA**
Extrusion Temperature	230 °C	250 °C
Screw Rotation Speed	100 rpm	130 rpm

During startup, the initially extruded material was discarded to eliminate contamination from residual material remaining inside the screws and barrel from previous runs.

After stabilisation of the extrusion process, the film was guided through the calendering system shown in Fig. 12. The first pair of rolls was adjusted to reduce film thickness, while the second pair operated with a 5% speed difference to maintain film tension during collection. Final film collection was performed manually.

Fig. 12: Calendering system (Process 11 Sheet Take off unit form Thermofisher™)

Continuous films of all investigated compositions were successfully produced and collected for subsequent characterisation and testing.

During processing, qualitative differences in melt behaviour were observed between the compositions. Pure PMMA and PET exhibited comparatively stable film formation after calendering. Increasing PLA content resulted in reduced melt stability and increased handling difficulty during film collection. Blends containing higher PLA concentration showed lower melt strength, reduced shape retention, and greater difficulty during passage through the roll system.

The extruder has a length of 40 L/D with 8 different heat zones was left to preheat, as the flat head was mounted to the end of it which was also heated to the same temperature (230 ℃ for PMMA/PLA blends, and 250 ℃ for PET/PLA blends), the extruder could reach 350 ℃. The rotation of the screws given in round per minutes (rpm) was also adjusted to 100 rpm for the PMMA/PLA blends, and 130 rpm for the PET/PLA blends. All the parameters can be adjusted using the touch screen available, which can also display the pressure at the exit and the aforementioned torque.

2.2.2 Die Cutter (AMSE):

Sample preparation was performed using a pneumatic die cutter operated using compressed air. The cutting force was adjusted to ensure complete specimen cutting without excessive die penetration, thereby minimising the risk of sample damage or material adhesion inside the die.

For PET/PLA blends, specimens were prepared using the die cutter shown in Fig. 13. Samples were cut from the central region of the extruded film and aligned parallel to the extrusion direction. Film regions containing visible defects or irregularities were excluded.

For PMMA/PLA blends, die cutting was not feasible due to the brittle nature of the films, which resulted in cracking during the process. Consequently, PMMA/PLA specimens were prepared manually by trimming the film edges and cutting defect – free section from the central region of the film. Prior to specimen preparation, the undulated film edges produced during extrusion were removed. This procedure was adopted following preliminary tensile tests, which showed that films with the undulated edge and edge irregularities exhibited premature failure and reduced mechanical performance.

Fig. 13: the die cutter on the left and the die used to cut the samples into shape

Pneumatic die cutter *Die*

The cutting force of the pneumatic die cutter was adjusted for each specimen to achieve complete cutting while avoiding excessive penetration of the die into the supporting surface.

Test samples suitable for subsequent mechanical characterisation were successfully prepared for both PET/PLA and PMMA/PLA blends. However, the difference in sample preparation methods reflected the different mechanical behaviour of the film. Particularly the increased brittleness observed in PMMA/PLA blends.

2.2.3 Artificial Aging (QUV):

Artificial aging was performed using QUV accelerated weather tester equipped with UV lamps operating at a wavelength of 340 nm shown in Fig. 14. The system simulated environmental aging by alternating cycles of ultraviolet radiation and condensation.

Extruded film samples of the PMMA/PLA and PET/PLA compositions were prepared prior to aging and placed inside the appropriate sample holder in the QUV chamber.

The aging consisted of repeated cycles of:

1. 8 h UV radiation where temperature was maintained at:
    - 60 ℃ for the PET/PLA blends
    - 45 ℃ for the PMMA/PLA blends
2. 4 h of condensation which was conducted at 40 ℃.

For most aging experiments, the radiation condensation cycle was maintained throughout the exposure period. However, PMMA/PLA samples that were aged for 24 h and 72 h were subject to consecutive UV irradiation cycles, without the intermediate condensation cycles.

Artificially aged specimens were obtained for subsequent mechanical, rheological, and thermal characterisation. This enabled the evaluation of the influence of accelerated aging on the properties of the different blends.

Fig. 14: QUV [21]

2.2.4 Tensile Testing Machine (Instron 5966):

Mechanical and tensile tests conducted serve to verify how the addition of PLA varies the resistance, Young's modulus, and/ or the deformation at rupture.

To ascertain of the maintainment, or to quantify the variation of the previously mentioned properties many different tests can be adopted. Starting with mechanical tests where a simple tensile test was adopted. This is done by clamping a sample from both sides and having the top grip shown in Fig. 15 pull. Mechanical results are heavily influenced by not only the polymer chains, but the interaction between the two polymers in the blend as well.

Fig. 15: Tensile test of a film following ASTM D882 standard [22]

Mechanical characterization was performed using the tensile testing machine shown in Fig. 16. Samples were pneumatically clamped before testing. Clamp pressure was adjusted to ensure the samples were properly mounted, while minimising slipping and premature failure near the grips.

Tensile test samples prepared from the extruded films, as described previously were used for the test here. Prior to testing, the thickness of all the samples was measured. For PMMA/PLA blends the width of the sample was also measured, given the manual sample preparation method (mentioned in section 2.2.2) employed instead of die cutting. All specimens were set up with a gauge length of 30 mm.

The pneumatic clamp pressure was usually maintained between 4 and 6 bars, depending on sample behaviour during testing. As stated before, the clamping pressure was adjusted to prevent slippage and premature fraction within the grips.

Tensile tests were conducted with constant crosshead speed of:

- 1 mm/min for PMMA/PLA blends
- 10 mm/min for PET/PLA blends

During the tests, the samples were elongated until fracture.

Tensile tests provided measurements of:

- Young's modulus
- Deformation at fracture

Differences in clamp pressure required, and failure behaviour were observed for the different blends.

Fig. 16: Tensile testing machine

2.2.5 DSC (Differential Scanning Calorimetry):

DSC scans will be used to evaluate thermal transition, crystallinity, and any variation after aging. These evaluations were then utilised to better understand the variations we obtained in the tensile test results.

As the polymer is subjected to controlled temperature change or temperature gradient (given in °C/min), the DSC test (Differential Scanning Calorimetry) measuring the heat flow shall be considered. Since the whole sample is analysed in the sample pan in Fig. 17, DSC blends will present different peaks due to the presence of different polymers. Different information that characterizes our material can be extracted from the DSC graphs including where applicable T_g (glass transition temperature), T_m (melting temperature), ΔH (enthalpy of fusion), and thus the crystallinity. [23]

Fig. 17: Diagram of a DSC chamber [24]

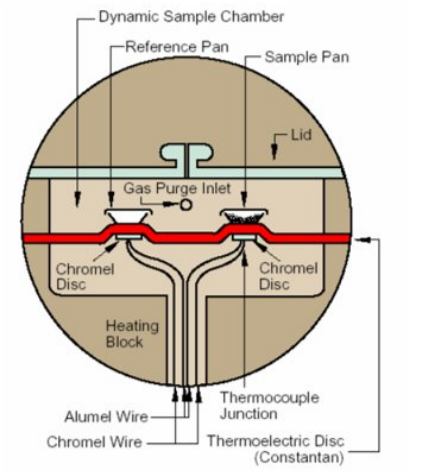

Thermal characterisation was performed using DSC (differential scanning calorimetry). This technique measures the difference in heat flow between a sample and a reference as a function of temperature under controlled heating and cooling conditions. The DSC measurements were carried out in the instrument shown in Fig. 18, in a Nitrogen atmosphere to minimise oxidative degradation during testing.

Samples for the DSC tests were prepared by cutting small sections from the extruded films using scissors. These pieces could be obtained from unused film, or alternatively from the samples previously subjected to mechanical testing. In case of the latter, material was taken from regions sufficiently far from the fracture zone, to avoid any possible influence of localised deformation or damage. Samples were placed in aluminium crucibles and sealed using the appropriate lids. Sample masses were maintained between 6 and 8 mg.

For the PMMA/PLA blends, the DSC temperature program is:

- First heating from 0 °C to 225 °C
- Controlled cooling
- Second heating

For the PET/PLA blends, the DSC temperature program is:

- First heating from 0 °C to 300 °C
- Controlled cooling
- Second heating

A temperature gradient of 10 °C/min was always used, and all measurements were conducted in a Nitrogen atmosphere.

DSC measurements were used to obtain the following information on the thermal behaviour of the polymer blends:

- T_g (glass transition temperature)
- Melting behaviour
- Crystallisation behaviour
- Degree of crystallinity.

Thermal properties of the film were obtained from the first cycle, while the intrinsic properties of the material were obtained from the third cycle.

Fig. 18: DSC

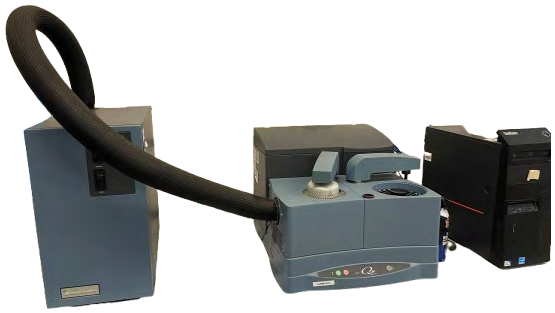

2.2.6 Rheometer (ARES – TA instruments):

Rheological tests were used to obtain information on the processibility of the blend, the viscosity, and the interaction between phases.

Parallel plate rheometers can be used for many different things by measuring the way a liquid (in our case a molten polymer) flows in response to an applied stress through various shear rates as well. Lower shear rates help in understanding how materials behave at rest, which has a marked effect on the stability of heterogeneous systems and gives insight into the material's microstructure. Said insight is what we desire from the rheology tests that we conducted, to understand the difference between blends, and the variation with aging.

The rheological measurements were conducted using a rotational rheometer equipped with a parallel plate geometry shown in Fig. 19.

The rheological samples were prepared by cutting strips from the extruded films. Before the tests were conducted, the samples were dried overnight (for 12 or more hours) to minimise the influence of moisture during the measurements.

The drying temperatures used were:

- 70 $°C$ for the PMMA/PLA blends
- 60 $°C$ for the PET/PLA blends

The higher drying temperature used for the PMMA/PLA blends was used due to the greater moisture retention observed in those blends due to the presence of PMMA. Following the drying the samples were left to cool to ambient temperature before being removed from the vacuum oven.

All measurements were performed in a Nitrogen atmosphere to reduce thermal and oxidative degradation during testing. The measurements were conducted at the following temperatures:

- 230 $°C$ for the PMMA/PLA blends
- 250 $°C$ for the PET/PLA blends

Fig. 19: Rheometer on the left and vacuum oven on the right [25]

Rheometer

Vacuum oven

An initial strain sweep was conducted to determine the linear viscoelastic region and identify the maximum deformation amplitude for which the viscoelastic response remained linear. The strain sweep conditions are shown in Table. 2. Strain sweep measurements were performed only for the 100/0 and 50/50 compositions. For each polymer system, the lower strain value obtained from these was used for all the following frequency sweep experiments.

Table. 2: Strain sweep settings

Frequency	10 rad/s
Initial strain	0.1
Final Strain	300
Points per decade	10

Frequency sweep measurements were conducted using the conditions shown in table. .used the settings shown in table. with the temperatures varying as stated before. From these frequency sweeps the values of the storage modulus (G'), and the viscosity (η) were obtained.

Table. 3: Frequency sweep settings

Strain	20% for PMMA/PLA and 10% for PET/PLA
Initial frequency	100
Final frequency	0.1
Points per decade	10

The strain sweep measurements were used to determine the linear viscoelastic region, and establish a suitable deformation amplitude for the following tests.

The frequency sweep measurements provided the following information:

- G' (storage modulus)
- η^* (complex viscosity)

The measurements obtained were used to evaluate the influence of composition, and aging on the rheological behaviour of the polymer blends.

2.2.7 UV-Vis (UV-2600i Shimadzu):

UV-Vis tests are especially useful to quantify the transparency and haze.

Transparency tests are also important especially for the aesthetics aspect. Since we are dealing with transparent materials, and transparency is a desirable characteristic for our case, variations must be quantized especially when not easily visible to the naked eye. As a result, a machine such as the one in Fig. 20 is used, emitting radiation from ultra-violet to visible range and measuring the amount reflected or transmitted (one is the compliment of the other) to give a measurement of transparency.

The spectrophotometer shown in Fig. 20 was used for the optical characterisation. This instrument measures the absorbance of light as a function of wavelength of the electromagnetic spectrum. The wavelengths utilized range from with the ultraviolet to the visible regions. Variations in absorbance and transmittance were used to evaluate the transparency of the films.

Film samples were cut into strips and placed into the integrated sample holder of the spectrophotometer before starting the test.

Before testing the lamp was allowed to warmup to ensure stability in the measurements. The measurements were conducted over the range of 200 nm to 800 nm.

These measurements provided wavelength dependant absorbance spectra of the polymer films. This data was in turn used to assess the optical transparency of the different blends, and the variation with aging.

Fig. 20: UV-2600i Shimadzu

2.2.8 ZEISS EVO 15 SEM (Scanning Electron Microscope) :

Images obtained from microscopy are used to observe any phase separation, morphology, and interfacial adhesion.

For further information on the microstructure, the phase structure of samples, and gain further information on the miscibility a SEM (Scanning Electron Microscope) is used. In a SEM the electron beam scans the sample in a raster pattern. Electrons are initially generated at the top of a column by a source as shown in Fig. 21 by heating the source material. These generated electrons are then accelerated by the anode, condensed, and collimated towards the target or sample to be analysed.

Fig. 21: Diagram of how a SEM works [26]

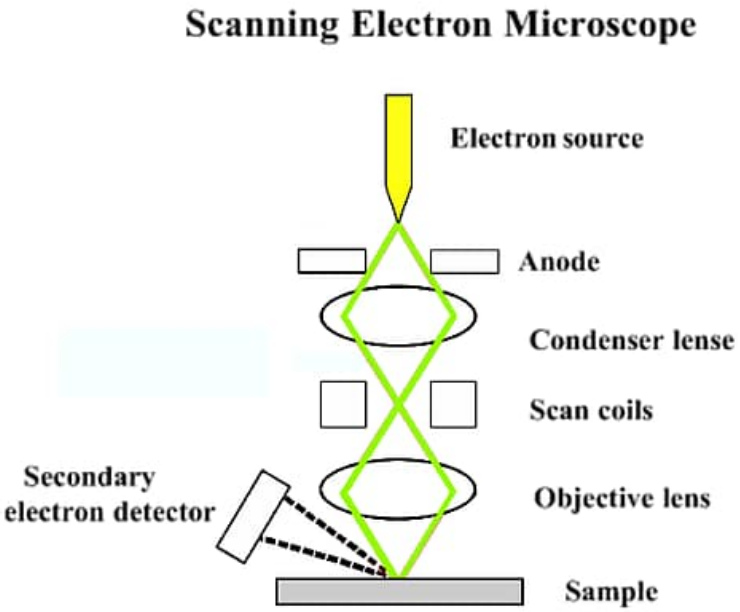

The morphological characterisation was performed using the scanning electron microscope. SEM generates high resolution images through the interaction of a focused electron beam with the sample surface. The image is formed mainly based on the detection of secondary, and backscattered electrons emitted from the sample. [26]

A completely fragile fracture is required for the SEM. As a result, to prepare the samples they were first submerged in liquid nitrogen for 20 s to 30 s, and subsequently, using pliers the sample was fractured. The fractured sample was appropriately placed onto a sample holder to undergo an in-vacuum sputter coating procedure. The coating was necessary to make surface imaging and characterisation possible. Since polymeric materials tend to be electrically insulating, charges usually accumulate at the surface, causing image distortion and poor imaging. The conductive coating thickness was maintained below 10 nm in order to preserve the original morphology.

SEM imaging was conducted on the fractured surface under vacuum.

The SEM images were used to assess the fracture morphology, and potential phase distribution and phase separation within the blends. The images were utilised to gain further information on miscibility and morphological homogeneity.

Fig. 22: ZEISS EVO 15 [27]

3 Results and Discussion:

In this chapter, results obtained from all experimental testing are presented. Following the presentation of each set of results (a comparative analysis is conducted and supported by the relevant literature. This will be presented as per the following sections:

- Mechanical tests and analysis: these are the tests that were conducted using the Instron machine for tensile test with a focus on Young's Modulus and deformation at fracture.
- Results and analysis of the DSC tests: to get more information on the phases present and crystallinity.
- Results of the rheological tests presenting the viscosity curves of the blends.
- Analysis for the SEM results: to gain a further understanding of the microstructure and bonds in relation to our results.
- Transparency (UV-Vis) tests: showing the variation in absorption with the PMMA/PLA blends as they age.

The obtained results will follow the variations found with the different levels of PLA (0%, 20%, 40%, and 50%), in the PMMA/PLA and PET/PLA blends with aging.

3.1 Test on PMMA/PLA Blends

3.1.1 Mechanical Tests on PMMA/PLA Blends

3.1.1.1 Mechanical Tests of PMMA/PLA samples at time 0

"Time 0" means right after extrusion, or to be more precise without any aging. Reported in the following figures are bar graphs with standard deviation bars. Young's Modulus is reported in Megapascal (MPa) and denoted by E, whereas the deformation is given as a percentage $\frac{final\ length - initial\ length}{initial\ length}$ and denoted by ε.

Young's Modulus was originally calculated through Instron's automatic program. However, since we are dealing with a quite fragile and thin film that already had a slight curve due to the calendering process without any correction, this would have resulted in a much lower Young's Modulus since the result given in that initial part is just due to the straightening. As a result, the modulus was usually calculated after a deformation of about 1%. This percentage was chosen by observing the stress – strain curves closely, and monitoring where their behaviour starts representing the film.

In Fig. 23 below, we can see that the material maintains its value for the Young's Modulus. As a matter of fact, the values do slightly improve with the increase of PLA. Values can be seen in table. 4.

Fig. 23: Bar graph of PMMA/PLA blends' Young's Modulus at time 0

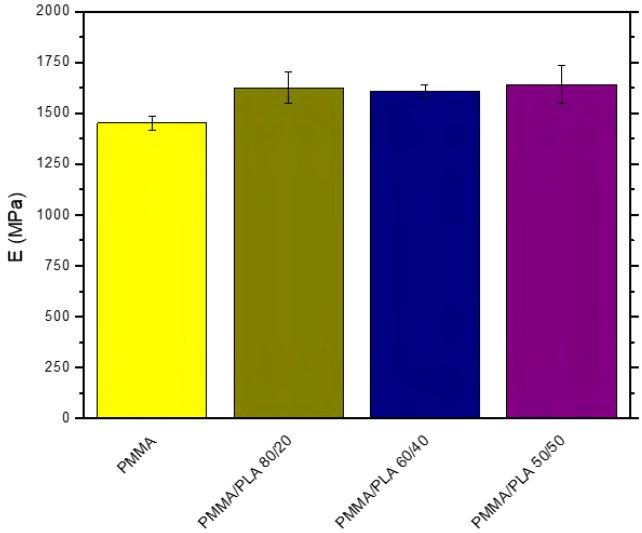

On the other hand, as shown in Fig. 24 below, the deformation shows a substantial improvement and increase in value. While the increase in deformation is not noticeable for PMMA/PLA 80/20, the difference becomes quite noticeable for the 60/40 blends. This difference was also apparent to the touch.

Fig. 24: Bar graph of deformation of PMMA/PLA samples at time 0

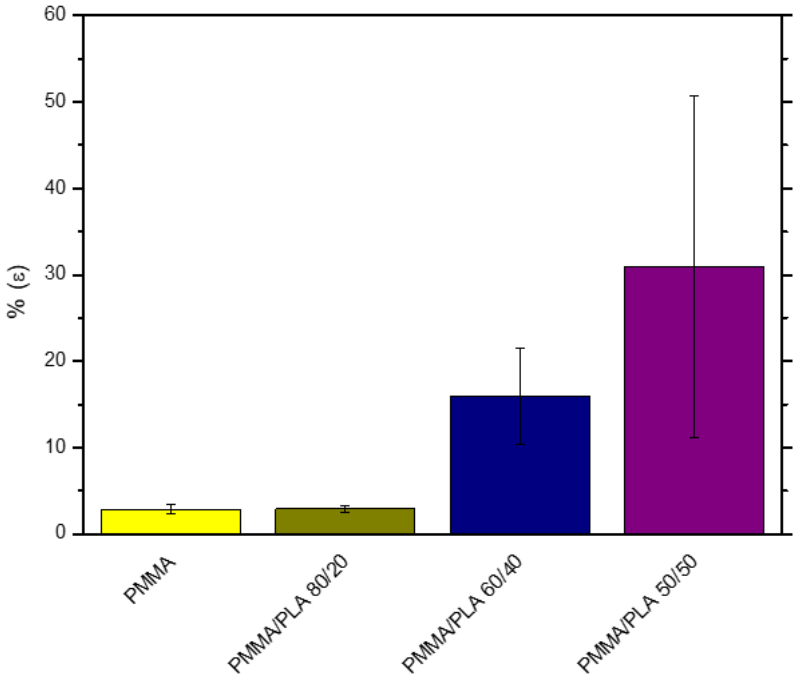

Despite this increase in deformation, all samples still exhibit fragile behaviour which was seen in the test samples. This made the sample preparation more difficult as stated before.

3.1.1.2 Mechanical Tests of PMMA/PLA samples at time 48 hours

Aging was done in this case in 12 hours cycles, 8 hours of UV (Ultraviolet) radiation at 340 nm (a non-aggressive blue) at 45 °C followed by 4 hours of condensation at 40 °C. It must be noted that an attempt to age these films for 96 hours at 60 °C in UV radiation was initially attempted, but the results did not prove to be useful since a measurement was not possible after ageing. The film was effectively "dead", and the samples with 50% PLA became warped and lost their shape, as seen in Fig. 25 below.

Fig. 25: PMMA/PLA 50/50 film coiling after going through QUV for 96 hours at 60 °C

Following this aging process samples remained brittle. As seen in the Fig. 26. below, pure PMMA film had a brittle fracture.

Fig. 26: Pure PMMA film aged for 48 hours at 45 °C

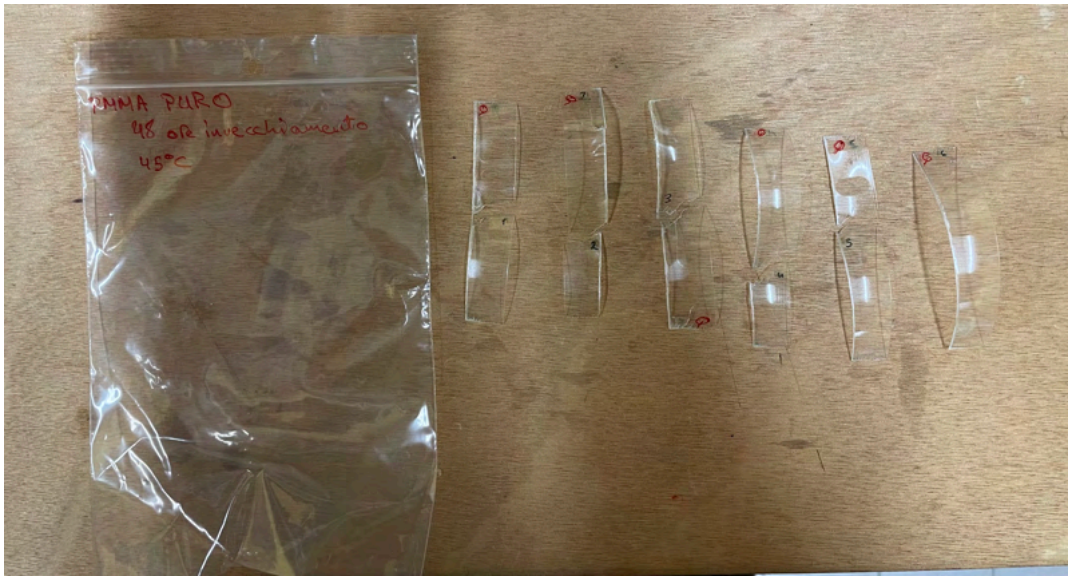

PMMA with 20% PLA was still quiet brittle as seen in Fig. 27 below. Samples with more PLA caused the clamps to lose grip. As a result, some samples were discarded from the calculations and not considered.

Fig. 27: PMMA/PLA 80/20 film aged for 48 hours at 45 °C

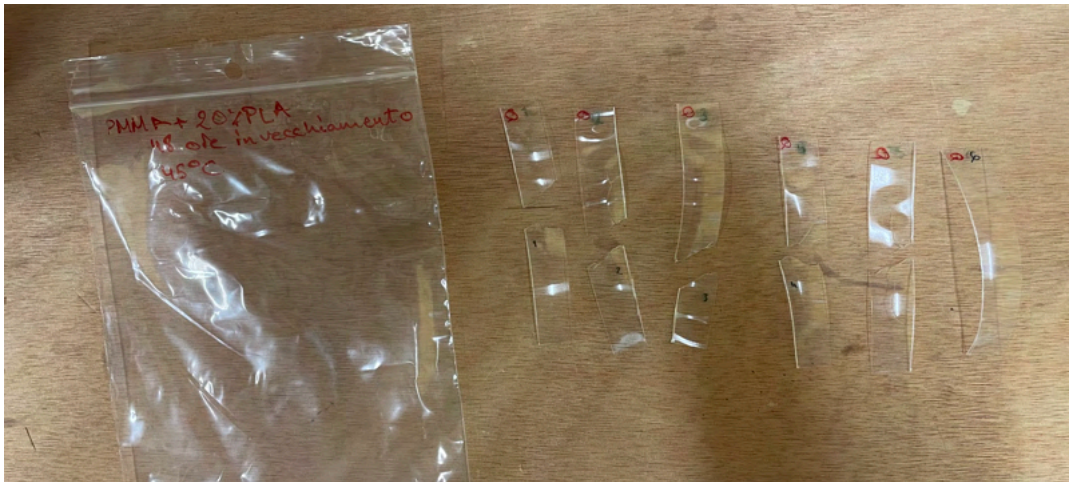

PMMA with 40% PLA shown in Fig. 28 was also brittle and had the same challenges as the blend with 20% PLA.

Fig. 28: PMMA/PLA 60/40 film aged for 48 hours at 45 °C

PMMA/PLA blend that was 50/50 became more evidently brittle as can be seen from the used samples in Fig. 29 below.

Fig. 29: PMMA/PLA 50/50 film aged for 48 hours at 45 °C

The samples maintained the same trends with the increase of PLA content even after ageing for the modulus (Fig. 30), and deformation (Fig. 31). Although, after the ageing we can see that the modulus peaks for the 60/40 blend. It can also be seen that the deformation drastically dropped, but an increase in deformation from the higher PLA content blends is still noticed.

Fig. 30: Average Young's Modulus of PMMA/PLA blends that were aged for 48 hours at 45 °C

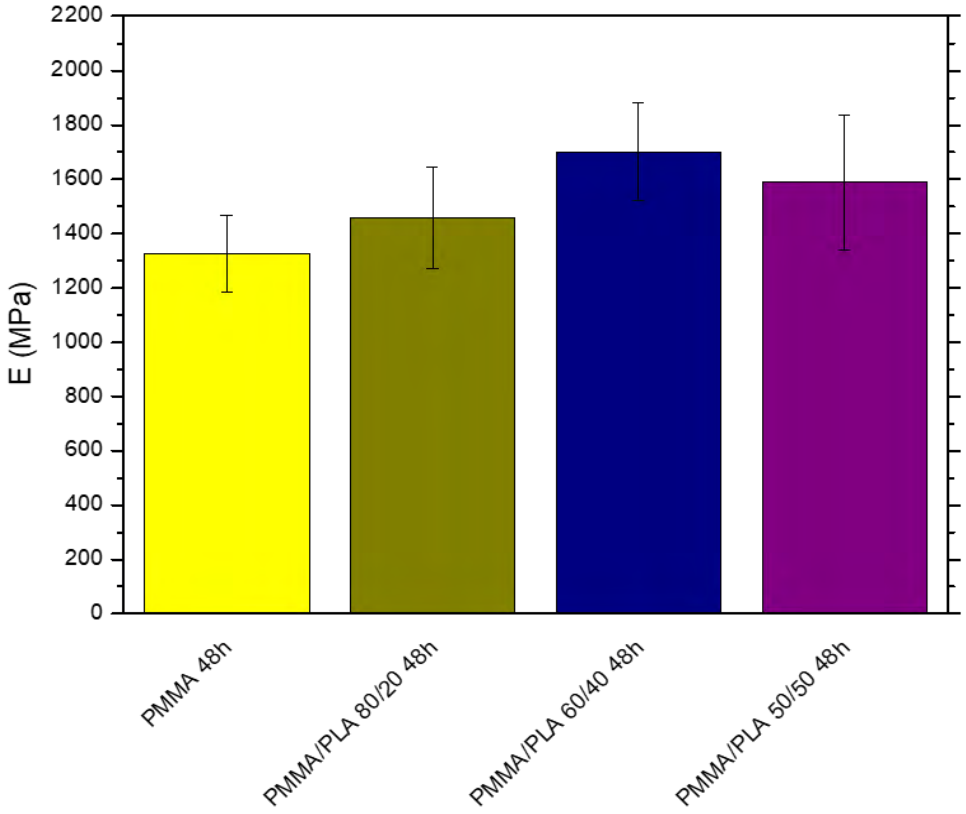

Fig.31: Average deformation of PMMA/PLA blends that were aged for 48 hours at 45 °C

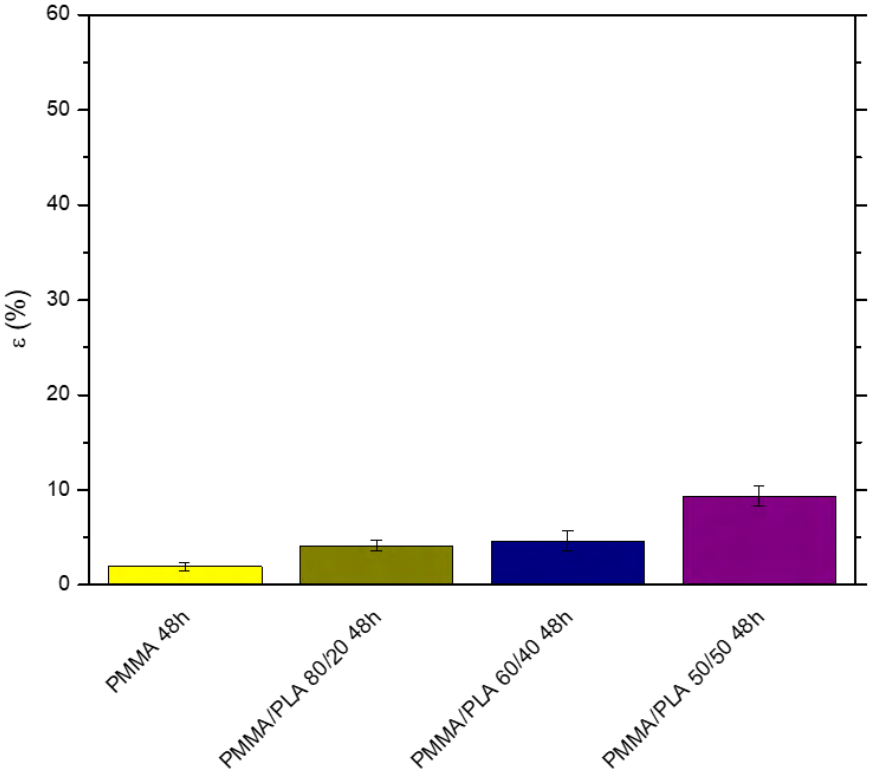

3.1.1.3 Mechanical Tests of PMMA/PLA Samples at Time 24 hours

For the 24 hours aging, the condensation step was skipped due to technical difficulties with the instrument. This means that the radiation cycles were applied consecutively. The UV radiation used is equal to the previous and was done at 45 °C as well.

The samples shown in the figures below show that the samples are brittle after 24 hours of aging as well. Starting with pure PMMA film in Fig. 32 which displays a net brittle fracture.

Fig. 32: Pure PMMA film aged for 24 hours at 45 °C

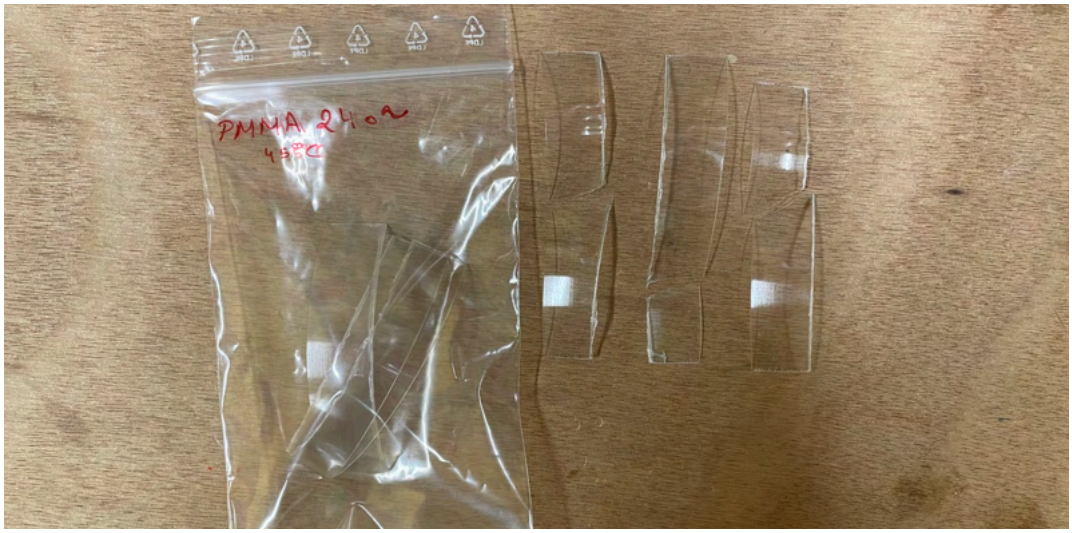

Moving on to the 24 hours aged PMMA with 20% PLA film. A brittle fracture can also be seen here in Fig. 33.

Fig. 33: PMMA/PLA 80/20 film aged for 24 hours at 45 °C

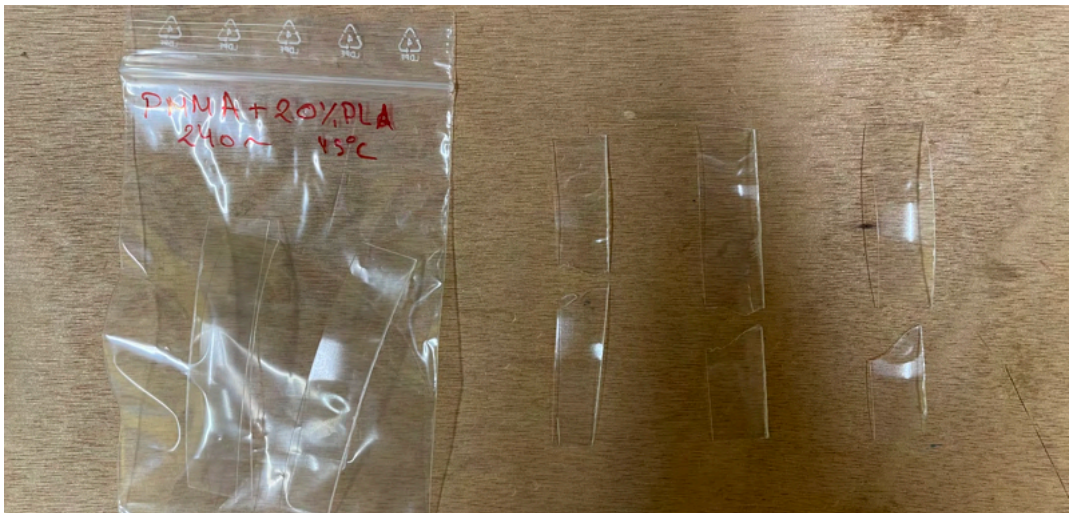

The PMMA with 40% PLA film also exhibited a fragile fracture in Fig. 34. In this case, the fractures were occurring closer to the clamps as well.

Fig. 34: PMMA/PLA 60/40 film aged for 24 hours at 45 °C

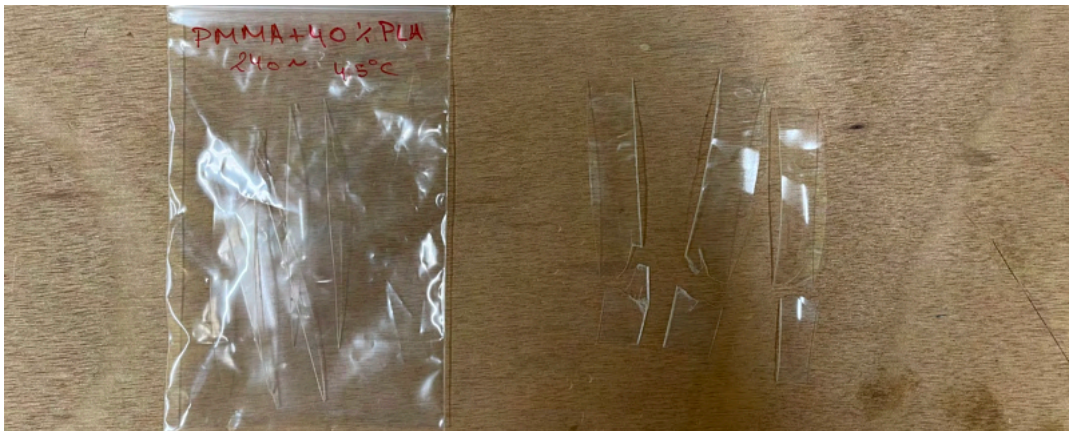

The PMMA with 50% PLA film also exhibited a brittle fracture as seen in Fig. 35.

Fig. 35: PMMA/PLA 50/50 film aged for 24 hours at 45 °C

Observing how the Young's Modulus varies with the increasing PLA content, a clear increase in the modulus in Fig. 36 is noted. The difference in the average values obtained of the modulus is also evidently bigger compared to the non-aged films, and to the 48 hours aged (with condensation step) films. Also, unlike the 48 hours aged films, there is an increase in the Young's modulus with every increase of PLA, and it doesn't peak at 40% PLA.

Fig. 36: Average Young's Modulus of PMMA/PLA blends that were aged for 24 hours at 45 °C

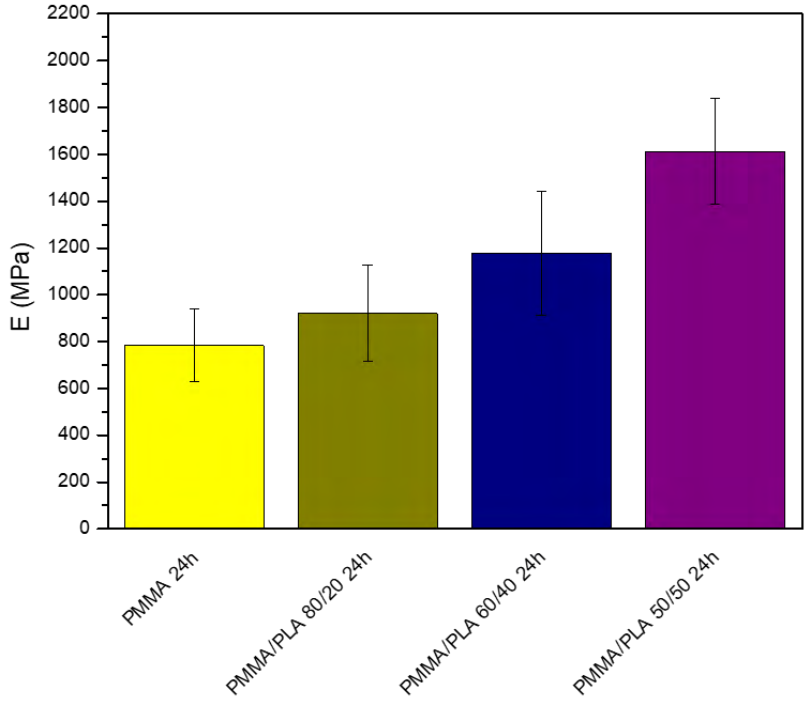

The deformation also followed the same trend that was seen previously for the non-aged and 48 hours aged samples as shown in Fig. 37. However, the deformation did decrease with respect to the values obtained, especially in the non-aged PMMA/PLA films.

Fig. 37: Average deformation of PMMA/PLA blends that were aged for 24 hours at 45 °C

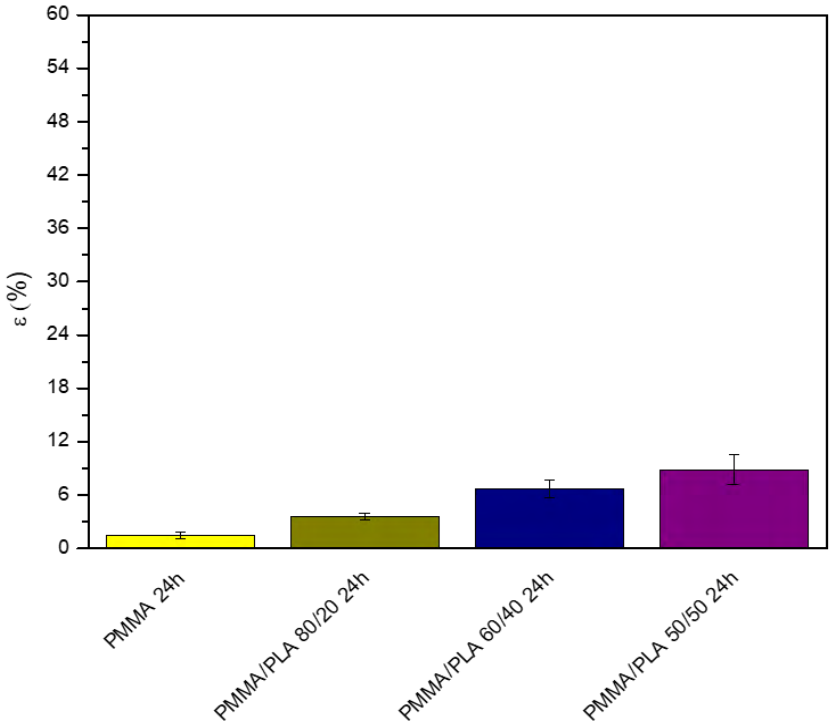

3.1.1.4 Mechanical Tests of PMMA/PLA Samples at Time 72 hours

For the 72 hours aging process, the cycles and stages were the same as the previous aging of 24 hours, using the UV radiation at 340 nm at 45 °C.

As always, the PMMA film exhibited fragile behaviour, and thus a fragile fracture as seen in Fig. 38. There were quite net fractures, and these films, even with increasing PLA content, still felt delicate and fragile to the touch.

Fig. 38: Pure PMMA film aged for 72 hours at 45 °C

PMMA films with 20% PLA remained brittle, as was expected based on previous results as well as seen in Fig. 39 below.

Fig. 39: PMMA/PLA 80/20 film aged for 72 hours at 45 °C

For PMMA films with 40% PLA were extremely brittle, and as can be seen in Fig. 40 below, where they seemed to shatter a bit (many small pieces breaking off to signify the end of the test).

Fig. 40: PMMA/PLA 60/40 film aged for 72 hours at 45 °C

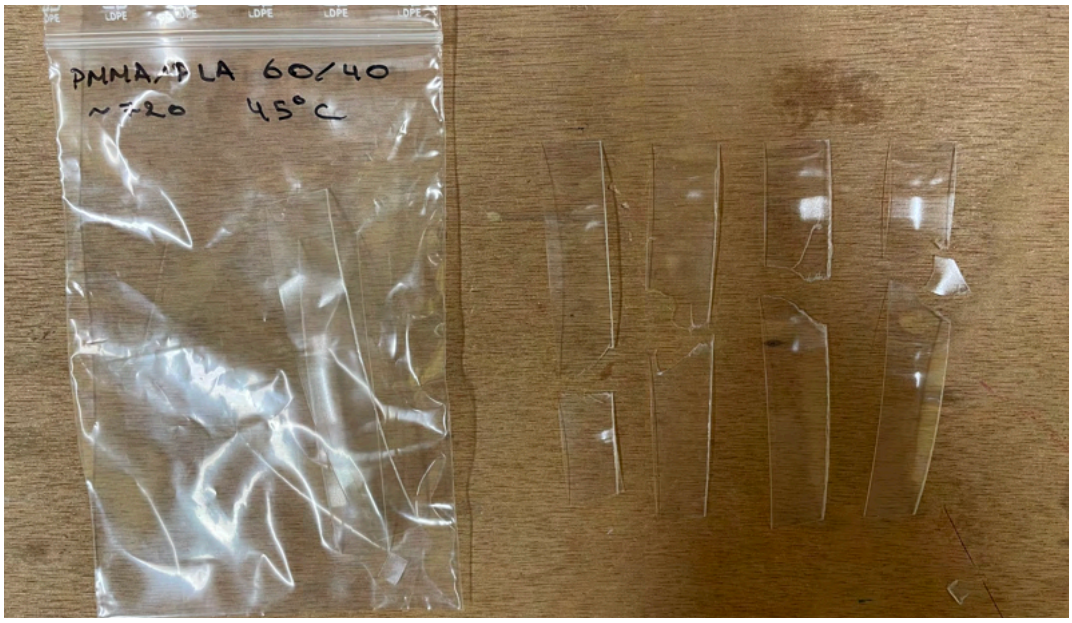

The final tested films were the PMMA with 50% PLA films which, as always were brittle, and as seen in Fig. 41 had brittle fractures. The seemingly undamaged samples are due to the slippery nature of the film with respect to the clamps.

Fig. 41: PMMA/PLA 50/50 film aged for 72 hours at 45 °C

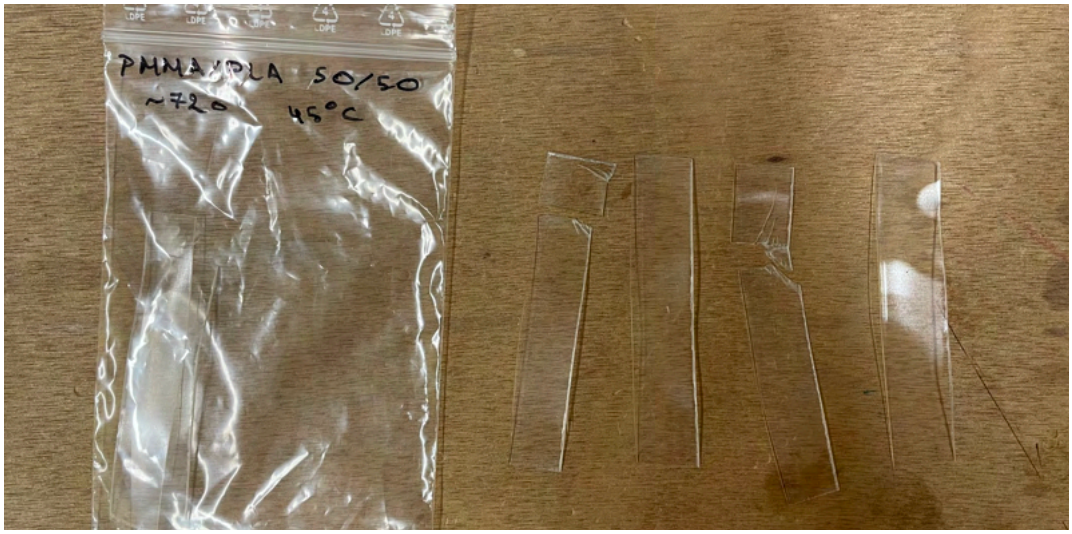

By comparing the films with varying percentages of PLA, it was observed that the trend of improving Young's Modulus with increasing PLA content is still present, as observed in Fig. 42. Despite a slight dip for the 20% PLA film, there was an evident increase for the 40% PLA and 50% PLA film.

Fig. 42: Average Young's Modulus of PMMA/PLA blends that were aged for 72 hours at 45 °C

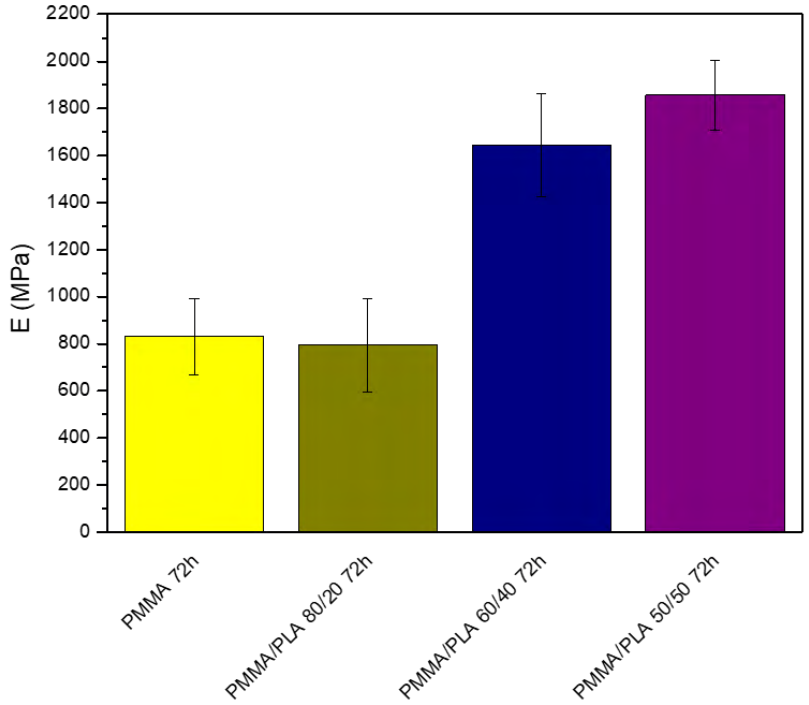

Deformation also improved with increasing PLA content in Fig. 43. In this case there was no dip for the 20% PLA, unlike what was seen for the Young's Modulus.

Fig. 43: Average deformation of PMMA/PLA blends that were aged for 72 hours at 45 °C

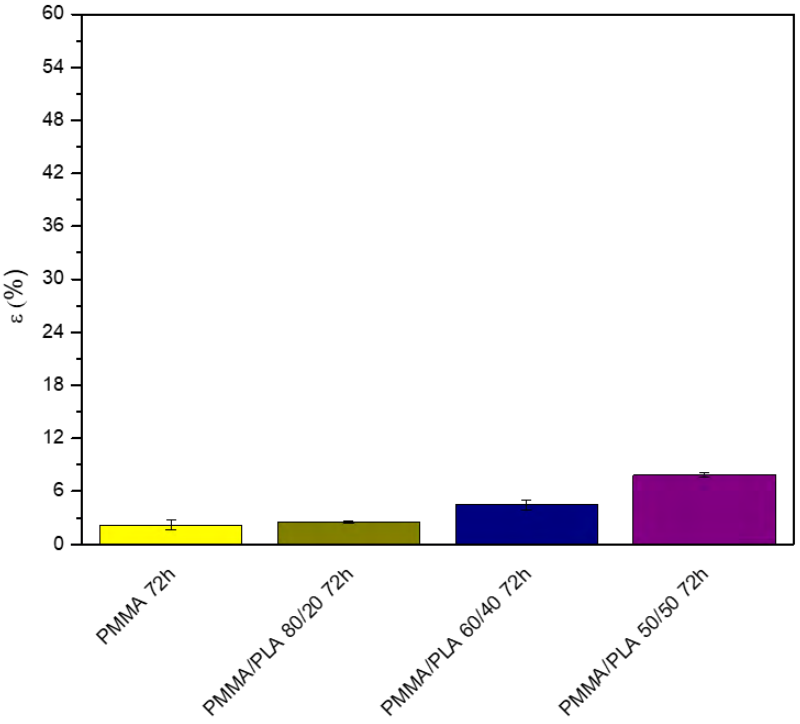

3.1.1.5 Summary of Results and Comments on PMMA/PLA Films

In the following Table. 4 all the numerical values for the mechanical test are shown. In **bold** are the maximum values obtained for the modulus and deformation.

Table. 4 Results of all the mechanical tests

	Young's Modulus (MPa)	Deformation (%)
PMMA 0h	1450	3
PMMA/PLA 80/20 0h	1625	3
PMMA/PLA 60/40 0h	1609	16
PMMA/PLA 50/50 0h	1640	**31**
PMMA 48h	1326	2
PMMA/PLA 80/20 48h	1459	4
PMMA/PLA 60/40 48h	1701	5
PMMA/PLA 50/50 48h	1589	9
PMMA 24h	782	1
PMMA/PLA 80/20 24h	920	4
PMMA/PLA 60/40 24h	1177	7
PMMA/PLA 50/50 24h	1611	8
PMMA 72h	830	2
PMMA/PLA 80/20 72h	793	3
PMMA/PLA 60/40 72h	1644	5
PMMA/PLA 50/50 72h	**1857**	8

As seen below in Fig. 44, the modulus generally decreases as the aging progresses.

Fig. 44: Average Young's Modulus evolution of PMMA with aging

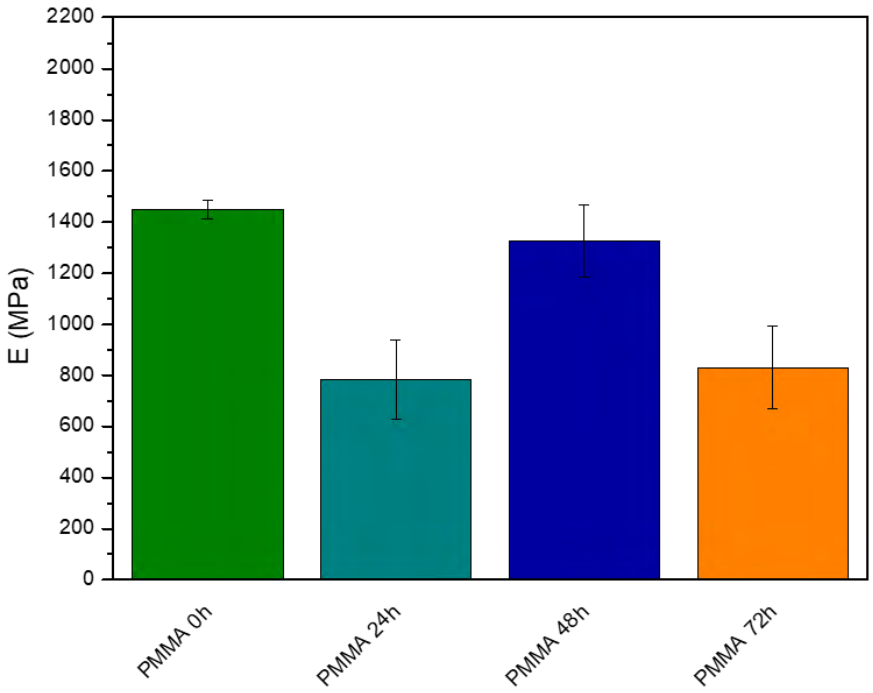

The highly brittle nature of PMMA means that variations are very little however a slight negative trend can be seen in Fig. 45 below.

Fig. 45: Average deformation evolution of PMMA with aging

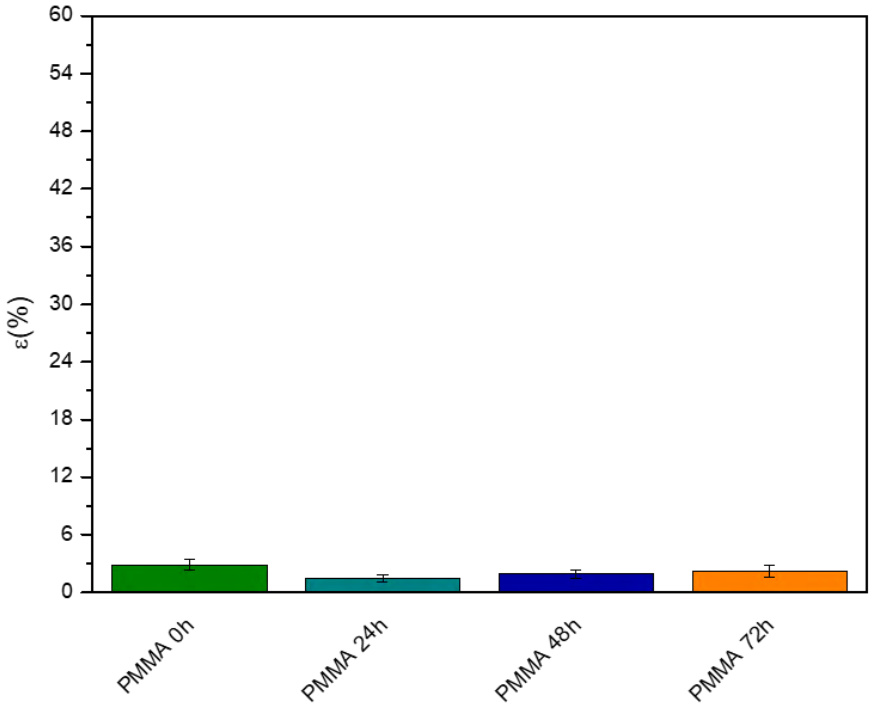

Again, in Fig. 46 the Young's Modulus decreases with aging in the case of the blend with 20% PLA.

Fig. 46: Average Young's Modulus evolution of PMMA/PLA 80/20 with aging

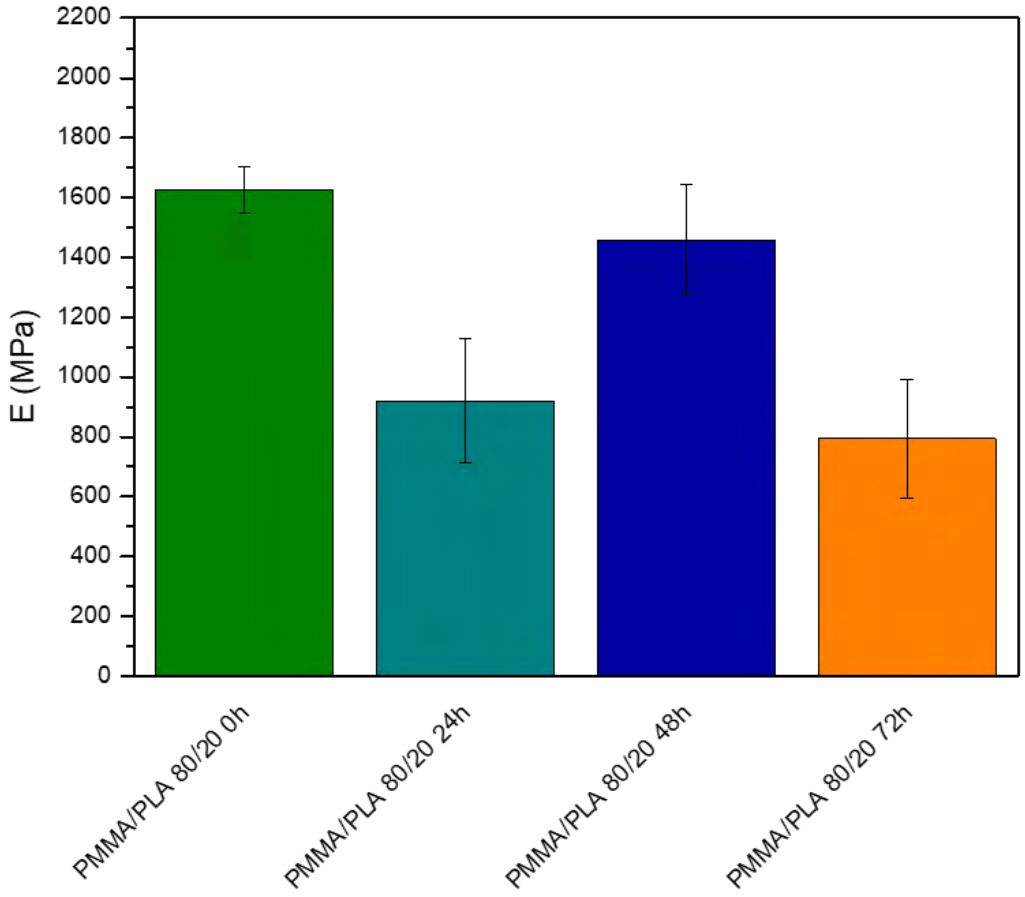

A common result of aging in many plastic materials is embrittlement, and it occurs due to a few reasons. The core reason and the main cause of embrittlement is the breaking of polymer chains. Since the mechanism, reasons, and conditions to set off the scission can be different, the resulting change in deformation may not be as intuitive. Noting that due to the original brittle nature of the blends, the variations are quite little as seen in Fig . 47.below.

Fig. 47: Average deformation evolution of PMMA/PLA 80/20 with aging

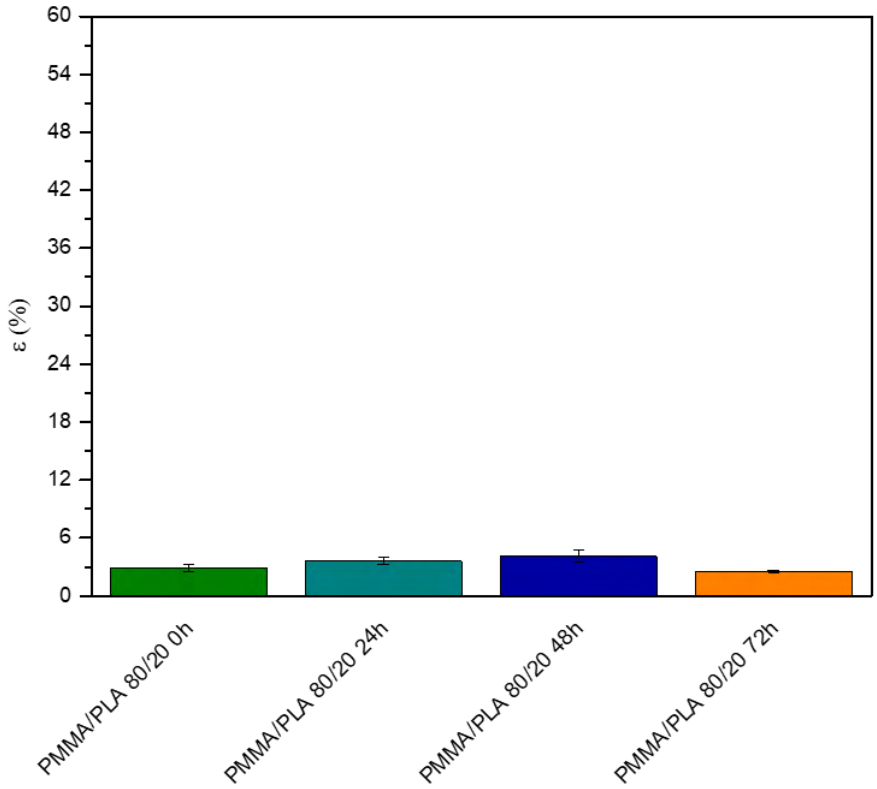

For the PMMA blend with 40% PLA we start seeing a slight improvement or maintainment of performance with the Young's Modulus is seen in Fig. 48.

Fig. 48: Average Young's Modulus evolution of PMMA/PLA 60/40 with aging

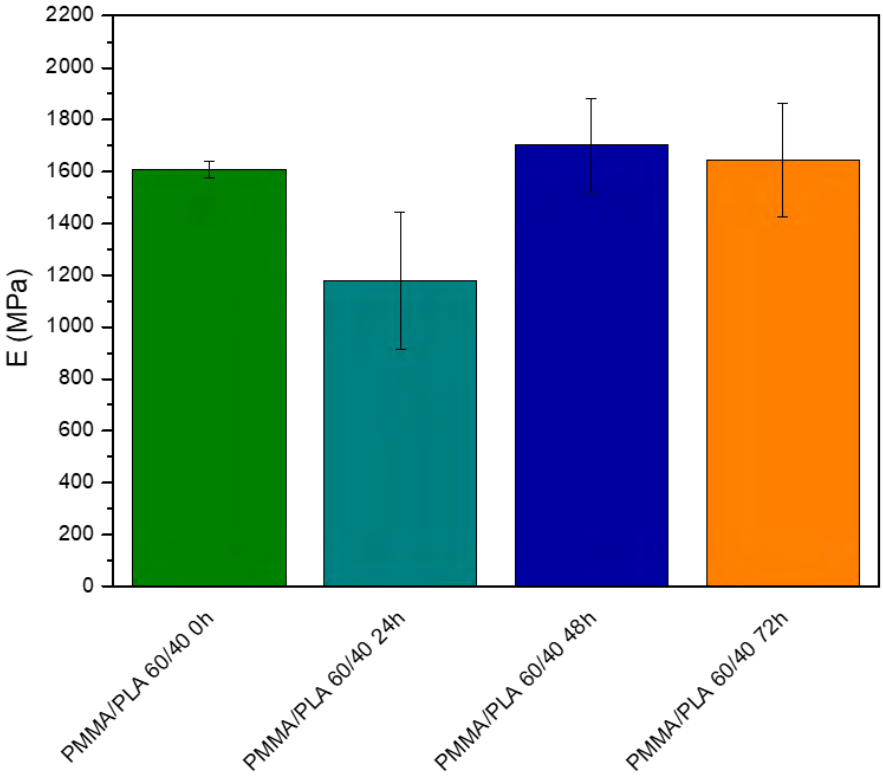

After adding 40% PLA in blends the drop in deformation becomes noticeable (Fig. 49). This is mainly due to the inferior ability of PLA to resist photodegradation. Studies indicate that amorphous PLA is particularly susceptible to radiation-induced degradation. [28]

Fig. 49: Average deformation evolution of PMMA/PLA 60/40 with aging

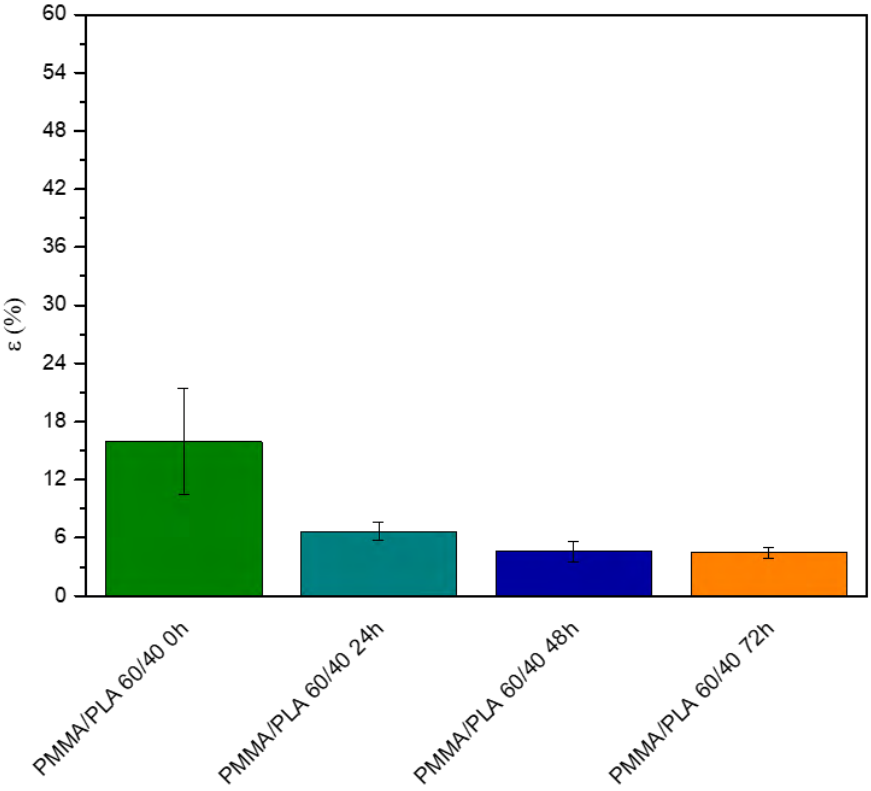

The Young's Modulus of the 50% PLA blend actually ends up having a slight improvement, as shown in Fig. 50. As a matter of fact, the PMMA/PLA 50/50 samples have the highest modulus value of all the samples that we tested.

Fig. 50: Average Young's Modulus evolution of PMMA/PLA 50/50 with aging

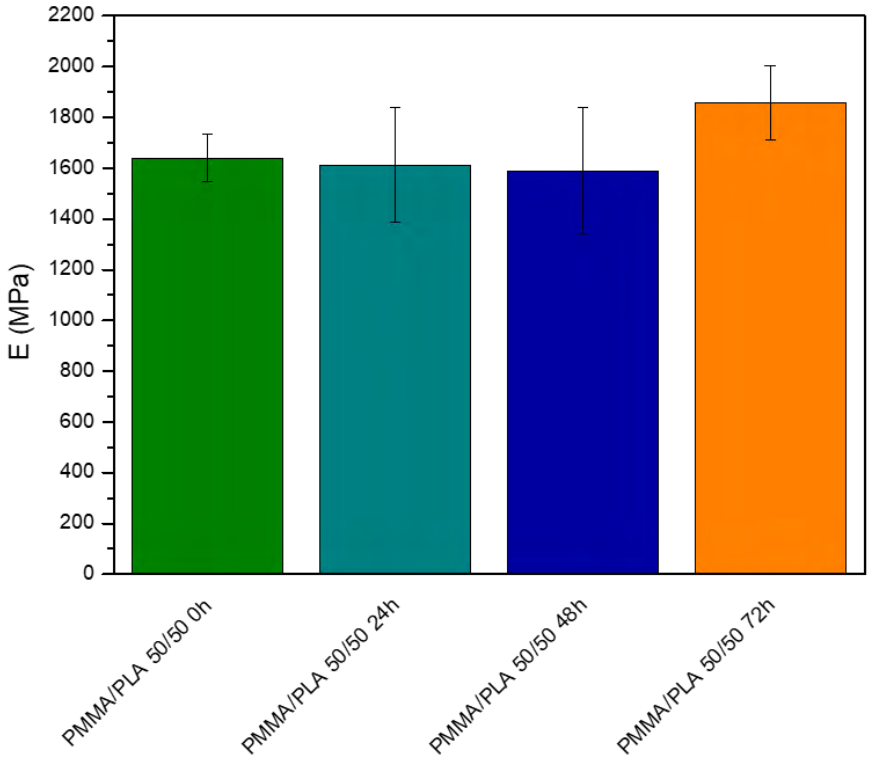

Unlike the Young's modulus, the deformation of the 50/50 blends suffers a dramatic decrease in Fig. 51. However, that does also come with the information that the samples with 50% PLA at 0 hours were by far the most deformed with a slight caveat of big error bars due to difficulties with the instrument.

Fig. 51: Average deformation evolution of PMMA/PLA 50/50 with aging

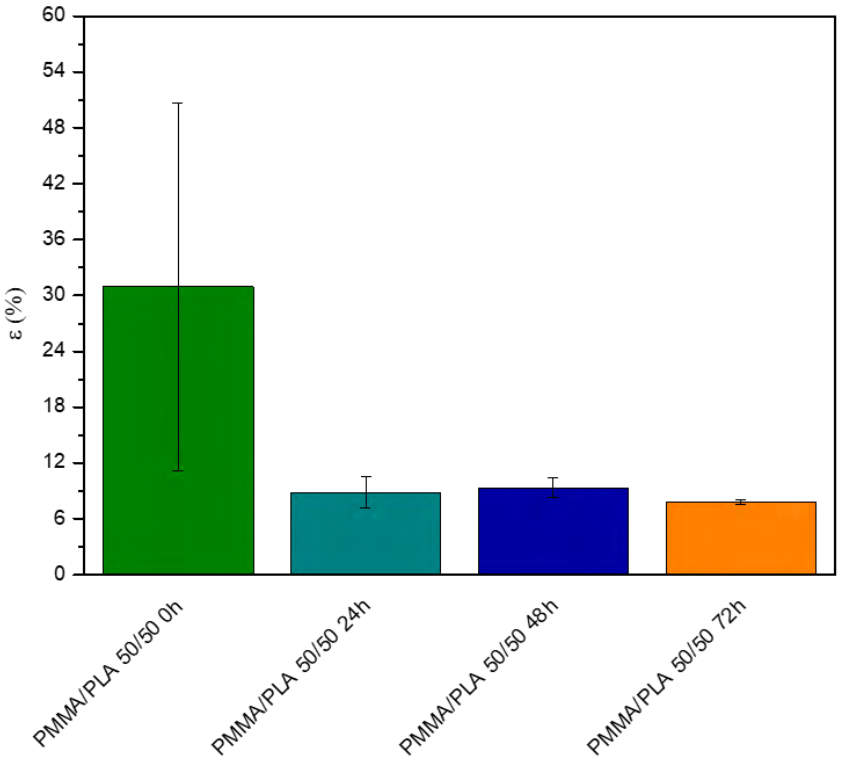

Attempts to explain the variations in behaviour of PMMA/PLA films have been researched, and simulations were carried out by Debashish Mukherji et al. [29], the method they used was the Kirkwood–Buff, theory of solution for investigating the thermodynamic properties of complex mixtures. The simulations were all–atom simulations carried out in four steps with different chain lengths, and number of chains which they chose to be short in order to not use entanglement but rather intermingle. Running the simulation box to a uniaxial tensile deformation akin to that of our own tensile test. They found that it was common for PMMA to be plasticised using another polymer - in this case PLA - and the larger the ratio of PLA present in the blend the lower the T_g , however that showed changes of only about 5% to the deformation at fracture. Thus, they investigated based on the chemical structure of the monomer units. Exploring this scenario, they found PMMA groups that can strongly interact with each other, thus increasing the interchain interlocking causing the brittleness of the samples, whereas a PLA chain can slide past other PLA and PMMA chains with little friction. Further investigations were also carried out for different lengths of PLA chains finding that the key factor for increasing the value of deformation is the mobility of these chains as they tend to attract to each other and move more readily when under a tensile load. Thus, for their simulations shorter PLA chains yielded better results for increasing the deformation.

3.1.2 DSC (Differential Scanning Calorimetry) of PMMA/PLA Blends

Further characterization was conducted in order to explain the behaviour seen. All samples that underwent mechanical testing were also subject to DSC scans characterization. All the graphs shown for DSC scans are displayed in an exo-up format. The table. 5 below shows all the values that were obtained using TA instruments from the DSC scans. N/A signifies that the value was not detectable from our DSC scans. That could be due to the fact that the signal was not there, for example T_g of PLA in the pure PMMA samples, the signal was weak, or even possibly the signal was covered by the background noise. From the DSC, a calculation of the crystallinity is made based on the formula $X_c = \frac{\boldsymbol{\Delta H_m}}{(1-x)\times \boldsymbol{\Delta H_{m0}}} \times 100$ [30], ΔH_m is the enthalpy of fusion that was found from our DSC scan, and in the case of PLA due to its slow crystallization between the glass transition and melt temperature, cold crystallization occurs presenting another peak [31] with the corresponding enthalpy being subtracted from the enthalpy of fusion. ΔH_{m0} is the enthalpy of fusion of the polymer when 100% crystalline, which is 93 J/g in our case [32] and that value is multiplied by (1-x) with x being the fraction in weight of the investigated polymer in the blend.

Table. 5 Results from the DSC scans

	Tg (°C) PMMA	Tg (°C) PLA	ΔH_m(J/g)	ΔH_{cc} (J/g)	X_c (%)
PMMA 0h	119	N/A	N/A	N/A	N/A
PMMA 24h	N/A	N/A	N/A	N/A	N/A
PMMA 48h	118	N/A	N/A	N/A	N/A
PMMA 72h	N/A	N/A	N/A	N/A	N/A
PMMA/PLA 80/20 0h	119	66	N/A	N/A	N/A
PMMA/PLA 80/20 24h	115	70	N/A	N/A	N/A
PMMA/PLA 80/20 48h	118	76	N/A	N/A	N/A
PMMA/PLA 80/20 72h	N/A	69	N/A	N/A	N/A
PMMA/PLA 60/40 0h	N/A	65	N/A	N/A	N/A
PMMA/PLA 60/40 24h	N/A	70	N/A	N/A	N/A
PMMA/PLA 60/40 48h	N/A	71	N/A	N/A	N/A
PMMA/PLA 60/40 72h	N/A	69	N/A	N/A	N/A
PMMA/PLA 50/50 0h	N/A	65	3.6	0.6	6.4
PMMA/PLA 50/50 24h	N/A	69	0.6	N/A	1.3
PMMA/PLA 50/50 48h	N/A	68	2.6	N/A	5.5
PMMA/PLA 50/50 72h	N/A	69	2.4	N/A	5.0

First, in Fig. 52 the different peaks for the PMMA/PLA blends are visible. While the dips indicating the T_g of PMMA and T_g of PLA (PLA further to the left meaning at lower temperatures) are detectable. As can be seen the peaks, valleys, and dips are not so strong which makes it hard to find the exact values.

Fig. 52: DSC scans of PMMA/PLA blends before aging

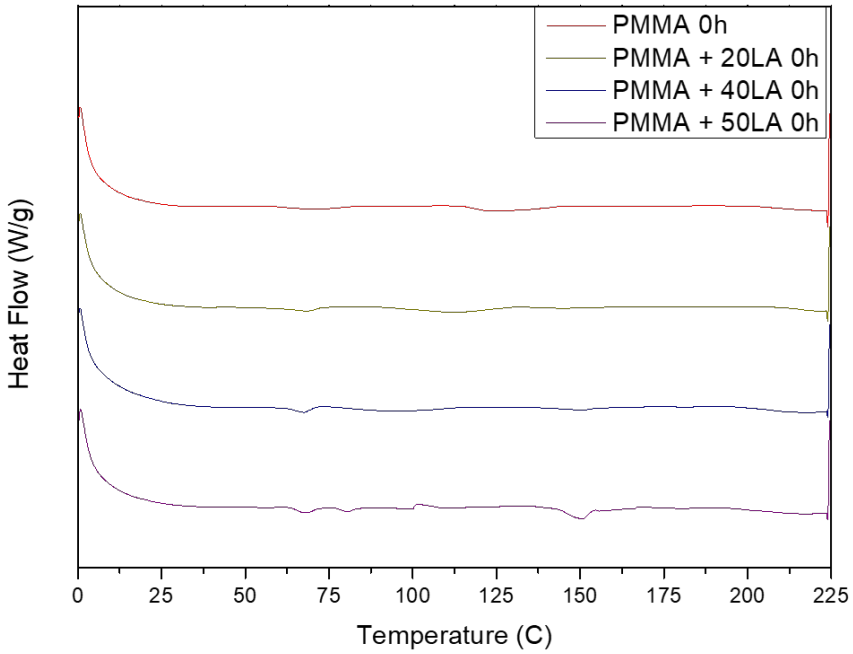

Observing the DSC scans of PMMA as it ages in Fig. 53 we can see that the form of the curves remains somewhat similar. We can also see how the dip for T_g of PMMA remains in the same place. This confirms the well-known durability of PMMA, as it doesn't show significant changes.

Fig. 53: DSC scans of PMMA as it ages

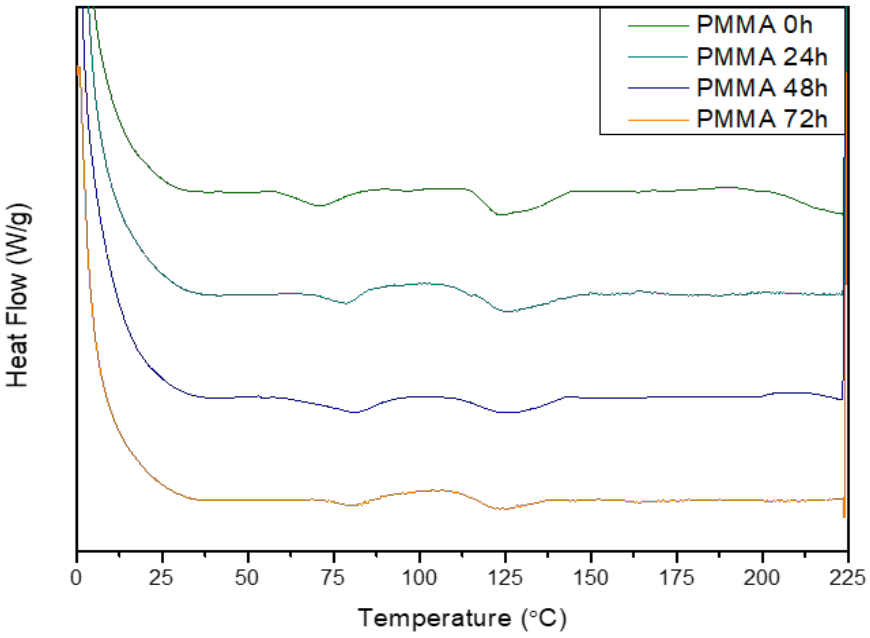

In Fig. 54 with the addition of PLA, as expected, the dip starts appearing at around 70 °C.

Fig. 54: DSC scans of PMMA/PLA 80/20 as it ages

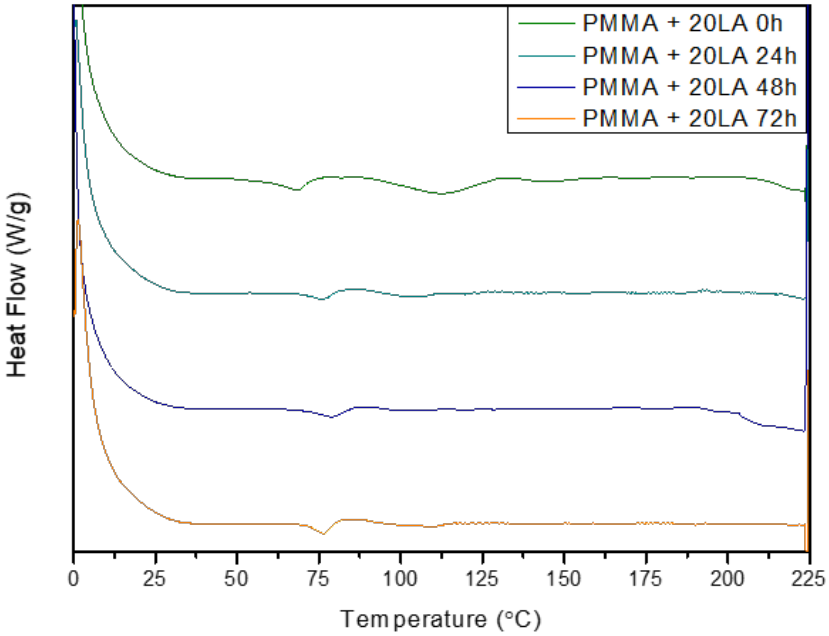

With the PMMA/PLA 60/40 blend in Fig. 55 the PLA signal becomes more pronounced. On the other hand, the PMMA signal became much harder to find. The enthalpy of fusion and cold crystallization were not detectable as well.

Fig. 55: DSC scans of PMMA/PLA 60/40 as it ages

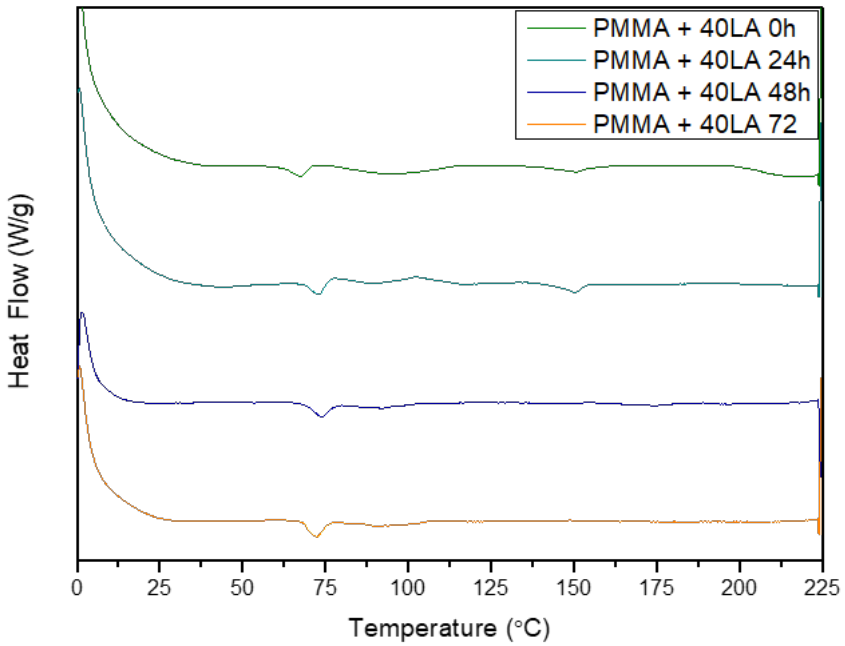

After increasing PLA to 50%, it was possible to not only detect the T_g of PLA, but the areas from which we get the enthalpies of fusion and cold crystallization were detectable. As seen in Fig. 56 below, we were able to locate the peak for fusion at around 143 °C, and the cold crystallization peak at around 101 °C.

Fig. 56: DSC scans of PMMA/PLA 50/50 as it ages

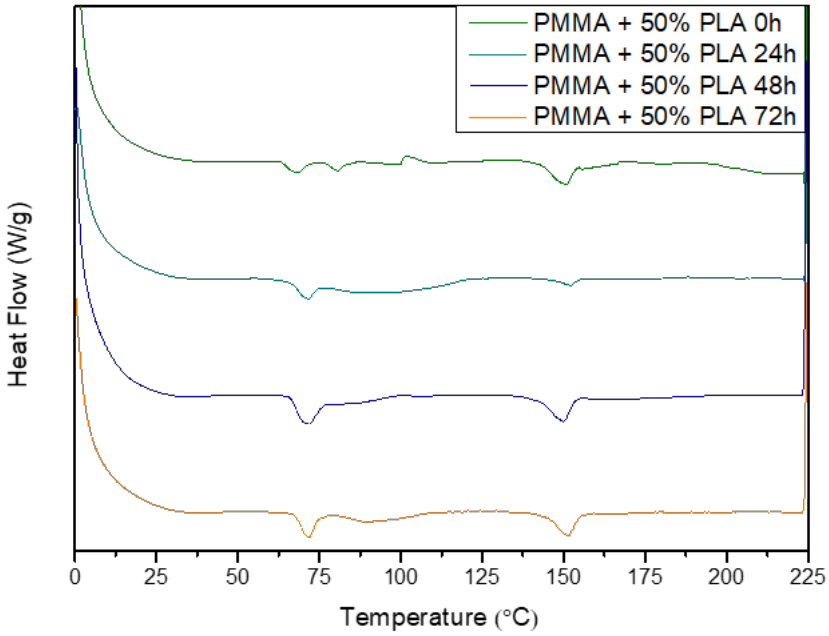

Given the stability of PMMA, further studies on PLA were researched, in particular the work of M. V. Podzorova, et al. [33]. They studied PLA films obtained from compressing granules in a hydraulic press at 180 °C irradiated at a wavelength of 254 nm for up to 100 hours. They found that the degree of crystallinity has a drastic drop at around 25 hours which coincides with the change in behaviour to brittle, and the crystallinity is halved by 100 hours. Their film also started cracking after 50 hours. They also observed a decrease of around 30 °C in the melting temperature as the film was irradiated and aged. These changes, and particularly the change in the melting temperature, were caused by the shortening of the polymer chains due to oxidative degradation.

Given this information, we can gain a deeper understanding of the mechanical tests shown in the previous section. The change in Fig. 51 for example, where the drop in deformation can be attributed to the shortening of the chains, and since in that example we have a high amount of PLA, the transition of PLA to brittle became apparent. On the other hand, the somewhat irregular behaviour of the Young's modulus as seen in Fig. 48 for example, can be attributed to two competing factors. First factor being that as PLA degraded and the chains became shorter, all of the mechanical properties decreased as seen from M. V. Podzrova et al.. Second factor being that of Debashish Mukherji et al's simulation, where the shortening of the PLA chains helped them to reaggregate, causing a reinforcement effect which we see in the 48 hours and 72 hours aged samples.

3.1.3 Rheology of PMMA/PLA Blends

Frequency sweeps are conducted at a constant shear strain rate and a constant temperature. Low frequencies coincide with longer times, also called stationary state. The force applied to the material comes from the velocity of deformation which in turn depends on the oscillation frequency.

With the dynamic frequency sweep curves conducted for the samples at 0 hours of aging in Fig. 57, they all showed a Newtonian plateau at lower angular velocities. A reduction in the viscosity with the addition of PLA can be observed signifying that PLA has a lower viscosity. The plateau did also get shorter for less PLA content. This means that the PLA impedes the alignment of the molecules confirming our explanation of the mechanical behaviour.

Fig. 57: Frequency sweep of PMMA/PLA blends before aging showing complex viscosity on the y – axis and angular velocity on the x - axis.

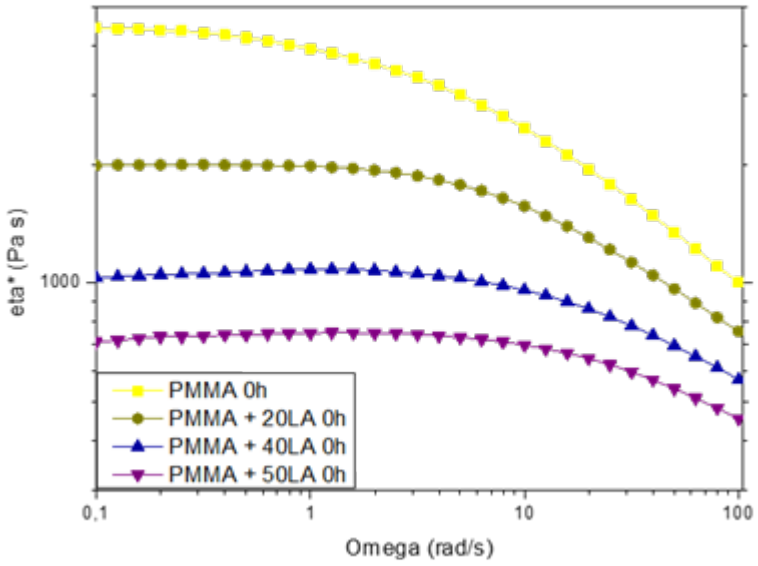

Observing the storage modulus (G') in Fig. 58 below. G' gives us information about the elasticity of the material, and how much energy the material can store when deformed. In this case, it shows that all the samples are viscoelastic, with the curves rising steadily with the increasing frequency. The polymer chains can rearrange and relax at low frequencies but are subject to elastic stiffening as they become constrained. Pure PMMA has the highest storage modulus, meaning PLA softens PMMA due to the aforementioned increased chain mobility. Other reasons could also contribute to this phenomenon such as partial plasticisation, and dilution of PMMA entanglements which is consistent with our findings from previous test as well. This is also confirmed by the larger separation at lower frequencies, and the easier flow which was observed during processing when PLA content increased. On the other hand, at higher frequencies we observe the separation getting smaller and the curves almost converging. This entire phenomenon shows the behaviour shifting form liquid like viscoelastic to a solid like viscoelastic material due to formation of interfacial bonds and network formations [34].

Fig. 58: Frequency sweep showing the storage modulus

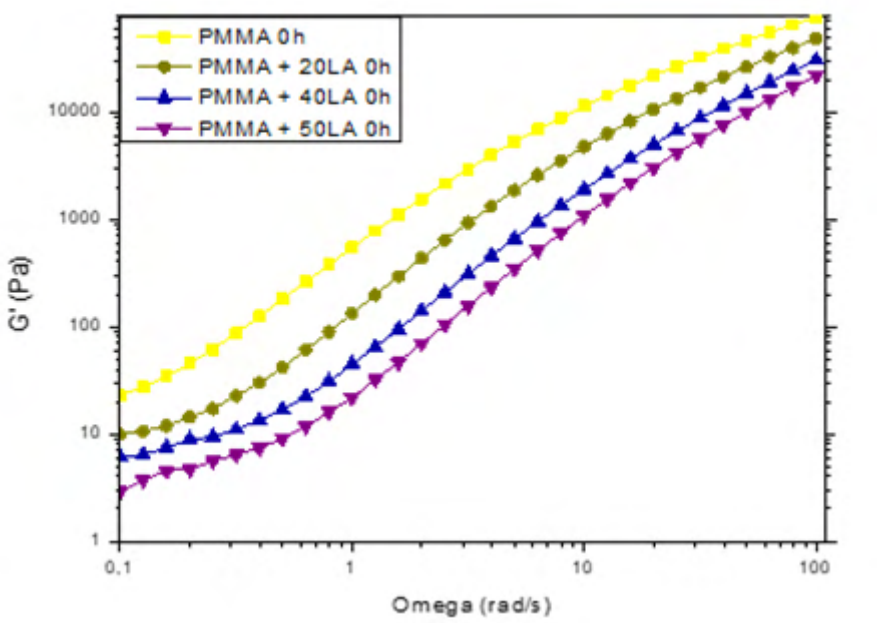

In Fig. 59 and Fig. 60 it is observed that the behaviour after 72 hours of aging is the same as the one prior to any aging.

Fig. 59: Frequency sweep of PMMA/PLA blends after 72 hours of aging showing the viscosity

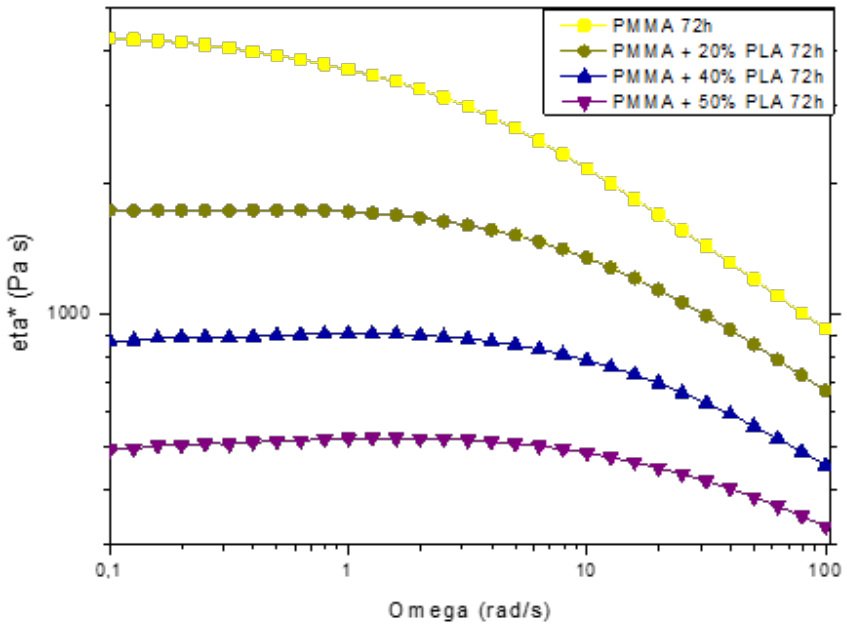

Fig. 60: Frequency sweep of 72 hours aged PMMA/PLA blends showing the storage modulus

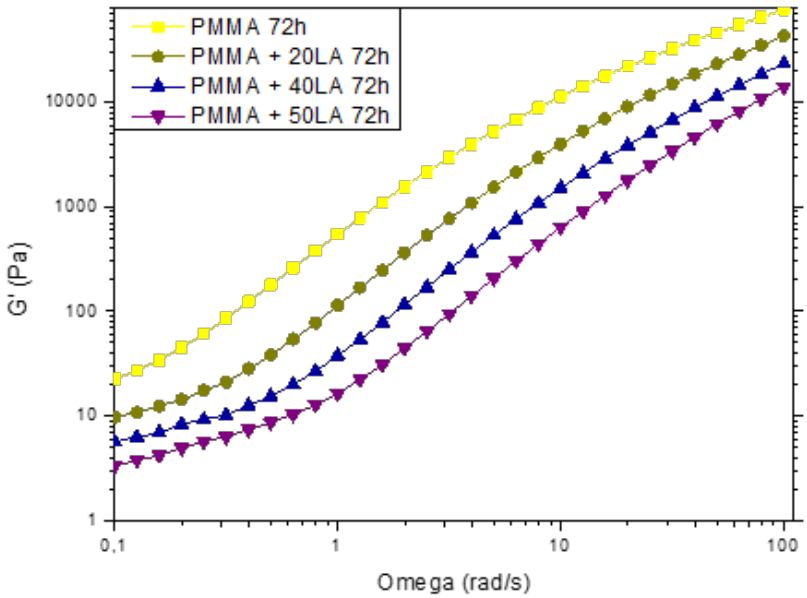

We can start seeing some comparisons for the rheological results of PMMA/PLA blends before and after aging. Starting with pure PMMA in Fig. 61 and Fig. 62. The behaviour of the viscosity curve is the same before and after aging, although there is a slight reduction which could be the result of chain scission with degradation. However, looking at the storage modulus, we can almost overlook the drop in viscosity since the curves before and after aging are coincident. This leads us to the conclusion that the PMMA remains stable and doesn't significantly degrade when aged under the conditions we have imposed.

Fig. 61: Frequency sweep of pure PMMA before and after 72 hours of aging showing the viscosity

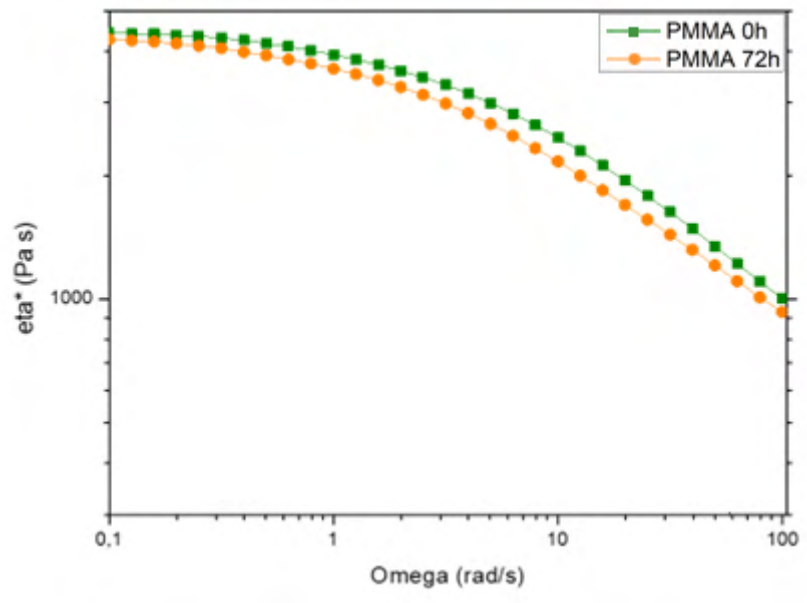

Fig. 62: Frequency sweep of pure PMMA before and after 72 hours of aging showing the storage modulus

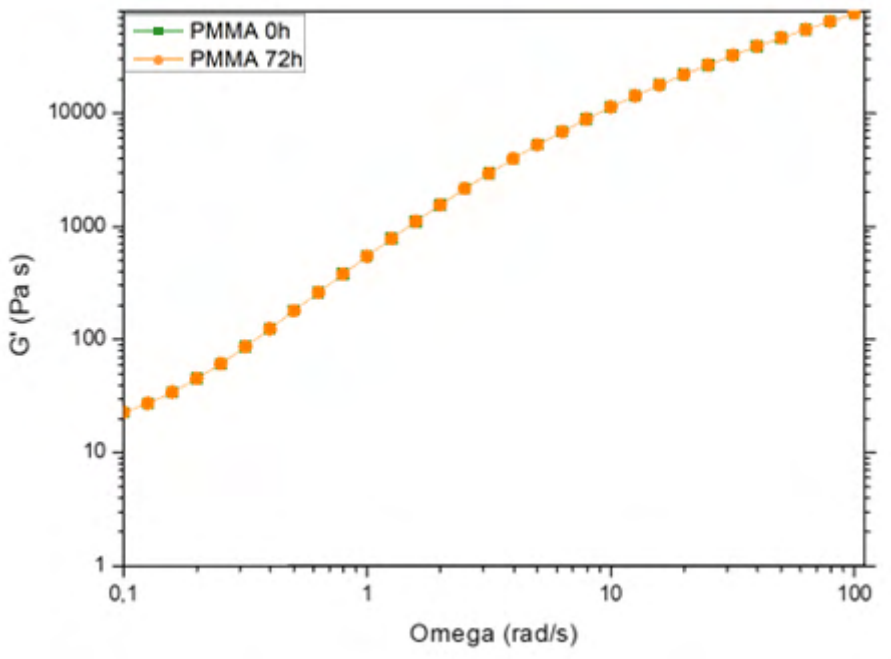

In the following figures, specifically from Fig. 63 to Fig. 68, we can confirm that the behaviour previously investigated is true for the blends with 20%, 40%, and 50% PLA even after aging. With the 80/20 blend the changes are still very small, since the PLA content which is more susceptible to degradation is still too small. With the 40% PLA blends the difference starts becoming noticeable, and the biggest difference is as expected in the 50% PLA sample. Specifically in Fig. 68, it is noted that the difference in storage modulus becomes larger at higher frequencies. This is possibly a sign of molecular weight loss from degradation, a common product of the degradation of PLA is lactic acid which could act as a plasticizer giving this result.

Fig. 63: Frequency sweep of PMMA/PLA 80/20 before and after 72 hours of aging showing the viscosity

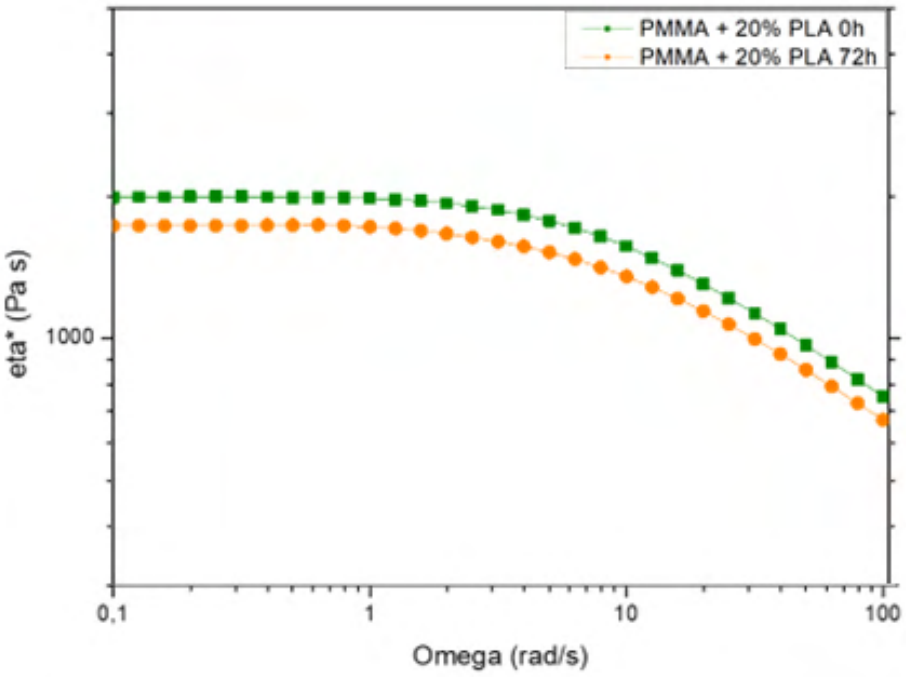

Fig. 64: Frequency sweep of PMMA/PLA 80/20 before and after 72 hours of aging showing the storage modulus

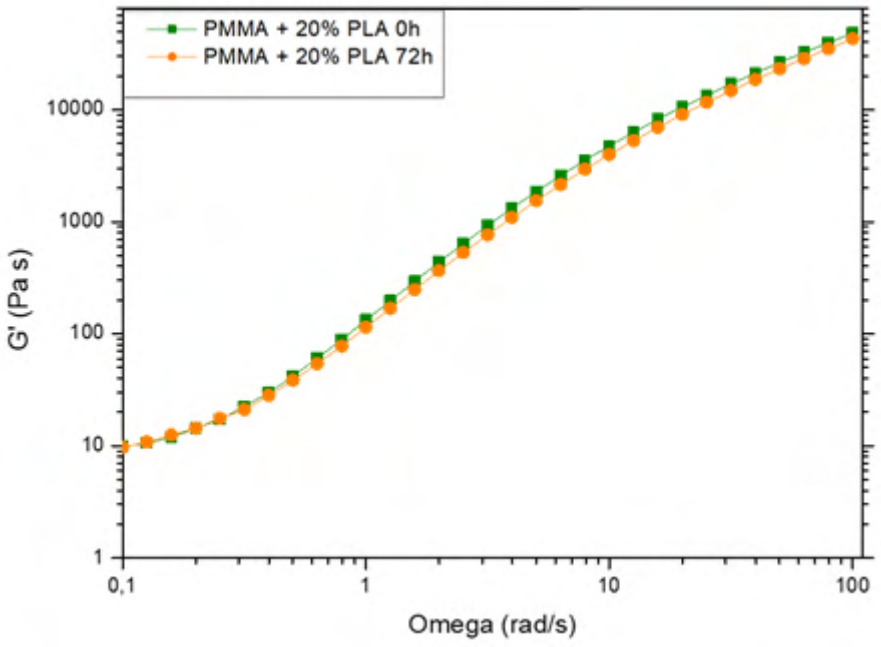

Fig. 65: Frequency sweep of PMMA/PLA 60/40 before and after 72 hours of aging showing the viscosity

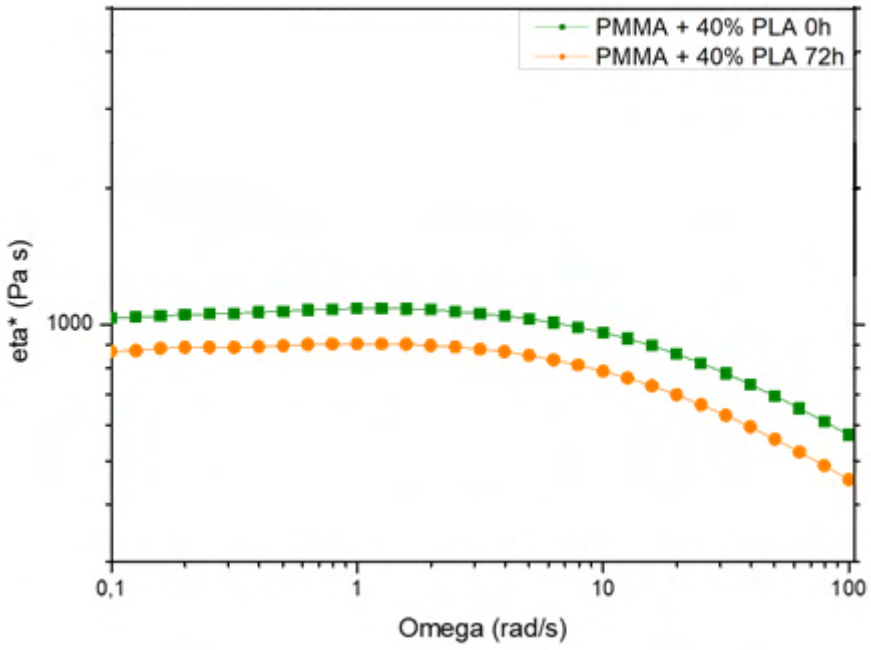

Fig. 66: Frequency sweep of PMMA/PLA 60/40 before and after 72 hours of aging showing the storage modulus

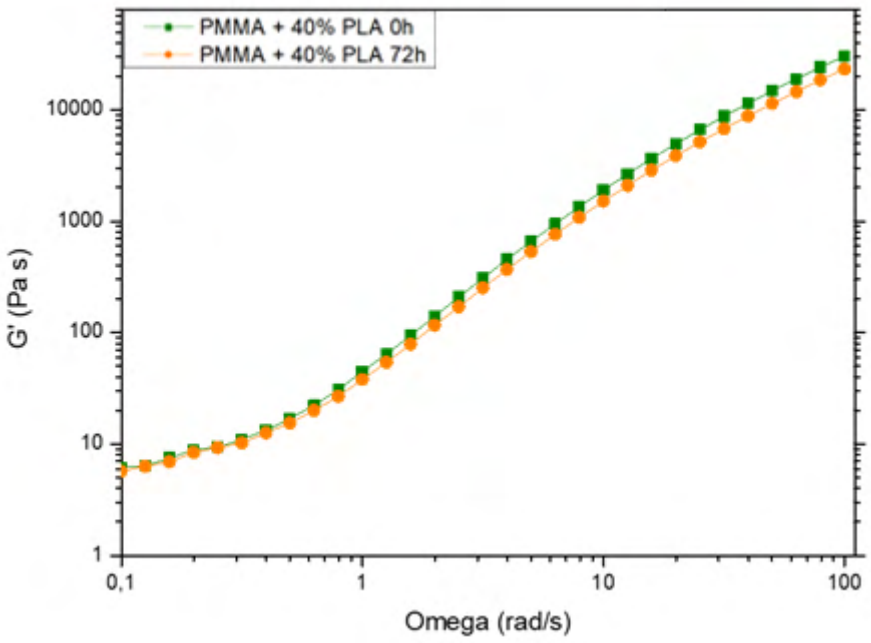

Fig. 67: Frequency sweep of PMMA/PLA 50/50 before and after 72 hours of aging showing the viscosity

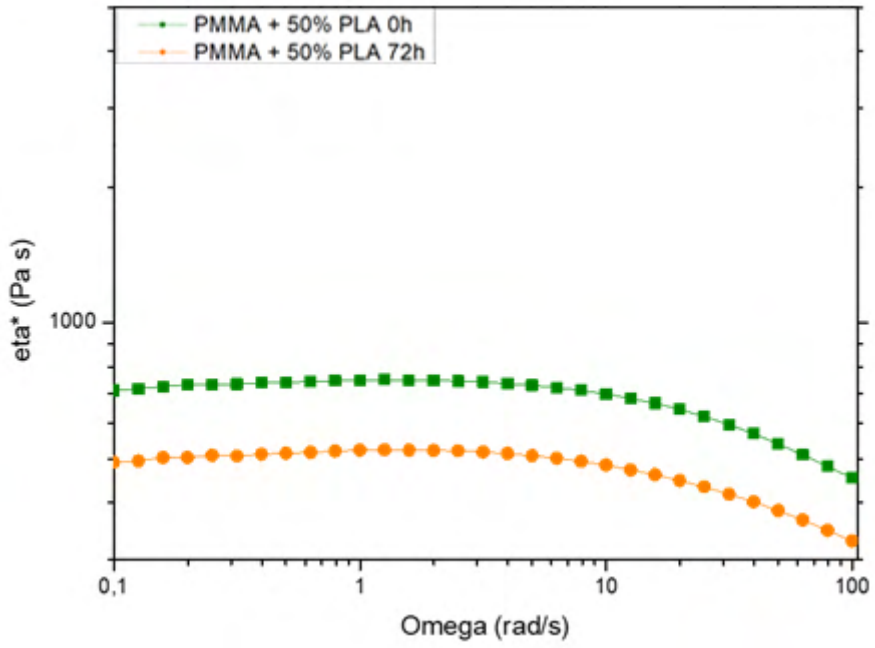

Fig. 68: Frequency sweep of PMMA/PLA 50/50 before and after 72 hours of aging showing the storage modulus

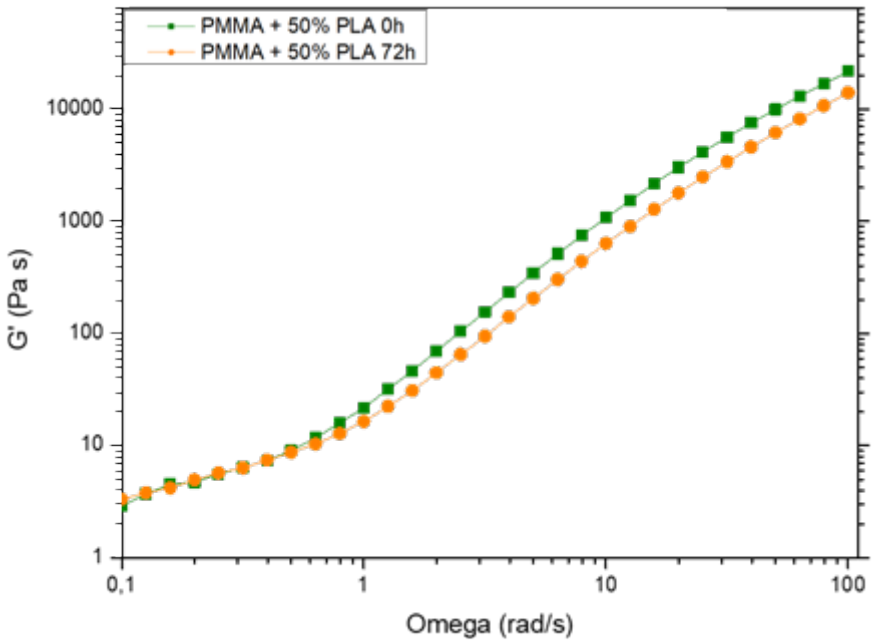

3.1.4 SEM (Scanning Electron Microscope) Images of PMMA/PLA blends

The images were taken in order to observe and investigate the miscibility of the blends further.

The results are quite consistent as shown in Fig. 69, 70, and 71. All the images are of a fragile fracture from a non-aged sample. Across all the samples for our PMMA/PLA films the two polymers proved to be miscible, and that is evident by the lack of spots which would be characteristic of non-miscible blends.

Fig. 69: SEM images of PMMA/PLA 80/20

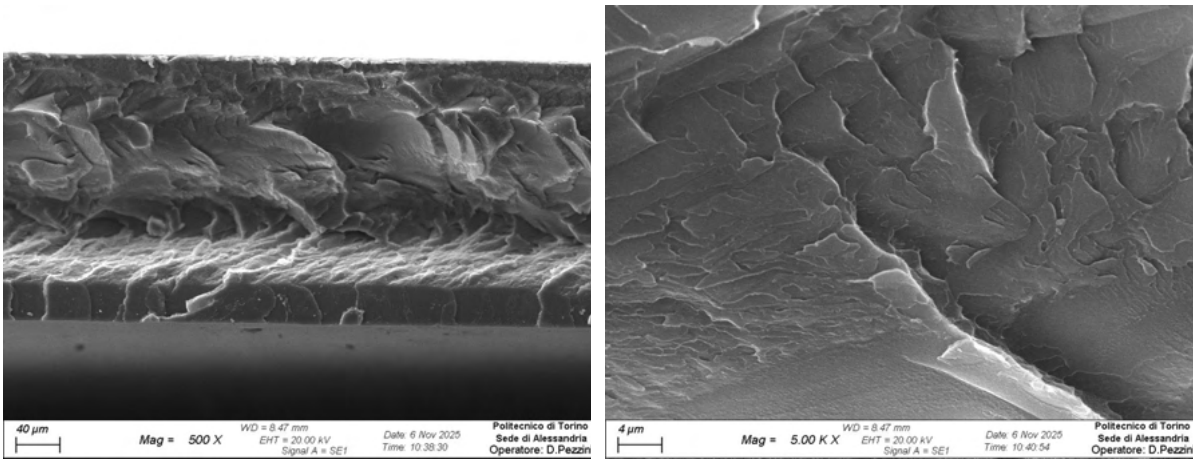

Fig. 70: SEM images of PMMA/PLA 60/40

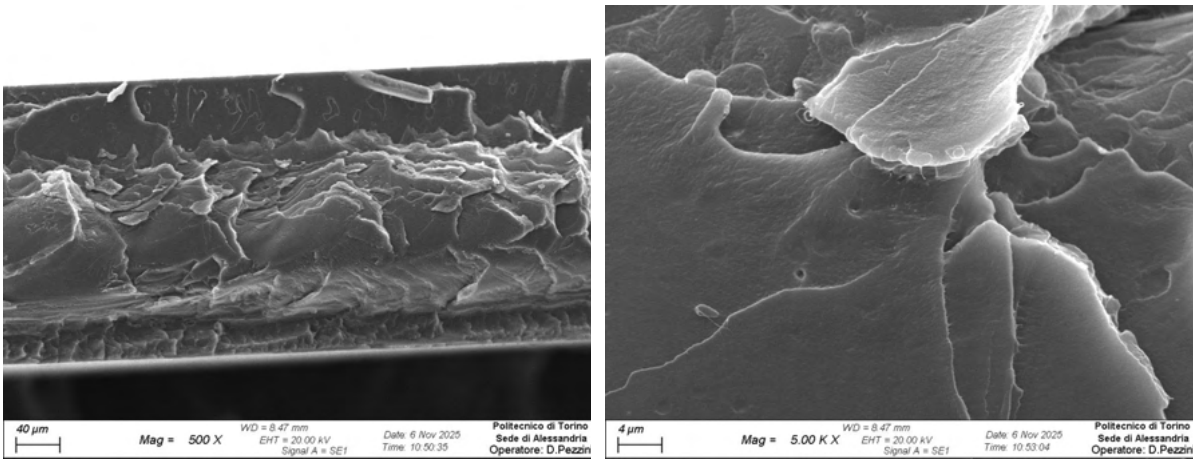

Fig. 71: SEM images of PMMA/PLA 50/50

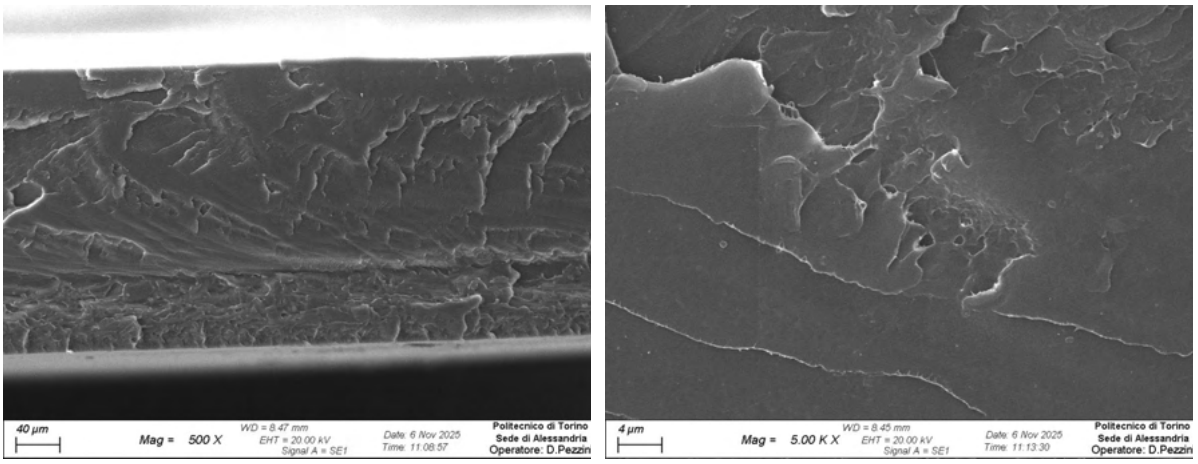

The miscibility of polymer blends is governed by the change in Gibbs free energy, $\Delta G_{mix} = \Delta H_{mix} - T\Delta S_{mix}$ with ΔH_{mix} being the enthalpic contribution and $T\Delta S_{mix}$ being the entropic contribution. If ΔG_{mix} is positive, then miscibility is not favoured, and the blend will tend to form separate phases which would appear as spots on our SEM images. In the case of PMMA/PLA the system is entropically stabilised as $T\Delta S_{mix}$ prevails over H_{mix}. Studies have shown that despite this miscibility PMMA tends to attract to PMMA while PLA attracts PLA as well. The length of the polymer chains could also have an effect, whereby longer chains could favour immiscibility as by the theory of Flory – Huggins where the mixing is inversely proportional to the degree of polymerization. PMMA/PLA blends also exhibited so called co-continuous phases. Which is a non-equilibrium morphology that is generated during mixing. The blend can remain co-continuous if cooled quickly. This miscibility is what conveyed the ductility seen in the PMMA/PLA 50/50 sample for example, but since it is highly governed by interfacial bonds between the two polymers when irradiated and PLA degrades, those bonds weaken or disappear causing the drop in deformation. [29, 35, 36, 37]

3.1.5 UV-Vis Transparency Tests

Figures 72 to 75 show the results obtained from the spectrophotometer in the range of 350 nm to 800 nm. Each figure represents a certain blend composition, and we can observe consistent behaviour within each blend. All the blends showed an increase in absorbance in the visible range (380 nm to 700 nm), thus, a decrease in transparency with aging. All samples however, showed a sudden increase at around 325 nm when approaching the UV range. A slight exception was observed for the PMMA/PLA 80/20 blend in Fig. 73, the differences with aging however remained marginal. The PMMA/PLA 50/50 blends also exhibited different behaviour with respect to the other blends as seen in Fig. 75, the results here showed a linear increase in absorbance with a decreasing wavelength in the visible range.

These results are also in accordance with the study of El Teoh and WS Chow, where they found that at the same wavelength pure PMMA and PLA showed a similar degree of visible light transmittance. However, PMMA possesses higher resistance against UV light, due to its low UV light absorption. That is because the photosensitive chromophores that activate

photooxidation in aliphatic polymers are not present in PMMA. These properties are the same ones that make PMMA suitable for outdoor use. [38]

Fig. 72: Results of absorbance with respect to wavelength for pure PMMA

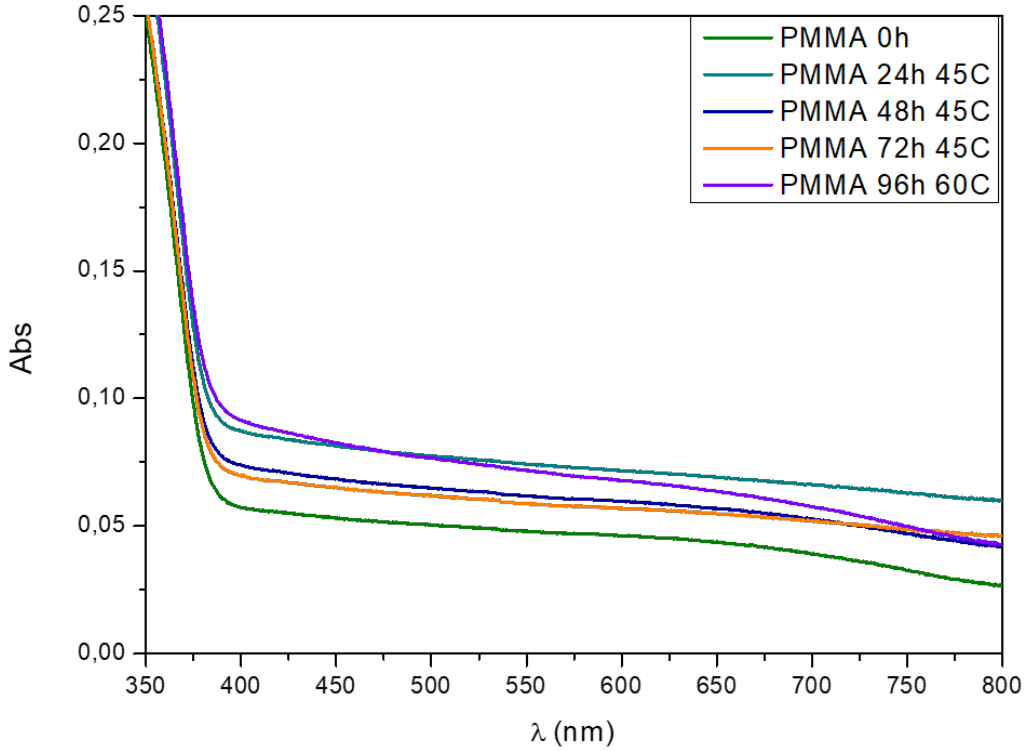

Fig. 73: Results of absorbance with respect to wavelength for PMMA/PLA 80/20

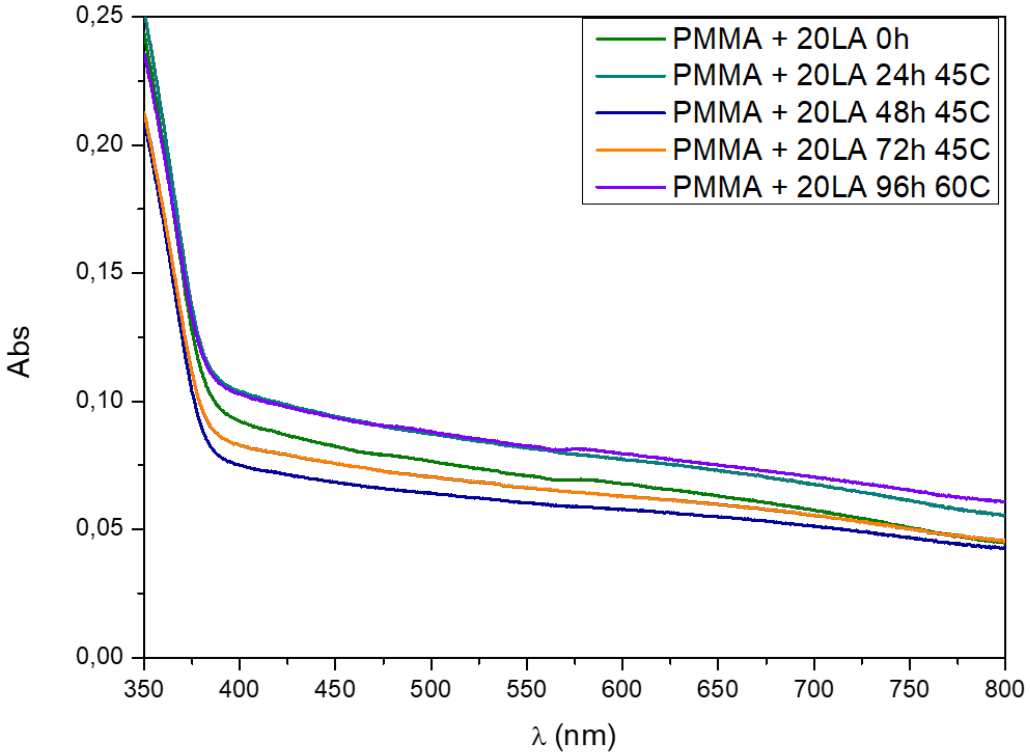

Fig. 74: Results of absorbance with respect to wavelength for PMMA/PLA 60/40

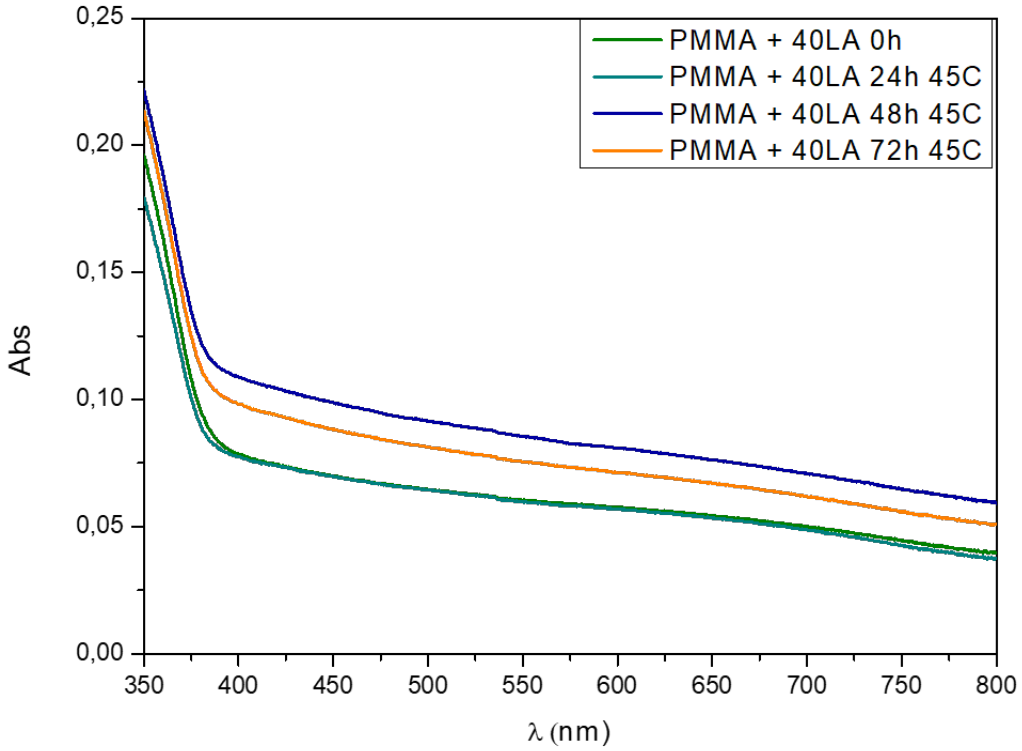

Fig. 75: Results of absorbance with respect to wavelength for PMMA/PLA 50/50

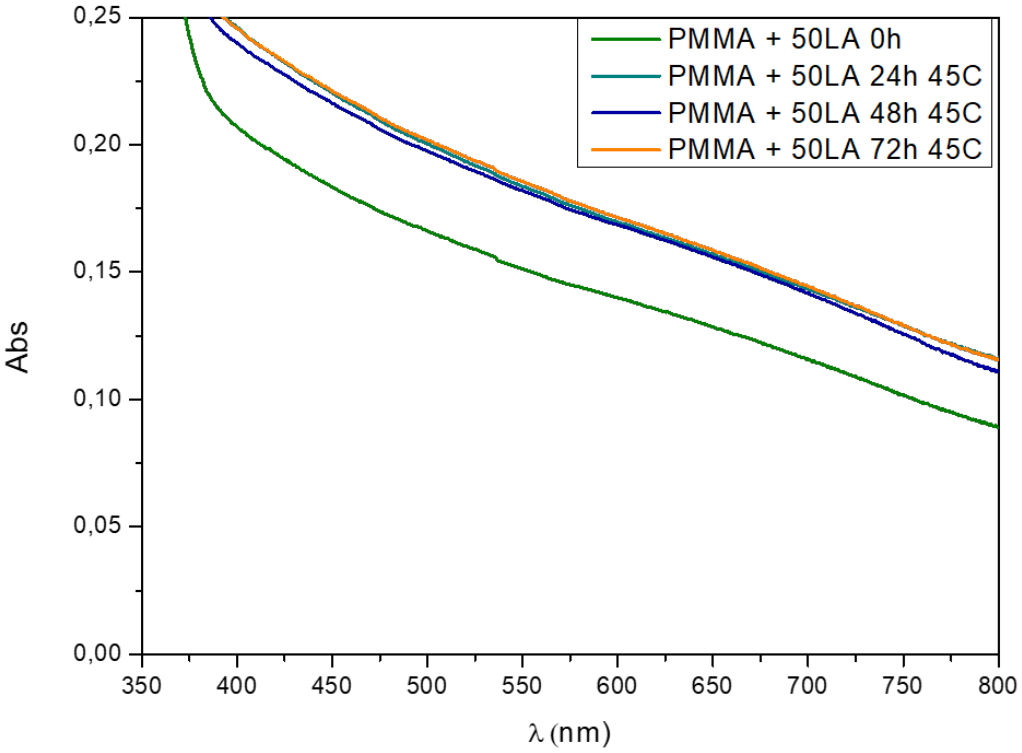

These results suggested that PLA lowers the UV protection properties of PMMA. This is because, despite the fact PLA has great optical properties and high transmission in the amorphous phase, when exposed to temperatures around 55 °C (wich is close to the 45 °C UV aging was conducted at), PLA started to crystallise which increased haze and reduced transparency. This is also consistent with our results from the 50/50 samples that were aged for 96 hours at 60 °C, they became coiled and also had a more visible yellow tinge to the film. [39]

3.2 Tests on PET/PLA

3.2.1 Mechanical Tests on PET/PLA Samples

3.2.1.1 Mechanical Tests of PET/PLA Samples at Time 0

As previously stated, time 0 refers to the samples and film straight after extrusion, and before any aging cycles. In the coming figures we will find again the Young's Modulus reported in MPa, and deformation given as a percentage.

These PET/PLA samples were less troublesome when setting them up for the mechanical tests compared to the PMMA/PLA samples previously tested. That is because it was possible for the PET/PLA samples to be prepared using the die cutter, thus the dimensions were consistent. In addition to that, the samples weren't as curved, so no further correction was applied to the results obtained from the stress – strain curves.

In Fig. 76 below, an instant improvement of the Young's Modulus with the addition of PLA was observed. The maximum in this case was for the blend with 40% PLA, however, the values started diminishing for 50% PLA.

Fig. 76: Bar graph of PET/PLA blends' Young's Modulus at time 0

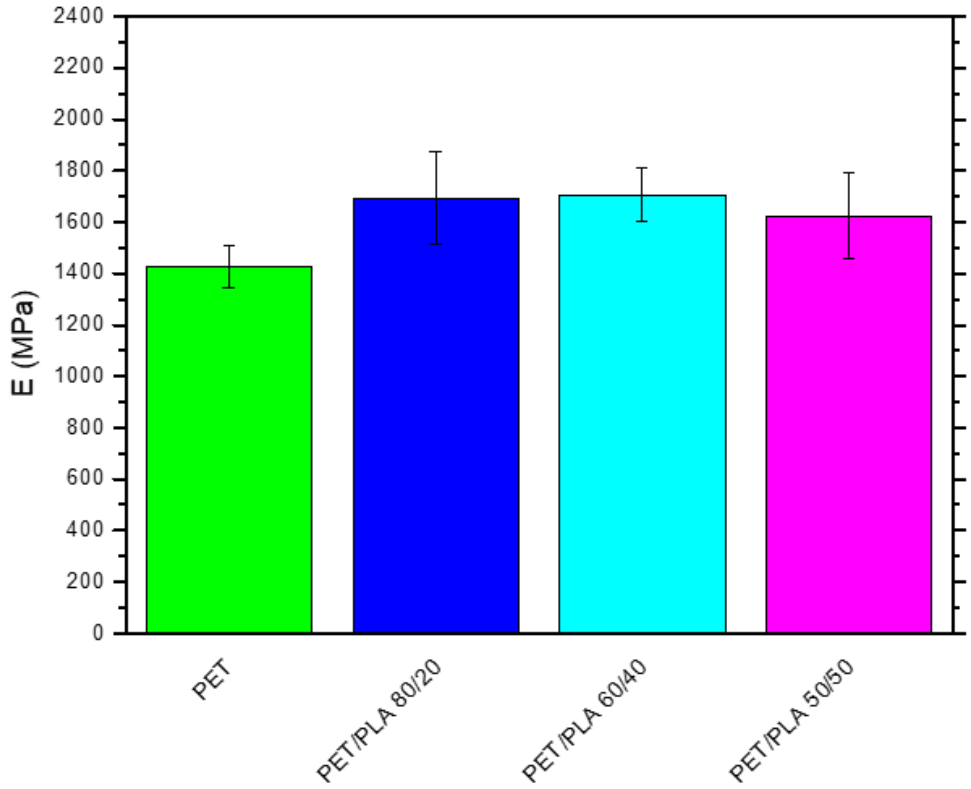

However, observing Fig. 77 we can see that the improvement seen for Young's Modulus was not observed for the deformation. In fact, the average deformation of the blends was at a minimum for the blend with 50% PLA. This difference was not readily perceptible by touch.

Fig. 77: Bar graph of PET/PLA blends' deformation at time 0

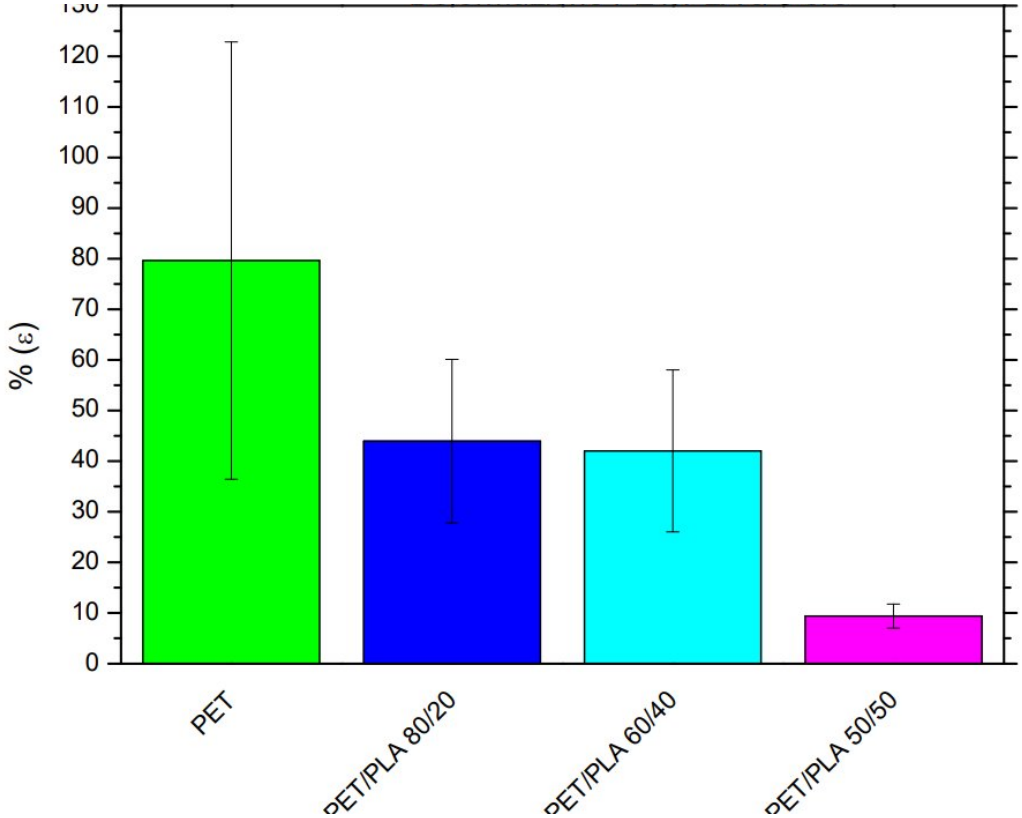

All samples were sufficiently malleable so as to create coils of film. The behaviour of the blends under the die cutter was also similar.

3.2.1.2 Mechanical Tests of PET/PLA Samples at Time 96 hours

Aging was done in 12 hours cycles divided into 8 hours of UV radiation at 340 nm (same as the radiation the PMMA/PLA samples were subject to) and 60 °C, followed by 4 hours of condensation at 40 °C.

Following the aging process ductility was maintained in the samples tested, and as we can see in Fig. 78 below, we can still see the necking that happened before the rupture of the film. This behaviour is characteristic of ductile materials.

Fig. 78: Pure PET film aged for 96 hours at 60 °C

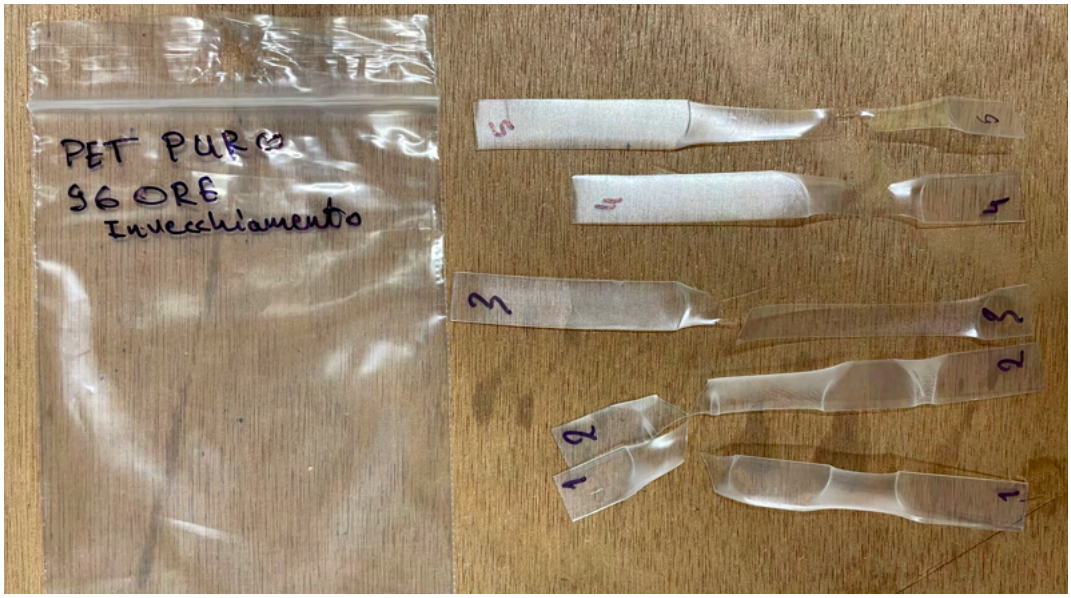

After the addition of 20% PLA, the main issue that was observed was the difficulty of the clamps in gripping the films as seen in the third sample in Fig. 79 below. Although some ductile behaviour remains observable, it is significantly reduced, as evidenced by the much shorter necking region.

Fig. 79: Pure PET/PLA 80/20 film aged for 96 hours at 60 °C

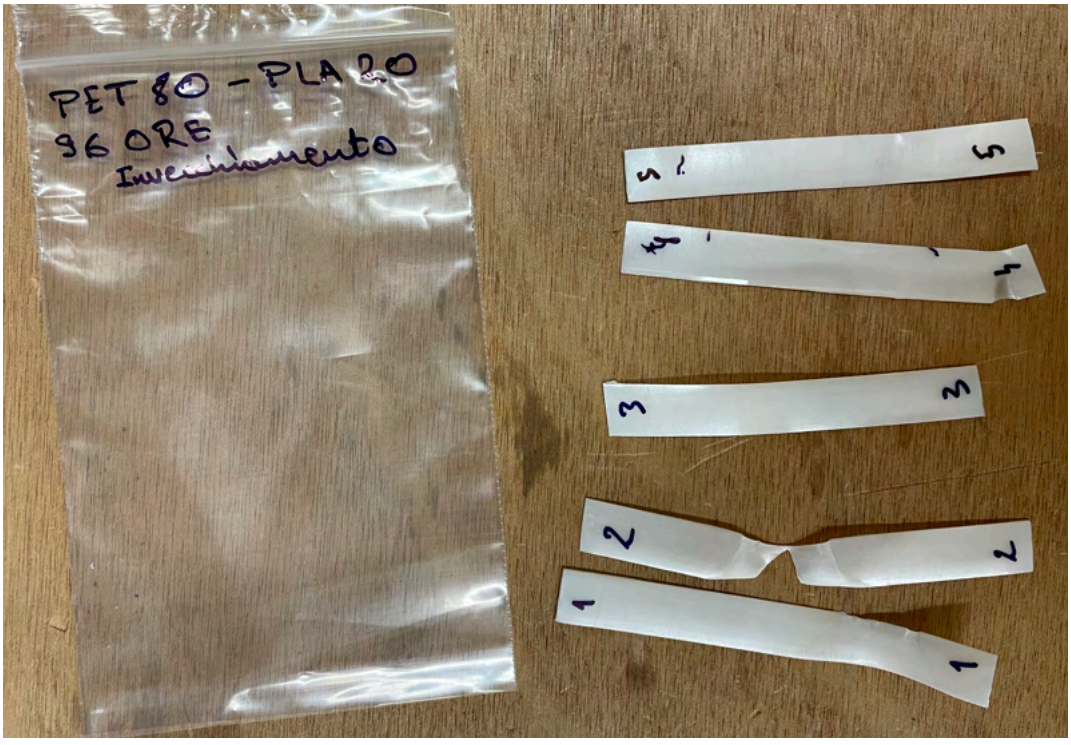

In the PET/PLA 60/40 samples in Fig. 80 below we can observe the disappearance of the necking phenomenon and thus, the ductile behaviour previously observed. Another particular

phenomenon did start appearing here which is the appearance of fibre-like strands upon the rupture of the sample.

Fig. 80: Pure PET/PLA 60/40 film aged for 96 hours at 60 °C

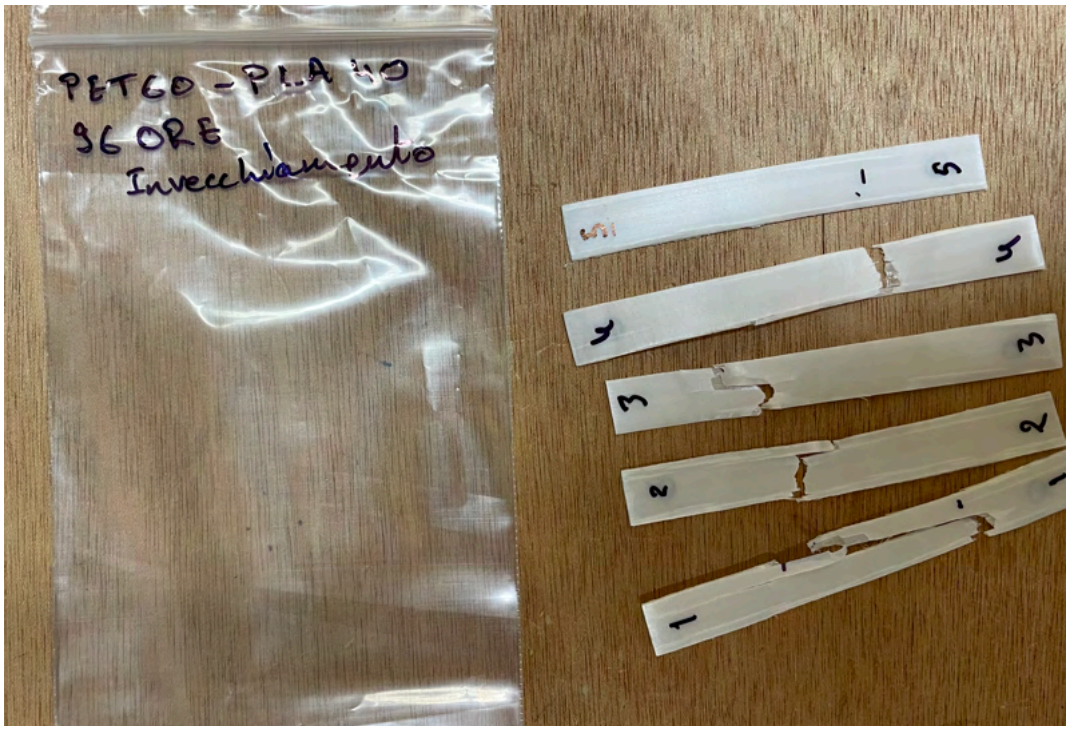

In Fig. 81 we see the behaviour of the PET/PLA 50/50 samples. Again, we see the brittle behaviour previously observed.

Fig. 81: Pure PET/PLA 50/50 film aged for 96 hours at 60 °C

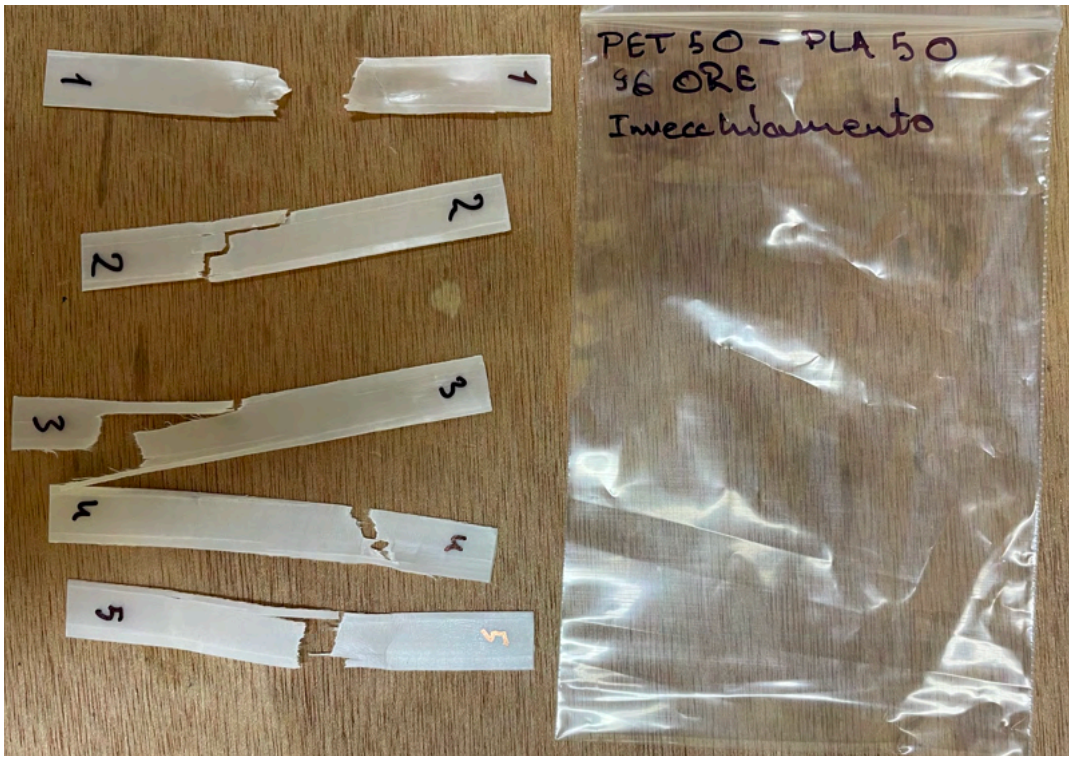

The samples continued to exhibit the same general trends seen for the non-aged samples. As observed in Fig. 82 and Fig. 83 below, the Young's modulus in this case though kept increasing and didn't just peak at the 60/40 blend.

Fig. 82: Average Young's Modulus of PET/PLA blends that were aged for 96 hours at 60 °C

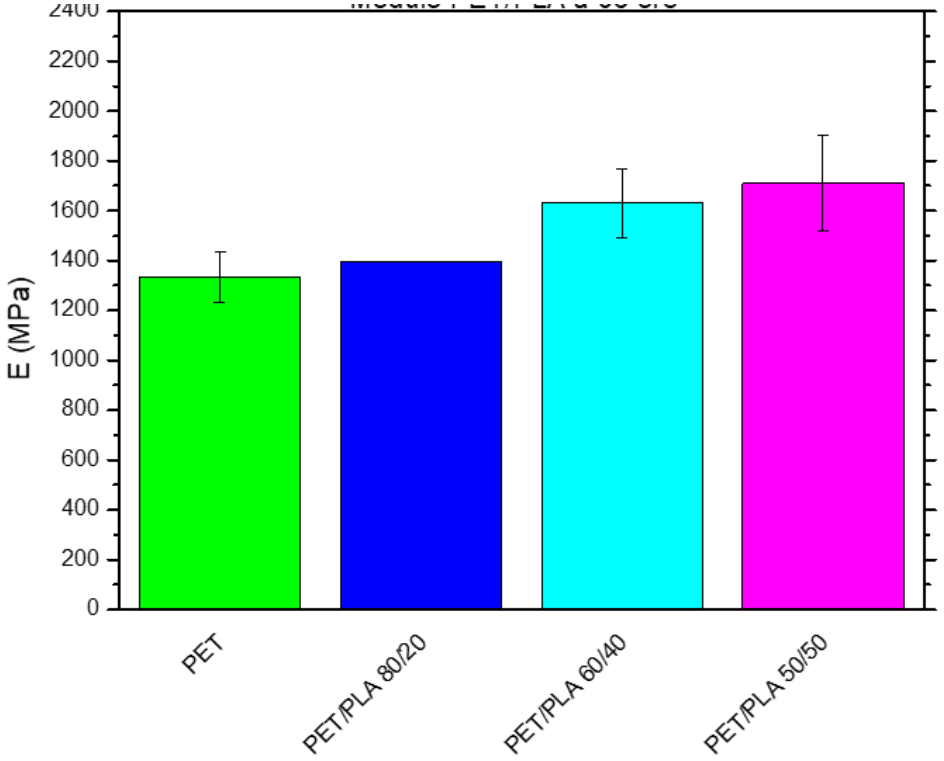

Fig. 83: Average deformation of PET/PLA blends that were aged for 96 hours at 60 °C

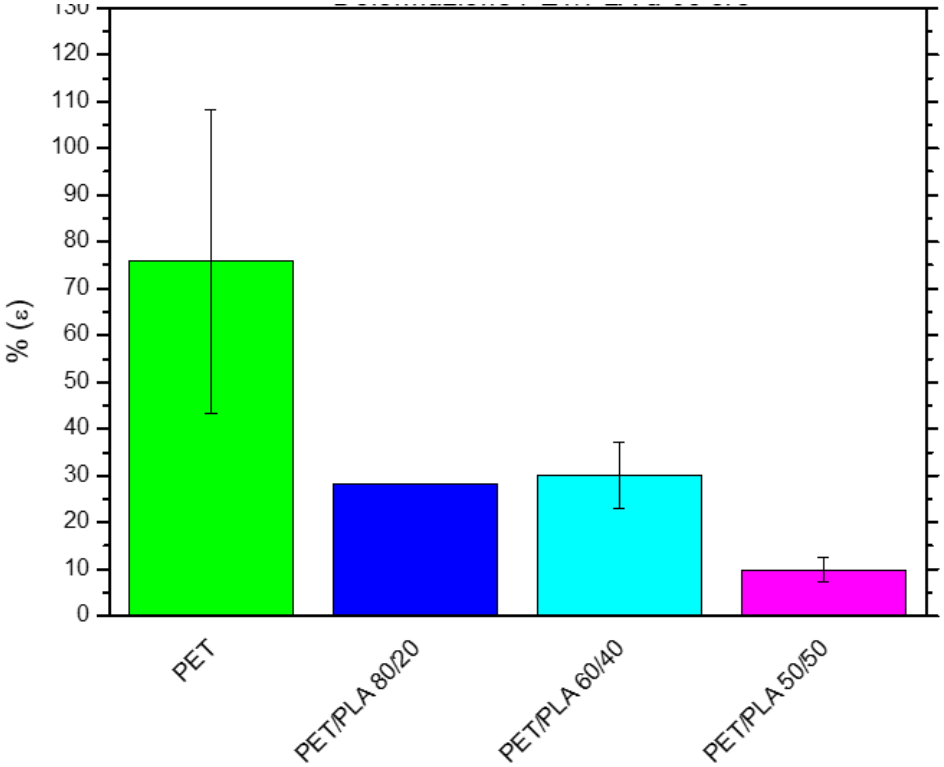

3.2.1.3 Mechanical Tests of PET/PLA Samples at Time 168 hours

Aging was done using the same 12 hours cycles as the 96 hours aged samples. With 8 hours of radiation and 4 hours of condensation, at 60 °C and 40 °C.

After 168 hours of aging even pure PET became visibly less ductile, as can be seen in Fig. 84 below with some samples exhibiting no necking at all.

Fig. 84: Pure PET film aged for 168 hours at 60 °C

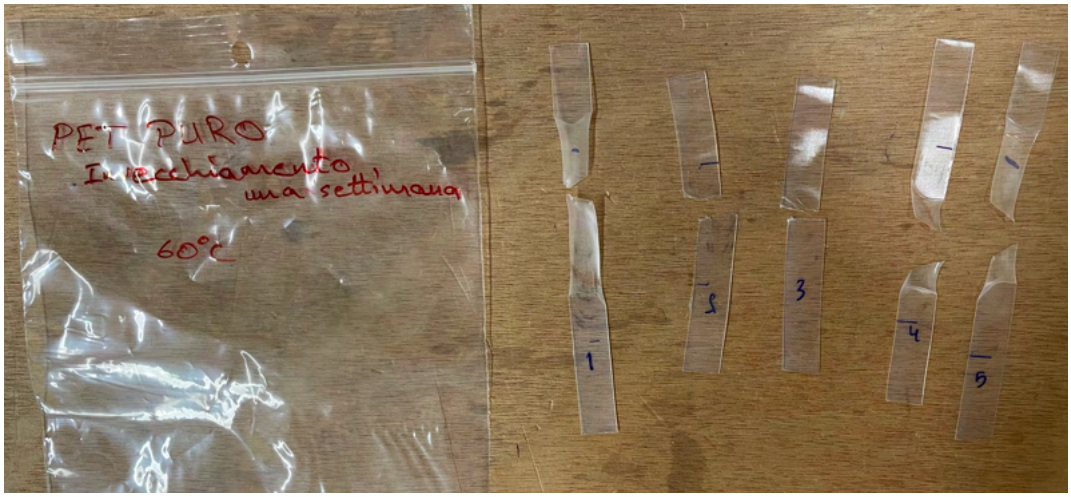

In Fig. 85, it was observed that the ductile behaviour in the case of the addition of 20% PLA was still observed after 168 hours of aging. As evident by the necking that was present in all the ruptured samples.

Fig. 85: PET/PLA 80/20 film aged for 168 hours at 60 °C

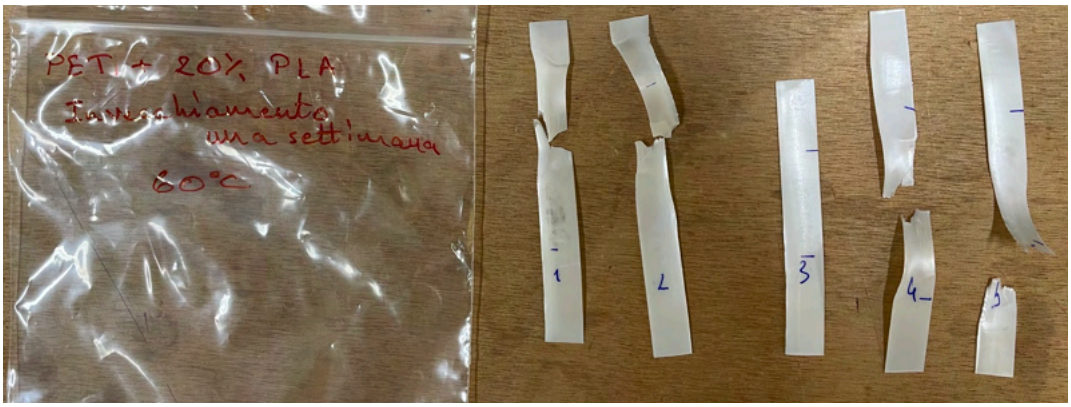

A return to more brittle behaviour was seen with the addition of 40% PLA. Fig. 86 below shows the brittle fractures and the fibre like phenomenon forming again, alongside an apparent separation of layers in the film.

Fig. 86: PET/PLA 60/40 film aged for 168 hours at 60 °C

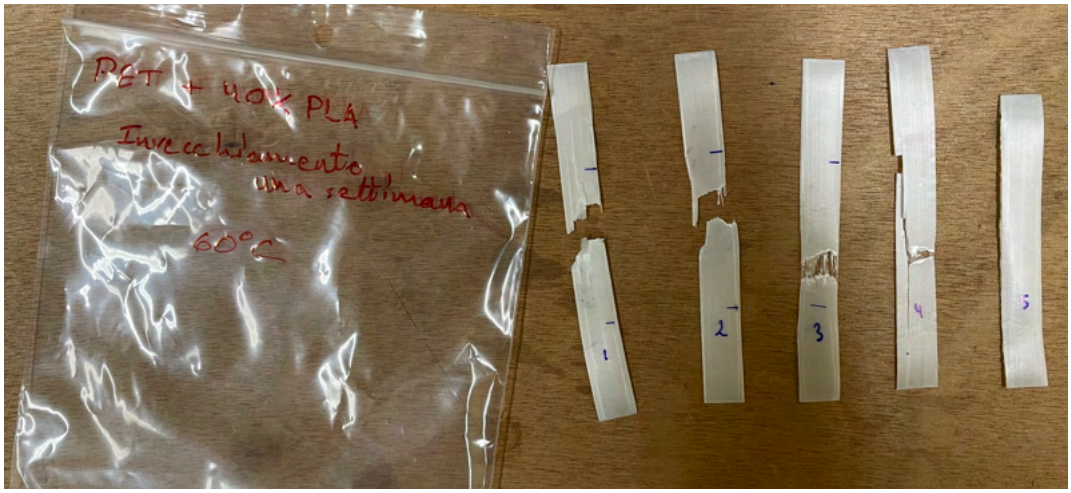

Similar to the previous blend of 60/40, after the addition of 50% PLA brittle behaviour was still observed, as seen in Fig. 87.

Fig. 87: PET/PLA 50/50 film aged for 168 hours at 60 °C

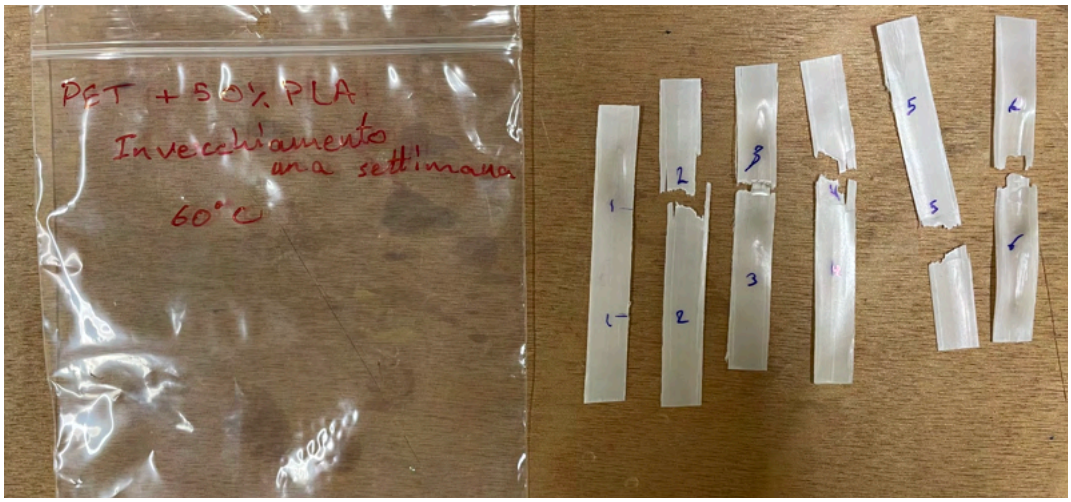

After 168 hours of aging the trend of the Young's Modulus became somewhat irregular. However, the main point of difference seen in Fig. 88 with respect to the trends observed in Fig. 76 and Fig. 82 for the non-aged and 96 hours aged PET/PLA samples was the drop in Young's modulus after the addition of 50% PLA. Another big difference was observed in Fig. 89 for deformation, where after 168 hours of aging the change in deformation after adding 40% PLA was less notable.

Fig. 88: Average Young's Modulus of PET/PLA blends that were aged for 168 hours at 60 °C

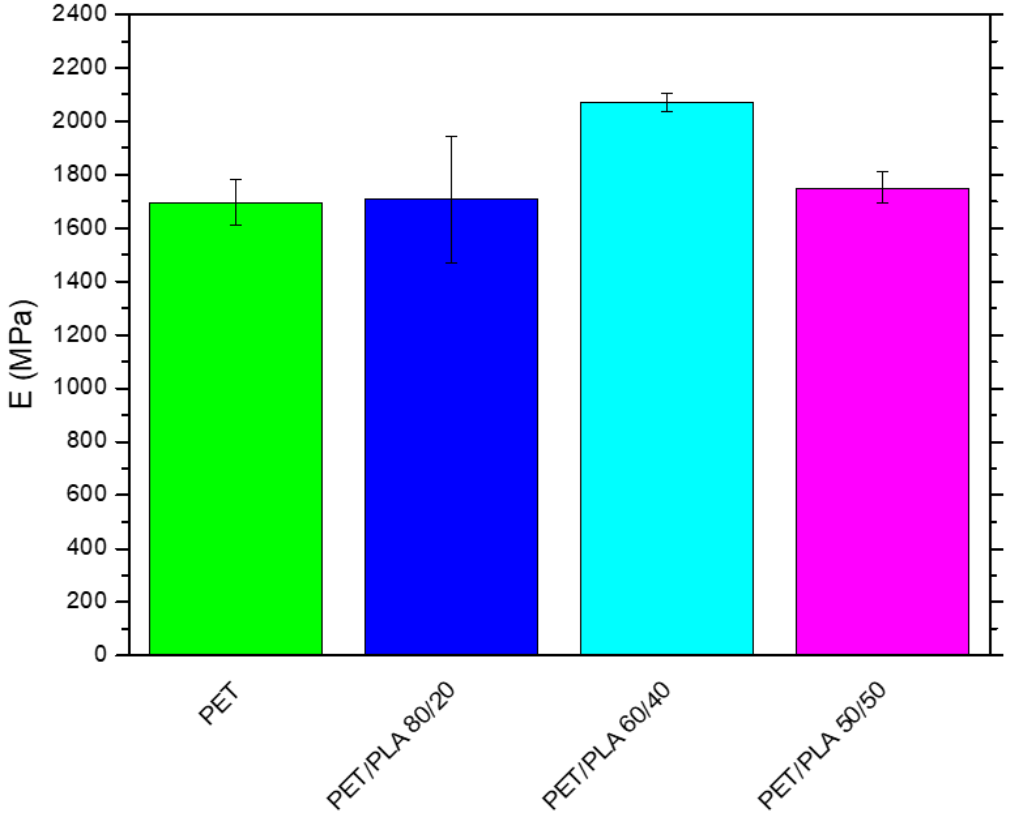

Fig. 89: Average deformation of PET/PLA blends that were aged for 168 hours at 60 °C

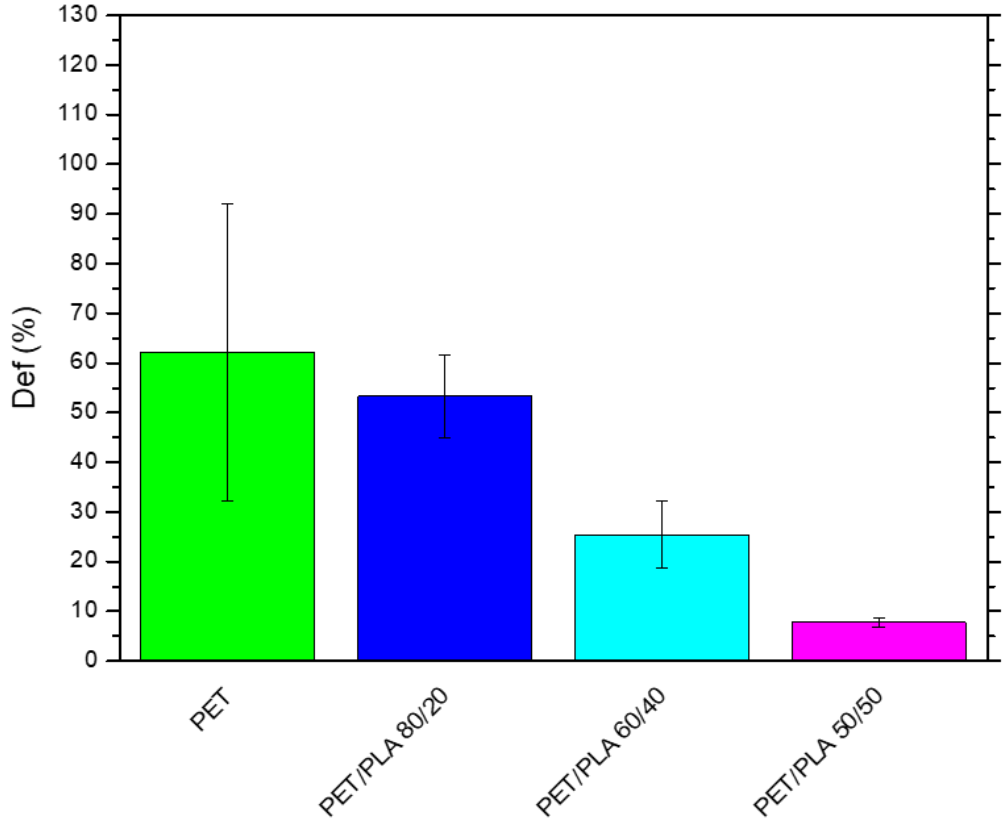

3.2.1.4 Summary of Results and Comments on PET/PLA Films

In the following Table. all the numerical values for the mechanical test are shown. In bold are the maximum values obtained for the Young's modulus and deformation.

Table. 6 Results of the mechanical tests

	Young's Modulus (MPa)	Deformation (%)
PET 0h	1426	**80**
PET/ PLA 80/20 0h	1693	44
PET/PLA 60/40 0h	1707	42
PET/PLA 50/50 0h	1625	9
PET 96h	1335	76
PET/PLA 80/20 96h	1393	28
PET/PLA 60/40 96h	1632	30
PET/PLA 50/50 96h	**1711**	10
PET 168h	1612	40
PET/PLA 80/20 168h	1459	53
PET/PLA 60/40 168h	1677	27
PET/PLA 50/50 168h	1101	9

The Young's modulus of PET generally increases with the aging process as seen in Fig. 90 below.

Fig. 90: Average Young's Modulus evolution of PET with aging

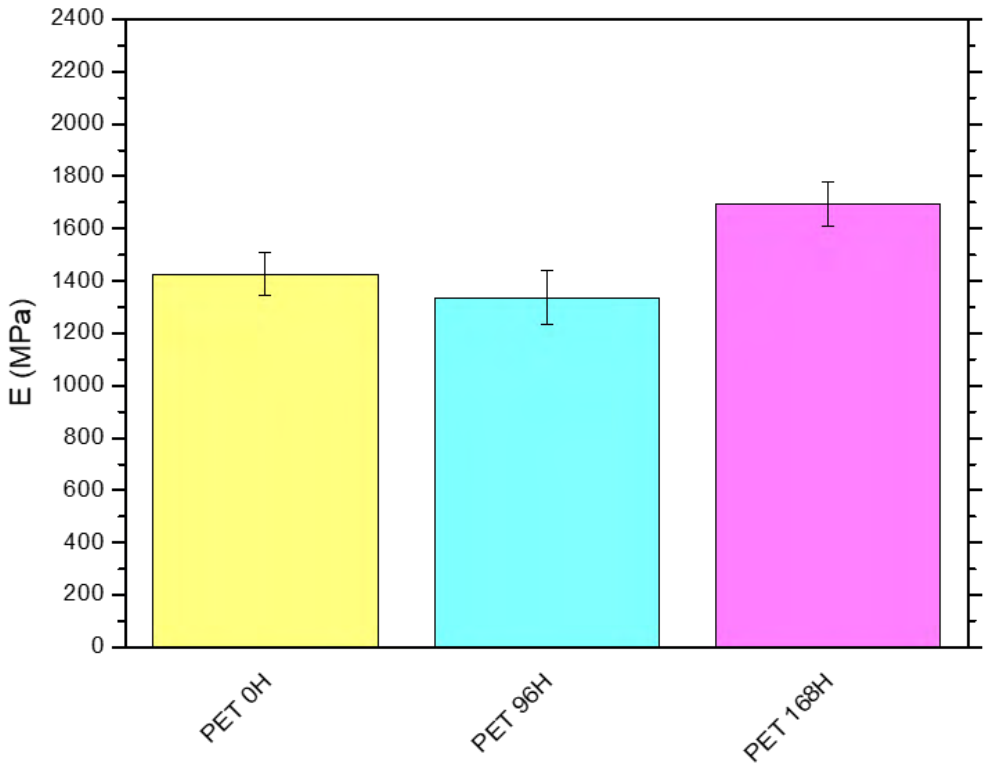

Opposite to the trend of Young's Modulus PET lost deformation as the aging progresses, as seen in Fig. 91. This phenomenon is very common among pure plastic materials.

Fig. 91: Average deformation evolution of PET with aging

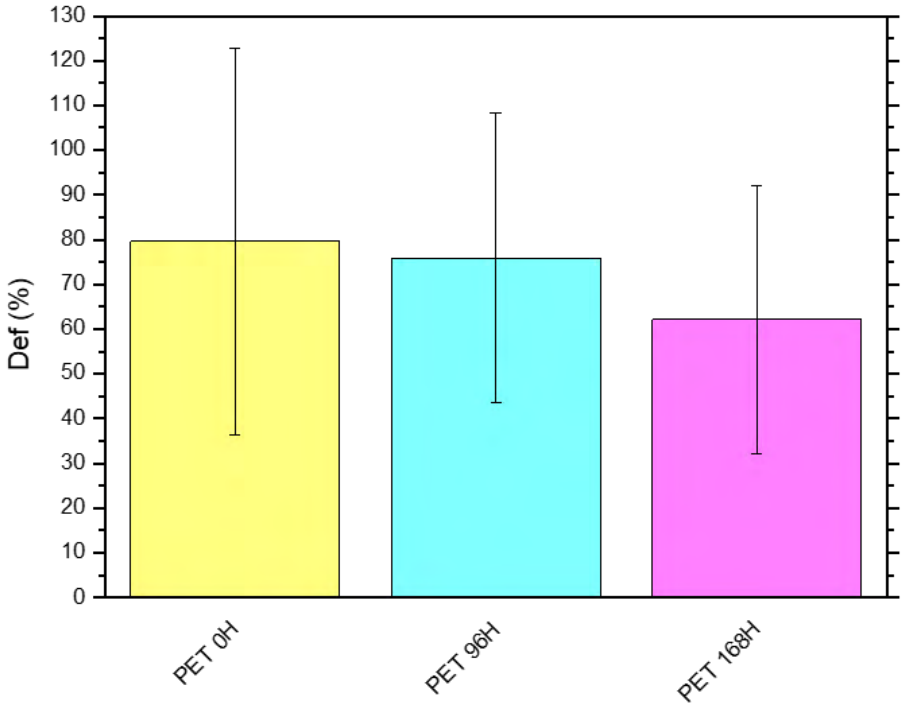

The same trend seen for the pure PET can be seen again for the PET blend with 20% PLA in Fig. 92.

Fig. 92: Average Young's Modulus evolution of PET/PLA 80/20 with aging

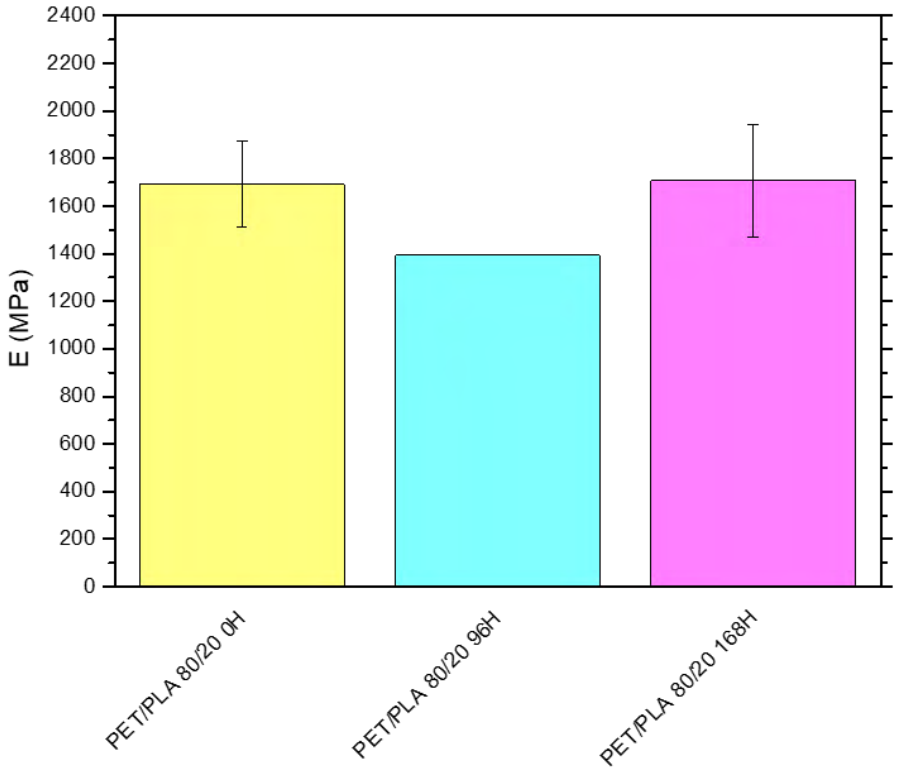

After the addition 20% PLA to the PET, a relative maintainment of the deformation evident in Fig. 93 was obtained.

Fig. 93: Average deformation evolution of PET/PLA 80/20 with aging

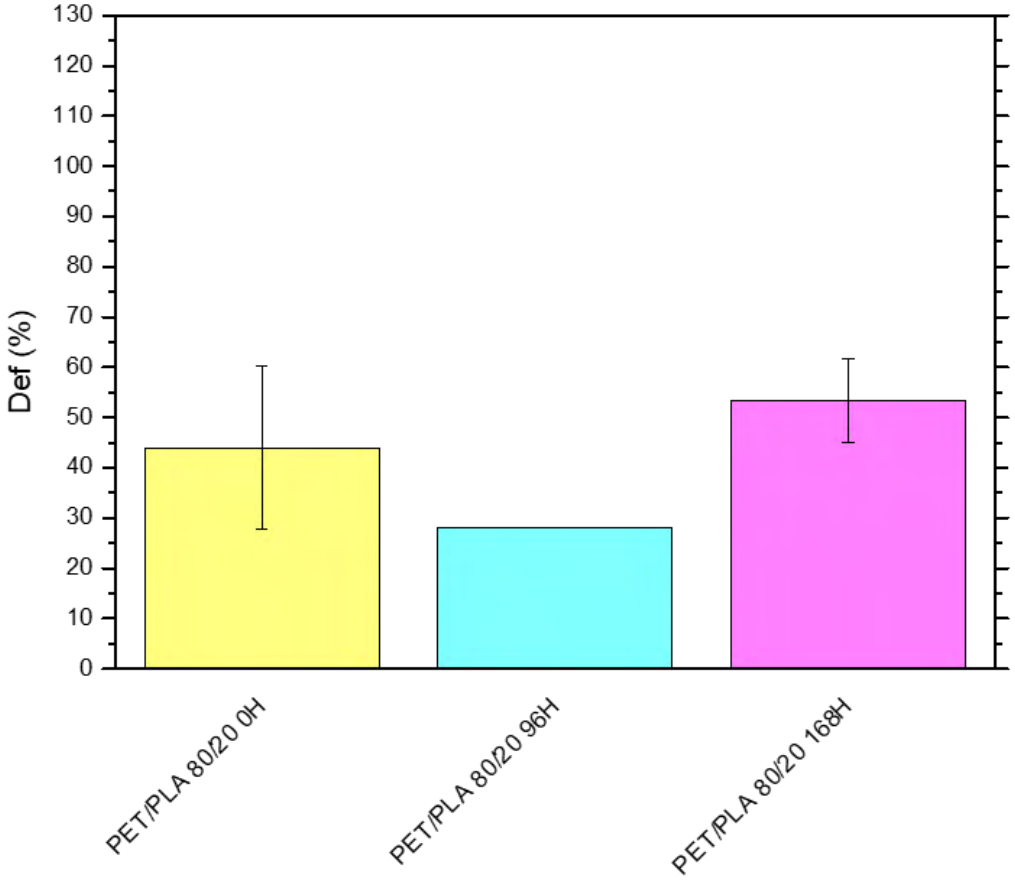

The trend of Young's Modulus remained similar even after the addition of 40% PLA. In Fig. 94 below a lesser reduction of the modulus was observed after 96 hours, but a more notable increase was evident after 168 hours.

Fig. 94: Average Young's Modulus evolution of PET/PLA 60/40 with aging

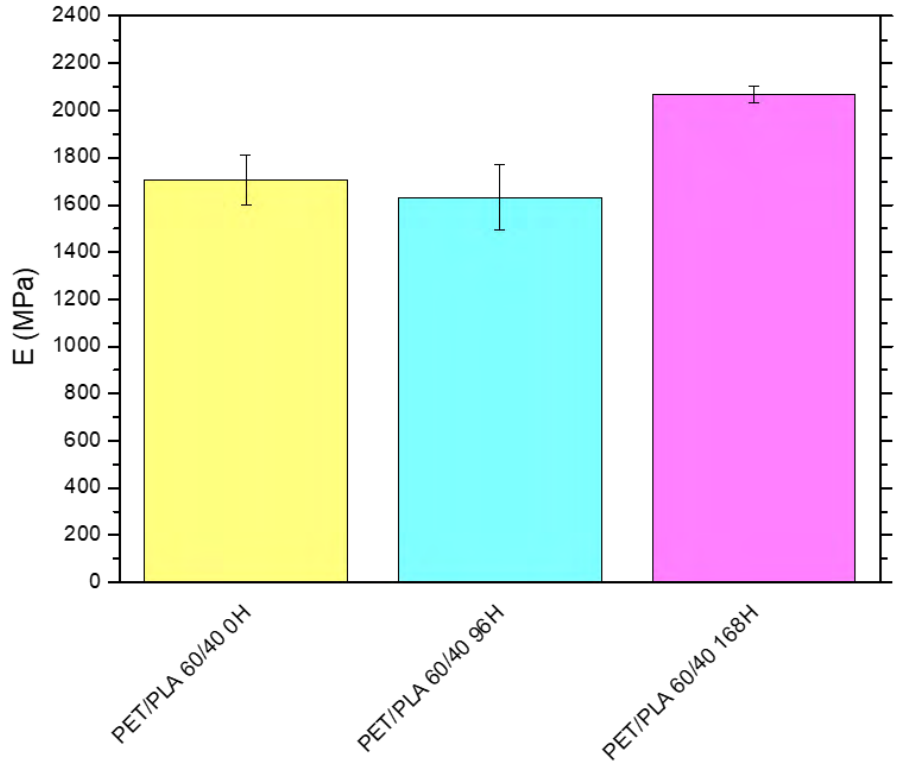

In Fig. 95 below while the usual trend for reducing deformation continues, unlike the previous case of PET/PLA 80/20 where an improvement was observed again after 168 hours, here only reduction was observed.

Fig. 95: Average deformation evolution of PET/PLA 60/40 with aging

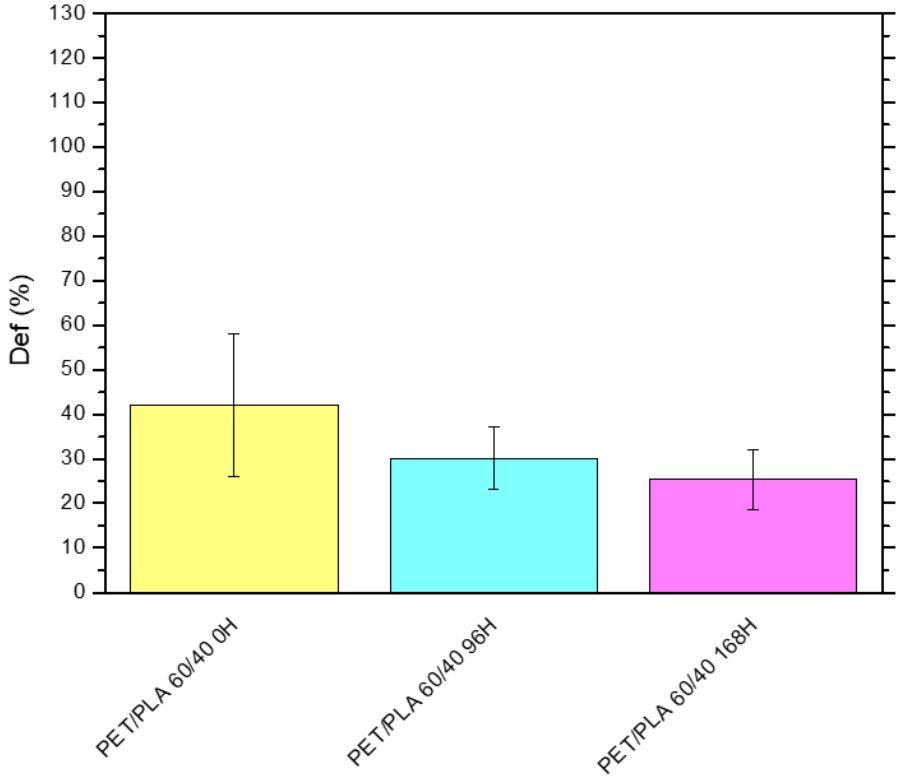

In Fig. 96 below, it can be observed that after the addition of 50% PLA, a continuous albeit slight improvement can be seen after each aging process.

Fig. 96: Average Young's Modulus evolution of PET/PLA 50/50 with aging

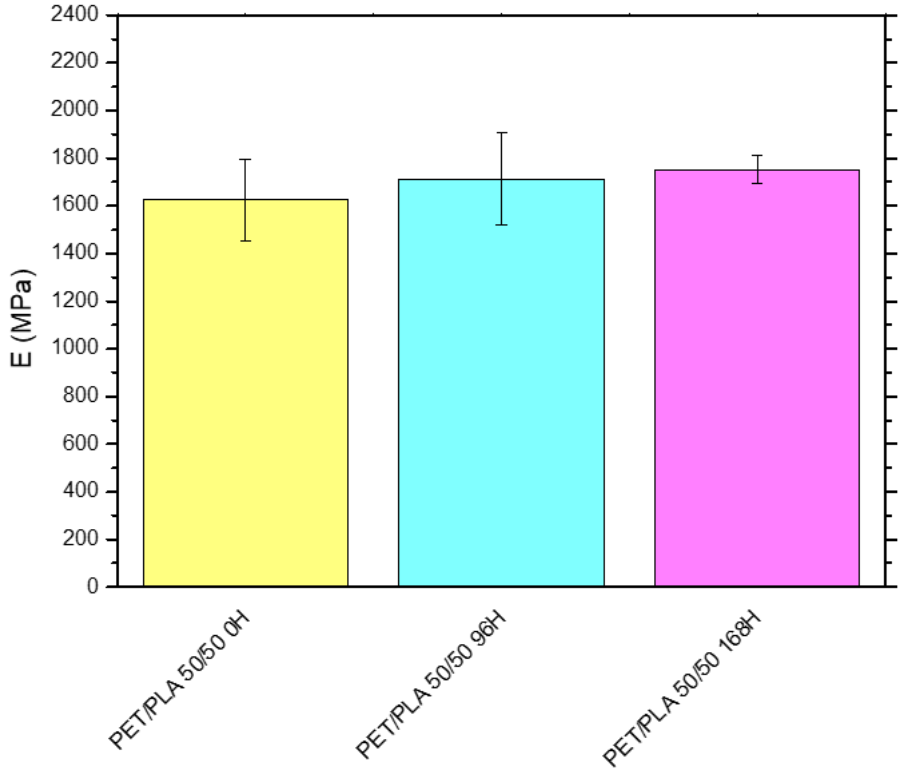

As is evident by Fig. 97 below, and the results in section 3.2.1.3 previously discussed, there was a big reduction in the deformation after adding 50% PLA even in time 0. However, it must be noted that the deformation was maintained quiet well with aging.

Fig. 97: Average deformation evolution of PET/PLA 50/50 with aging

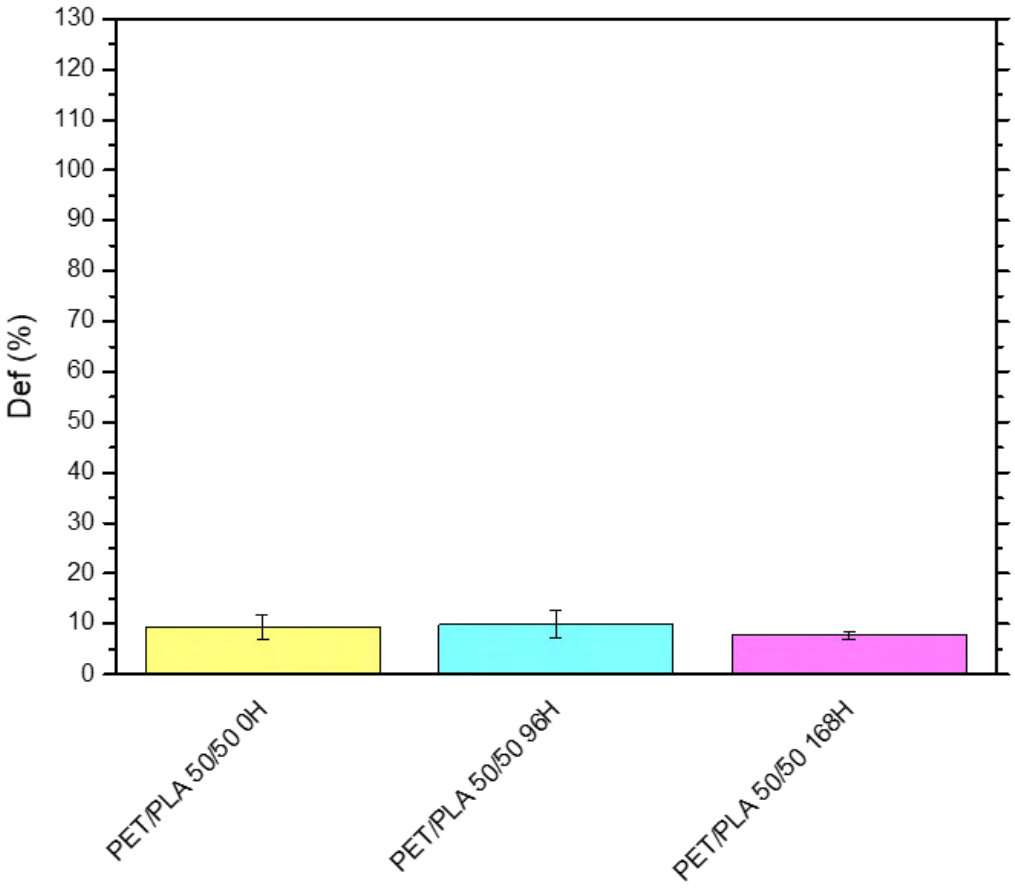

In an attempt to explain the behaviour seen here with PET/PLA blends, a study by A. M. Torres-Huerta et al. [41] was consulted. Although they produced filaments from a single screw extruder, rather than the twin extruder the films reported here used, meaning they were subjected to less shear and thus less efficient mixing. They studied the intermolecular interactions of the blend using FTIR (Fourier Transform Infrared spectroscopy) for the hydrogen bonds between the two polymers, because the specific interaction affected the local electron density. With the addition of PLA, they observed a lower wave number with respect to pure PET for the $C = O$ stretching. PET and PLA are compound of polar nature containing groups, which can form hydrogen bridges or new bonds when blends are synthesised for example as shown in Fig. 98 below. The behaviour shown in this thesis and the one in the study are strongly related to the miscibility which will be explored in more detail in coming sections. What can be deduced from these mechanical results, however, is that the fragility of hydrogen bonded polymer blends was strongly dependant on the fraction of segments that do form said hydrogen bonds. For higher PLA content they too experienced rougher surfaces at break, as well as the appearance of fibre-like structures as previously stated here. Such behaviour was attributed to the enhanced interfacial adhesion between PLA and PET. Thus, it can be assumed that in the cases where an improvement of the mechanical properties was exhibited the film

had a better distribution of PLA in PET which acted as reinforcement. If an excess of PLA was employed for the PET/PLA blends separation of phase can occur causing a reduction in the fracture energy. This matches the results obtained, where often relative peaks were observed with the addition of 40% PLA followed by a drop with the addition of 50% PLA.

Fig. 98: Physical Hydrogen bond interactions of PET/PLA [40]

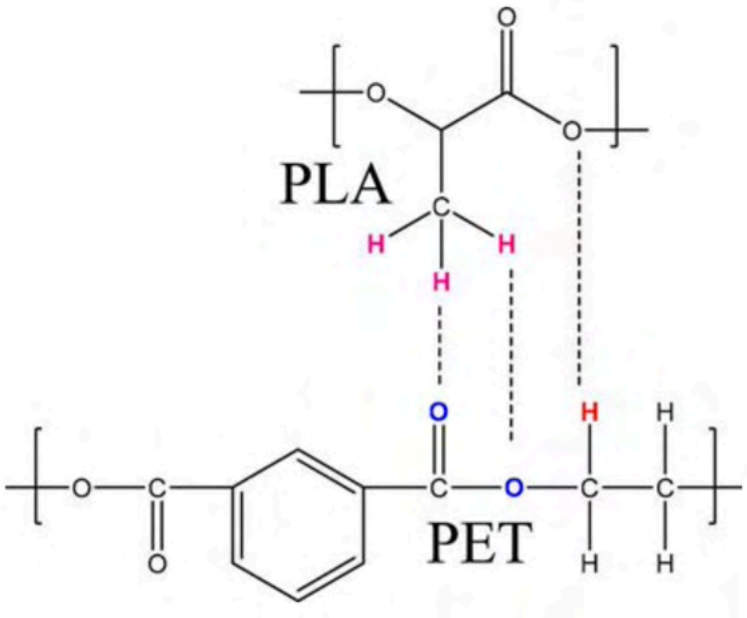

3.2.2 DSC (Differential Scanning Calorimetry) Scans of PET/PLA Blends

To confirm our findings from the mechanical tests in the previous section, DSC tests were conducted for all the samples. The values obtained from the DSC graphs using TA instruments are shown in Table. 7 below. As was done before for the PMMA/PLA blends N/A signifies a value that wasn't there or was not detectable. Also, similarly this time the crystallinity of PET was calculated using the same formula of $X_c = \frac{\boldsymbol{\Delta H_m}}{(1-x)\times \boldsymbol{\Delta H_{m0}}} \times 100$ [30], ΔH_m is the enthalpy of fusion from our DSC scans, and PET also exhibits cold crystallization so the corresponding enthalpy ΔH_{cc} must be subtracted from ΔH_m. The enthalpy of fusion of the polymer PET when 100% crystalline is ΔH_{m0} and is equal to 140 J/g [41], which is multiplied by (1-x) with x being the fraction in weight of the polymer being investigated.

Table. 7 Values from DSC tests of all PET/PLA blends

	T_g $(°C)$ PET	T_g $(°C)$ PLA	ΔH_m(J/g)	ΔH_{cc} (J/g)	X_c (%)
PET 0h	72	N/A	44.5	7.6	26.3
PET 96h	76	N/A	44.6	23.0	15.4
PET 168h	78	N/A	57.3	12.4	32.1
PET/PLA 80/20 0h	70	60	39.5	7.1	28.9
PET/PLA 80/20 96h	78	62	38.6	8.0	27.3
PET/PLA 80/20 168h	77	62	38.3	8.2	26.9
PET/PLA 60/40 0h	70	59	26.5	7.8	22.2
PET/PLA 60/40 96h	77	62	28.9	9.1	23.6
PET/PLA 60/40 168h	79	62	24.6	8.0	19.8
PET/PLA 50/50 0h	67	61	23.3	8.4	21.3
PET/PLA 50/50 96h	73	62	22.4	7.9	20.8
PET/PLA 50/50 168h	78	62	22.4	7.0	21.9

Starting with Fig. 99 we can see the different peaks for the PET/PLA blends before aging. The dips signifying the T_g can be seen around 75 °C for PET, and 60 °C for PLA. The peaks, valleys, and dips were well defined facilitating the identification of the values in the above table. Going from right to left, the valley at around 250 °C was the one attributed to the enthalpy of fusion of PET (ΔH_m), the valley at around 150 °C was for the fusion of PLA, and the peak at around 125 °C was attributed to cold crystallization of PET ΔH_{cc}.

Fig. 99: DSC scans of PET/PLA blends before aging

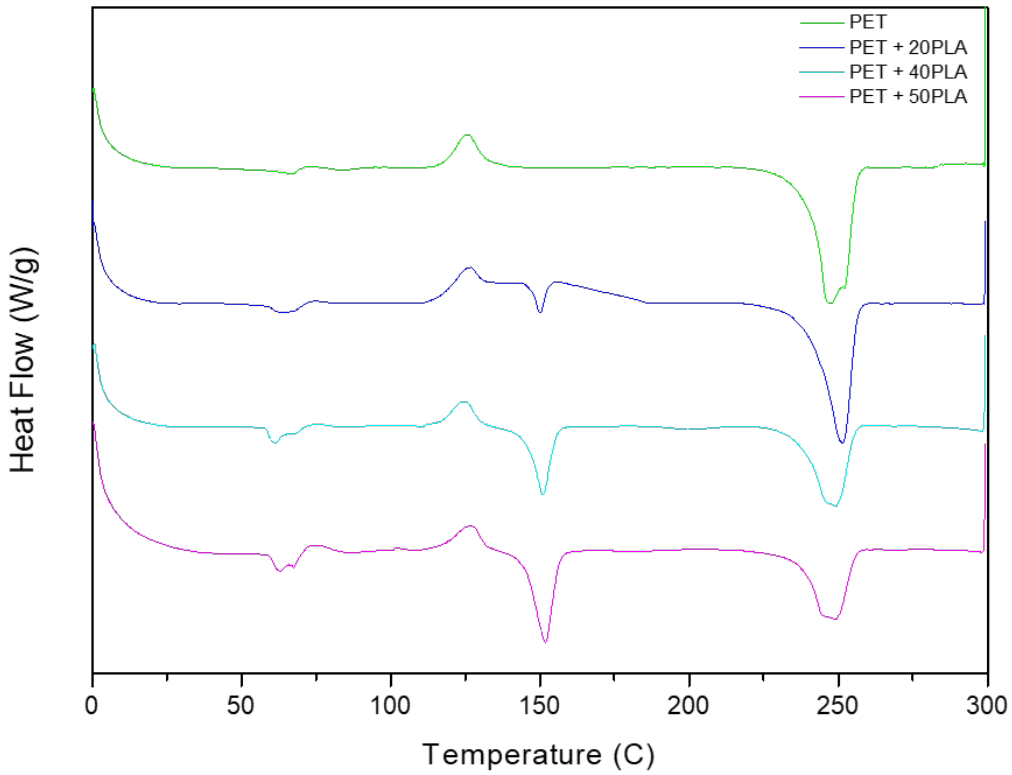

Observing the DSC scans of PET as it ages in Fig. 100 it can be seen that the form of the curves remained similar. Transition and fusion temperatures (T_g and T_m) remained constant and no significant changes to the position in the curves was seen. Although as the calculations made in Table. 7 showed, crystallinity was reduced after the first aging but was largest after 168 hours of aging. Such behaviour could be the result of chain scission, where after 96 hours the PET polymer chains were broken but did not have time to reorganise to regain crystallinity, however that time was available after 168 hours.

Fig. 100: DSC scans of PET as it ages

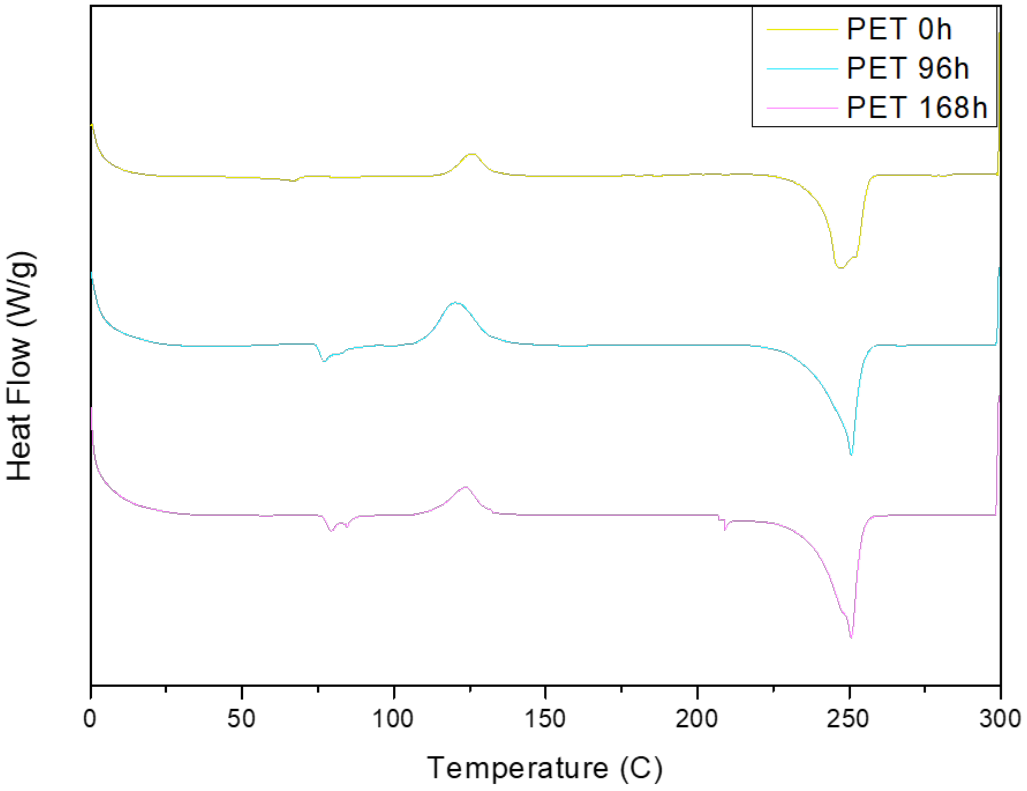

The appearance of the valley related to the cold crystallization of PLA starts appearing with the addition of 20% PLA, as can be seen in Fig. 101 below. Although, crystallinity didn't vary significantly in this case.

Fig. 101: DSC scans of PET/PLA 80/20 as it ages

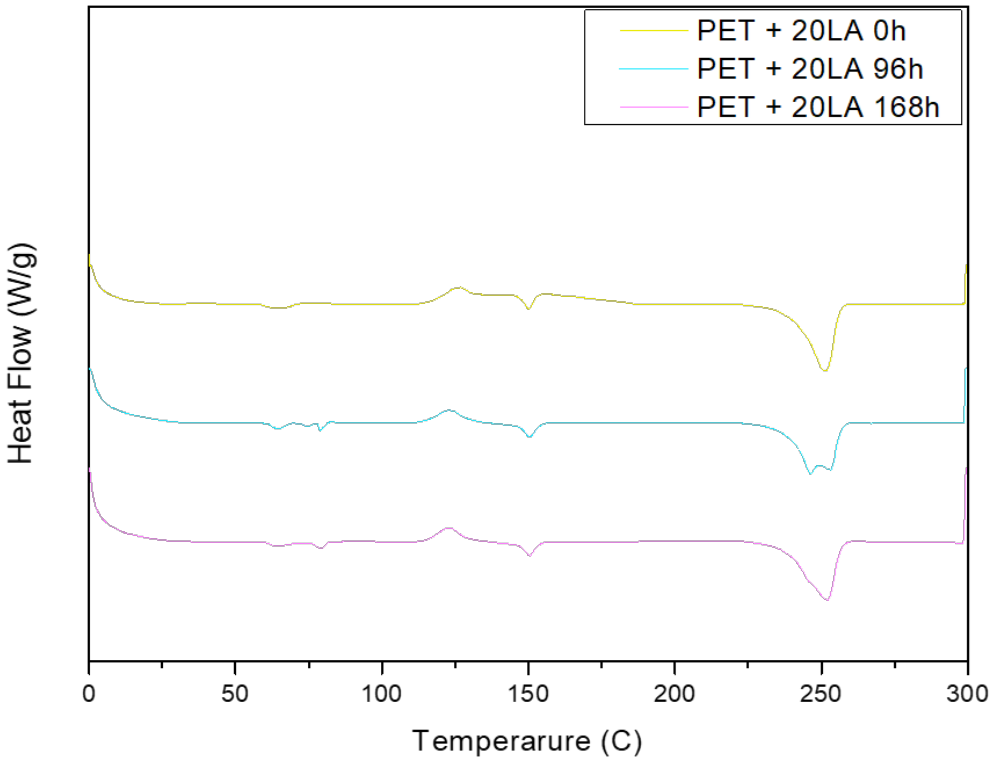

In Fig. 102 below the DSC scans of the PET blend with 40% PLA are shown to have the same behaviour with aging as the 80/20 blends. However, in this case the crystallinity dropped more significantly after 168 hours of aging. This is most likely due to the elevated presence of PLA that has a lower T_g, thus, degraded earlier maintaining the crystallinity at 96 hours, but dropped at 168 hours.

Fig. 102: DSC scans of PET/PLA 60/40 as it ages

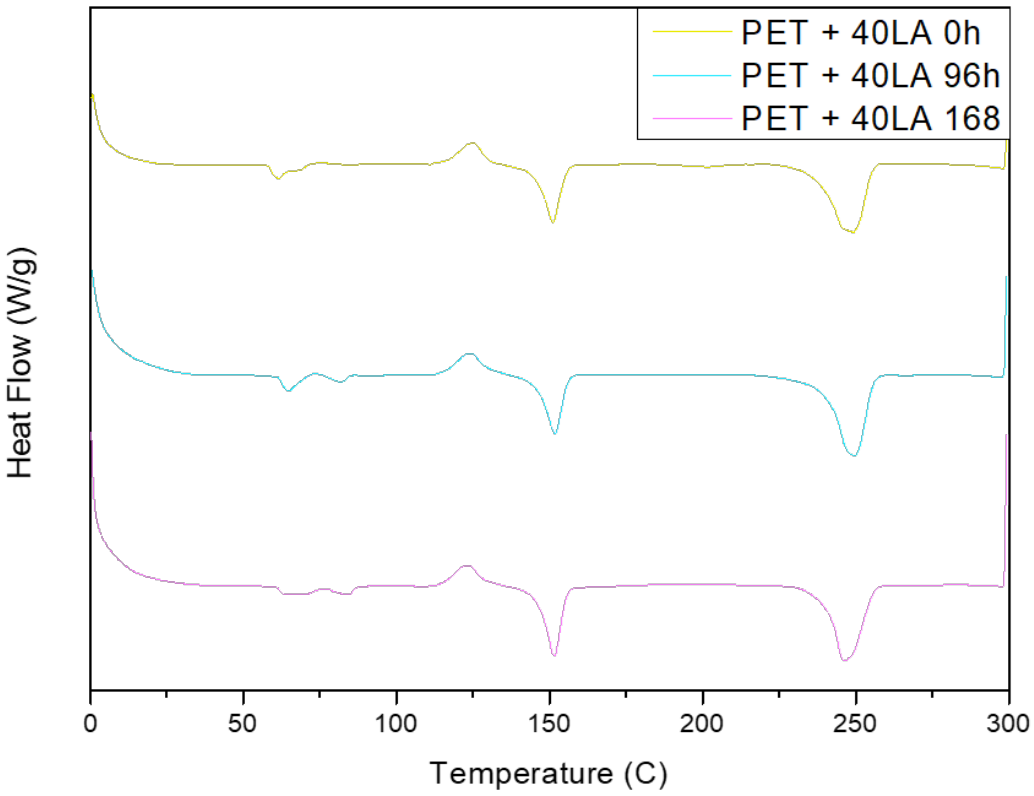

With the addition of 50% PLA shown in Fig. 103 below. This blend exhibited the same trends that were seen before.

Fig. 103: DSC scans of PET/PLA 50/50 as it ages

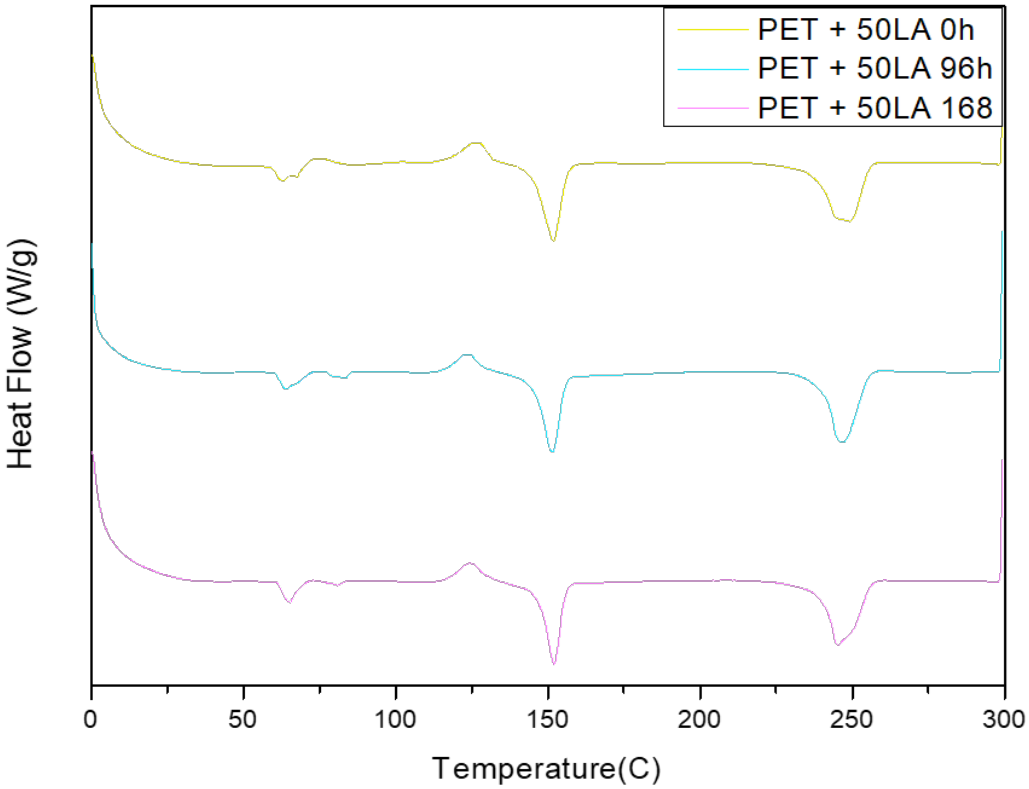

Semi-crystalline PET is known to have a T_g that is around 80 °C, while a combination of crystallinity and molecular weight can have an effect on the final characteristics as well. Other research has also been done to study the behaviour of PET/PLA blends, as Kuru Zehra et al. found that the crystallinity of PLA was inversely proportional to the crystallinity of PET. In their experiment with cold crystallized electrospun PET/PLA blends, they also found the immiscibility of the blend given by the presence of 2 unique and distinctive T_g. The crystallization of both PET and PLA was hampered by the presence of the other due to said immiscibility. They have also confirmed the reasoning that was deduced for the mechanical results, which is that the interactions governing the behaviour of the blends are the Hydrogen bonds and electrostatic contact [42]. The research by Hasan Azizi Topkanlo, et Al. expanded on that point by concluding that other process parameters such as the cooling rate have a considerable effect on crystal morphology which could lead even to fully amorphous blends. More specifically, as the cooling rate increased the relative crystallinity decreased for a specific temperature because there were less chances for polymer chains to overcome the nucleating obstacles. Furthermore, relative crystallinity approached 100% at higher temperatures as cooling rates decreased, signifying that crystal structures of the blend needs to be completed at higher temperatures [43]. They also got the same mechanical trends, whereby the Young's Modulus decreased with the increase of PLA.

The previously sited study by A. M. Torres – Huerta, found that the transition temperature (T_g) decreases about 15 °C with less than 10% PLA in the blend, whereas the temperature of crystallization increased with PLA rendering crystallization more difficult thus lowering crystallinity. The increase in the intensity of the exothermal peak, indicated that the number of polymer chains involved in the crystallization process also increased. PET could crystallize in all the blends, whether PLA is amorphous or crystalline.

3.2.3 Rheology of PET/PLA Blends

Frequency sweeps were as usual conducted at a constant shear rate, and a constant temperature. The instruments employed were the same as the ones employed for the PMMA/PLA blends, however for the PET/PLA blends a higher temperature was used. All the settings and methods employed were specified in the second chapter for materials and methods.

Fig. 104: Frequency sweep of PET/PLA blends before aging showing complex viscosity on the y – axis and angular velocity on the x – axis

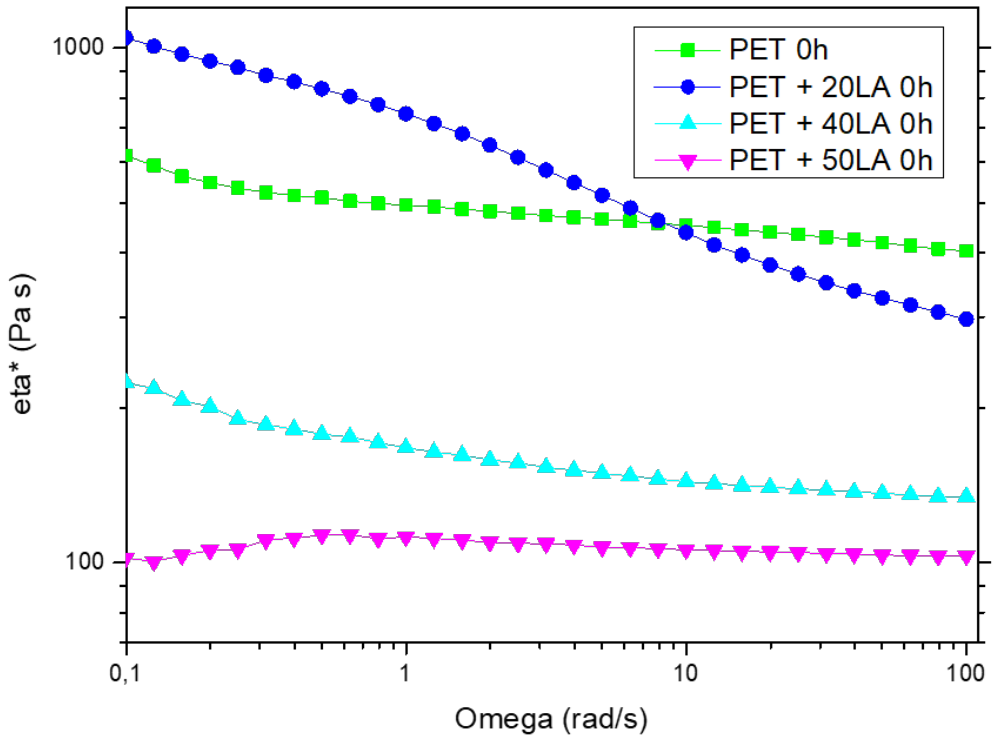

From the behaviour seen in Fig. 104 above we can conclude that unlike the case of PMMA/PLA, here PLA did not act as a plasticiser. The rheology of the PET/PLA blends point towards composition dependent structural or interaction effects, which is consistent with our earlier findings. The behaviour is not monotonic, and especially not monotonic for the storage modulus shown in Fig. 105.

The PET blend with 20% PLA stood out, due to having the highest viscosity and storage modulus as well as having the strongest dependence on frequency. This suggested that with this amount of PLA we got an enhancement of melt elasticity of PET. Due to a few possible mechanisms, such as increased molecular interaction reducing chain mobility. Another

possible explanation could be due to the anti-plasticization phenomenon, where - especially when the content of the additive is low - free volume could decrease, while local chain packing increases causing an increase in stiffness. There could also be present some transesterification induced intermolecular coupling, where even slight branching could dramatically increase the storage modulus [44].

For higher content of PLA (40% and 50%), the trend reverses seeing a drop in both viscosity and storage modulus signifying a drop in elasticity in this case. This indicates that above a certain point PLA started behaving as diluent, or mobility enhancer.

Fig. 105: Frequency sweep of PET/PLA blends before aging showing storage modulus on the y – axis and angular velocity on the x - axis

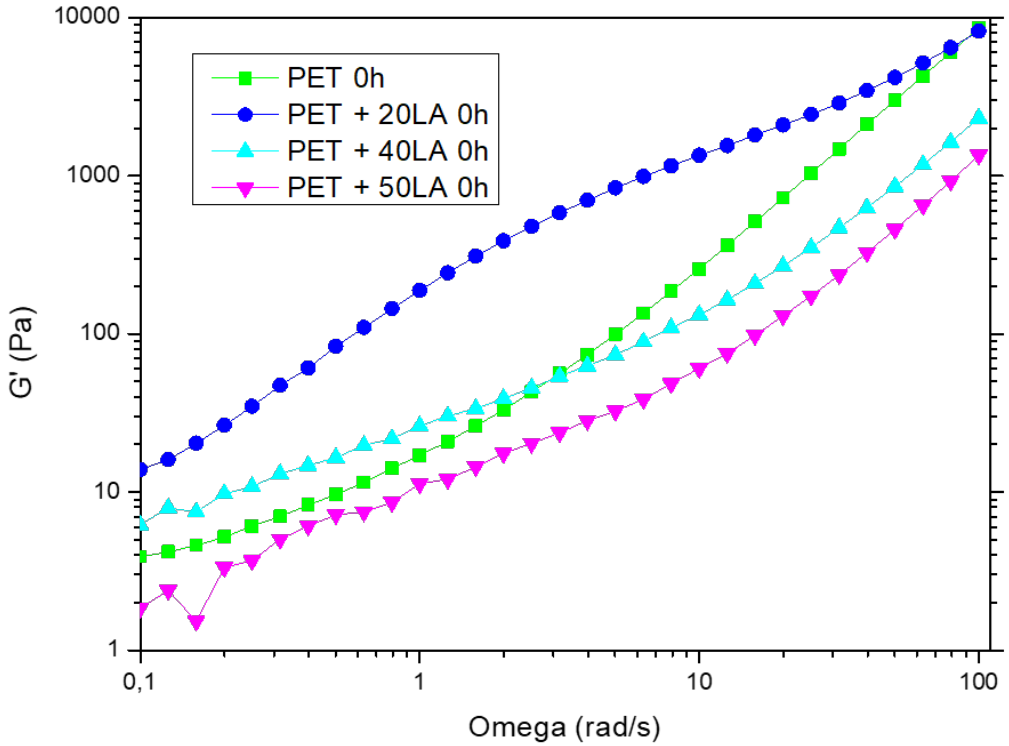

The behaviour at higher frequencies is of particular interest, where the separation between compositions became larger. This signifies that the PLA is strongly effecting segmental dynamics, local stiffness, and short time relaxation modes. The latter could also be seen in the DSC results previously obtained for the crystallinity from the DSC scans.

The trends seen from the rheology tests, expands on our understanding from the mechanical test and DSC scans. In particular, the apparent improvement of the Young's Modulus seen in Fig. 88 where we can see the instant increase upon the addition of 20% PLA.

3.2.4 SEM (Scanning Electron Microscopy) Images of PET/PLA blends

The images were taken in order to observe and ascertain information about the miscibility of the blends further.

The results obtained are consistent with our earlier findings. In Fig. 106 (a) below, the difficulty in obtaining the samples as the blend, even with as little as 20% PLA, can split giving us more than one plane. Magnifying more in Fig. 106 (b), the immiscibility of PLA in PET was evident by the spots. These spots also evidently followed the flow of the polymer, and in this case, they are following the curve at the edge of the sample.

Fig. 106: SEM images of PET/PLA 80/20

a) *b)*

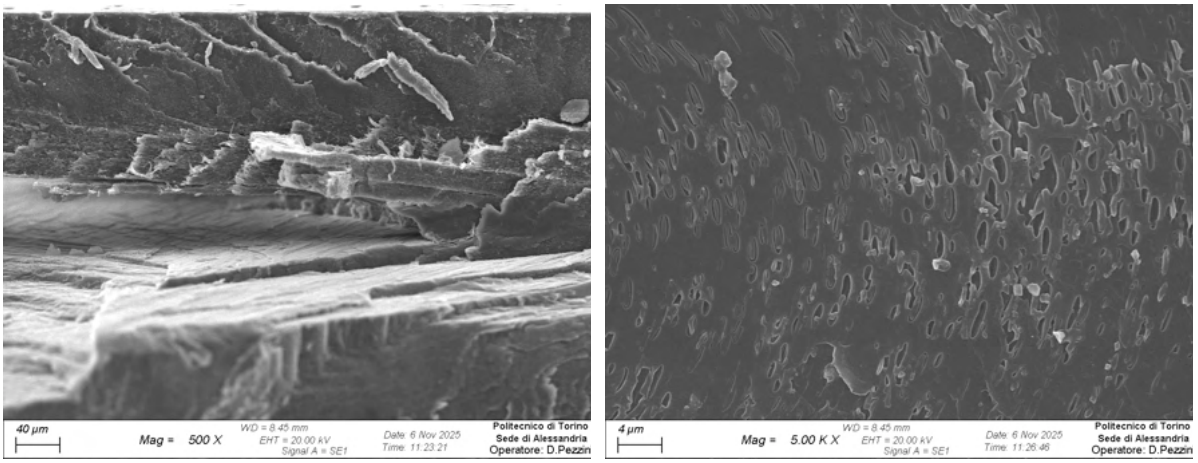

Observing the images of the PET/PLA 60/40 blend in Fig. 107 below. In Fig. 107 (a), it can be seen that the image at the break shows a somewhat smoother rupture, possibly attributed to the increased PLA content. In Fig. 107 (b), the PLA spots dispersed appear larger which is consistent with other research papers as well. [45]

Fig. 107: SEM images of PET/PLA 60/40

a) *b)*

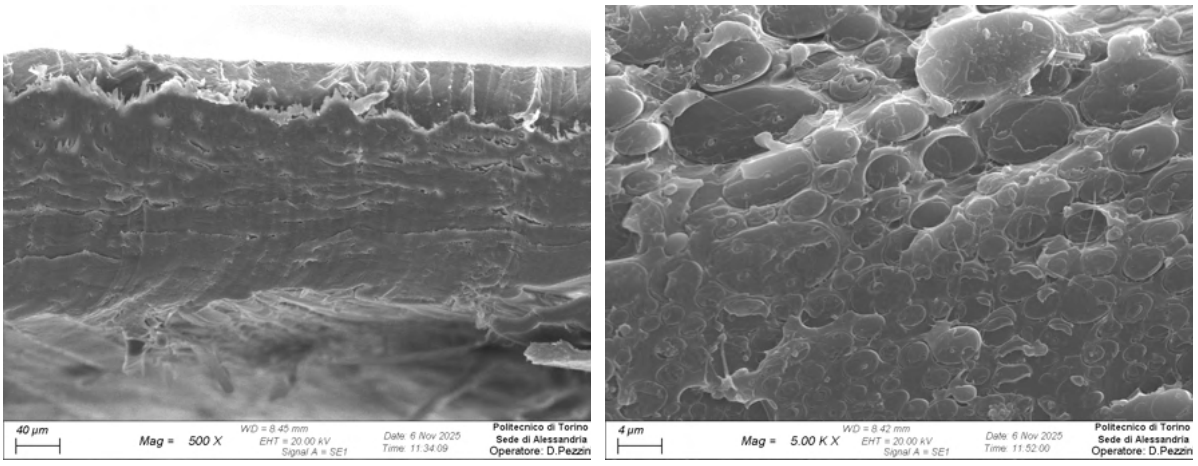

In Fig. 108 (a), the behaviour of the rupture can be seen to have become more brittle in line with the mechanical results of deformation. The rough “texture” on the top side of the sample, was a foreseen result due to the difficulty in obtaining the sample since when attempting to obtain a fragile fracture a separation of the film into two apparent layers occurred. In Fig. 108 (b), the immiscibility spots were again observed.

Fig. 108: SEM images of PET/PLA 50/50

a) *b)*

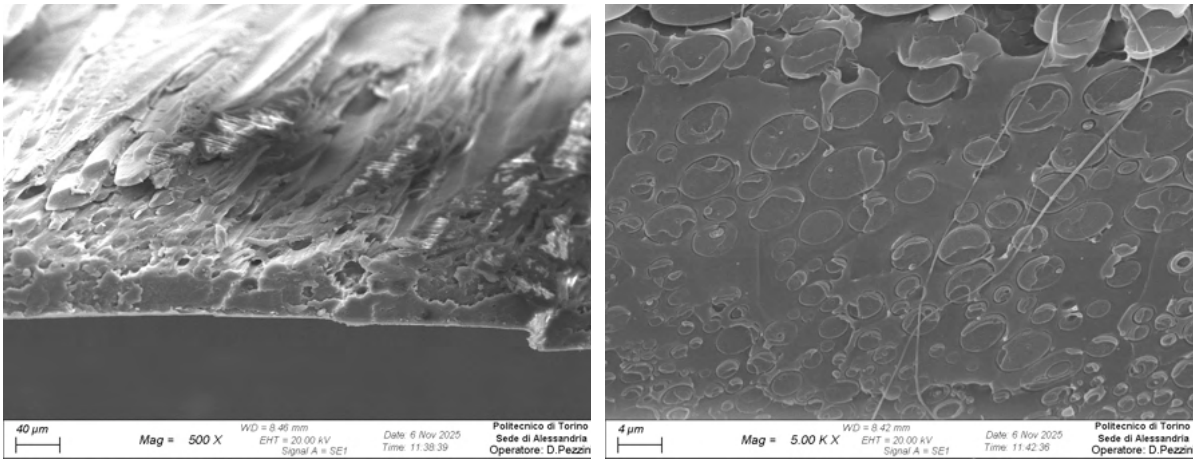

In the Fig. 109 below we can see all the fibrous behaviour, rendered visible thanks to the SEM. This behaviour is related to the phase separation, and the previously mentioned separation into layers.

Fig. 109: SEM images showing the fibrous behaviour of PET/PLA blends at rupture.
a) PET/PLA 80/20, b) PET/PLA 60/40, c) PET/PLA 50/50

a)

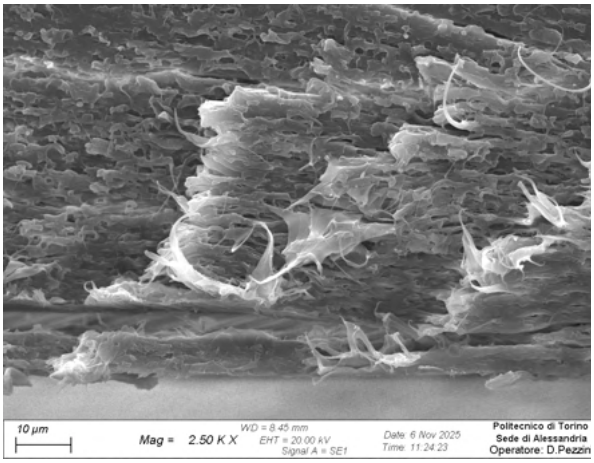

b)

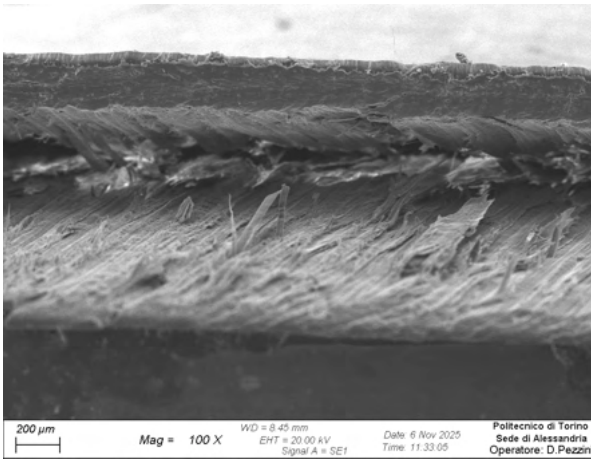

c)

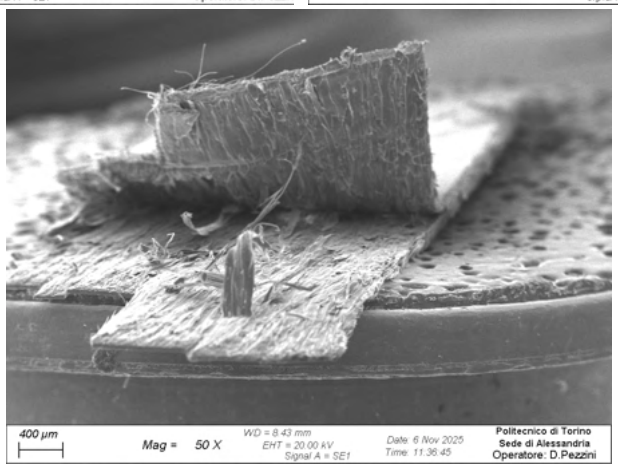

Generally speaking, and from the previous figures, a good dispersion was obtained in all the blends. The size and distribution were due to the flow, and the coalescence phenomena in PLA particles is divided into two categories. In the dynamic category, there was a flow induced process whereby the dispersed phase experienced a combination of breaking and coalescence of both particles. In the end, the dispersed phase matrix structure was coarsening. This coarsening phenomena and Ostwald ripening are late-stage phase separation. The main reason for this process is the minimization of interfacial energy surface tension by reducing the surface area [45].

Morphology of PET/PLA blends was found to be of the island – sea type, even with the employment of compatibilizers. However, an inversion was obtained once PLA content reached 50% as shown in Fig. 110 below [45]. Co-continuous morphologies are still possible, but they are mainly formed around the point of phase inversion, but not at a single volume fraction.

Fig. 110: Dispersed phase structure of different compatibilized and un-compatibilized PET/PLA blends [45]

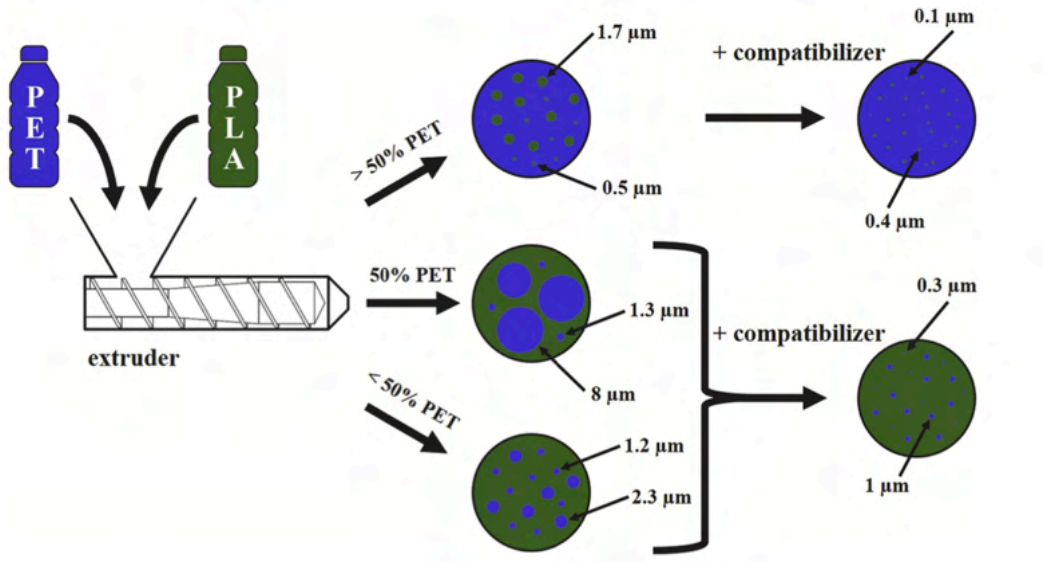

4 Conclusions:

The objective of this thesis was to create two sets of films made of PMMA / PLA and PET / PLA blends. The films were prepared in the following weight percentages: 100/0, 80/20, 60/40, and 50/50. The purpose of the blends was to reduce the use of fossil – based polymers, with a focus on the mechanical properties obtained, and the development of the properties with aging. PMMA and PET are some of the most commonly used polymers, while PLA is one of the most commonly used bio–based polymers. In summary, it was desired to obtain a more environmentally friendly material in the sense of reducing the reliance of fossils when producing virgin materials.

The films were extruded using a flat head attachment, and subsequently calendered and collected. Calendering also helps with orienting the polymer chains, and with the dispersion and distribution. From the extruded films, samples were prepared for all the subsequent mechanical tests, thermal analysis, rheological tests, SEM, imaging, and for the case of PMMA/PLA blends UV-Vis tests as well.

First, mechanical tests were conducted for the PMMA / PLA blends. An instant improvement of the mechanical results was observed for both the Young's modulus and the deformation at fracture, despite that the samples remained brittle even with the addition of 50% PLA. PMMA/PLA films were also aged for 48 h, 24 h, and 72 h where behaviour started varying. Whereas for the non-aged films Young's modulus increased upon the addition of PLA then remained constant after adding more PLA, the deformation kept on increasing with the increase of PLA content in the blend. On the other hand, samples aged for 48 h had a Young's modulus peak for the 60/40 blend, and despite a loss in deformation the 50/50 blend still showed the most deformation. Samples aged for 24 h and 72 h had both the Young's modulus and deformation peak for the PMMA / PLA 50/50 blend. The general observed trend is the increase of Young's modulus with aging and the increase of PLA, while deformation decreases with aging it still increases with PLA content.

Mechanical tests of PET / PLA showed initial increase in the young's modulus, and a decrease in deformation at fracture, with the increase of PLA content. The mechanical tests showed ductile fractures but transitioned to more brittle behaviour when PLA increased. After aging for 96 h, Young's modulus starts to increase with the increase of PLA, however deformation decreases, and brittle fractures are seen with the blends of 60/40 and 50/50 (which shows the biggest drop at this point). After 168 h of aging, a similar behaviour was seen where Young's modulus peaks for the 60/40 blend, but deformation continuously decreases with increasing PLA. In general, a small decrease was observed for the blends Young's modulus and deformation that were aged for 96 h, before an increase after 168 h, with exception to the PET / PLA 50/50 blend where the modulus kept increasing albeit slightly and the deformation did not change.

Thermal analyses were then conducted using the DSC for both PMMA / PLA and PET / PLA blends. No significant changes to the T_g were observed with aging, nor with varying PLA content. Although, when increasing PLA content, the T_g curve of PMMA became harder to detect. PLA films when irradiated are known to have their crystallinity drop, however, in the

PMMA / PLA 50/50 blends aged for 48 h and 72 h it was observed that the crystallinity remains constant. The behaviour can be attributed to PLA having enough time to reorganise. DSC scans of PET / PLA blends showed an increase in the T_g of PET with aging, but the T_g of PLA remains constant. The PET / PLA blends' crystallinity dropped with increasing PLA content, but there are no significant changes with aging.

Next, rheological tests were conducted. The results for the PMMA / PLA blends showed a Newtonian behaviour at low frequencies, and gradually as frequency increased a typical shear thinning was obtained. PLA acted as a plasticiser for PMMA, lowering the viscosity and storage modulus. Both were also lowered with aging. PLA in the PET / PLA does not act as a plasticiser, the rheological tests indicated towards the immiscibility as well. PET / PLA 80/20 had the highest values for both viscosity and storage modulus.

Further microstructural characterisation was done using SEM. PMMA / PLA blends showed clean surfaces indicating miscibility. Another test that was conducted exclusively for the PMMA / PLA blends is UV-Vis for transparency, all the samples remained transparent and minimal changes were seen. However, the general trend was that transmittance is reduced in the UV range, increased PLA content, and aging also reduced transparency. Images of PET / PLA blends on the other hand showed the immiscibility of PLA in PET, with clear visible spots present. The PET / PLA images also showed rough fractures, given the more ductile nature of the blends, another aspect that was highlighted by these images is the phase separation that occurs in the form of fibre-like structures.

Given these results, the following conclusions can be made:

1. Aesthetically, PLA doesn't significantly affect PMMA, however the addition of PLA to PET instantly resulted in an opaque material.
2. PMMA/PLA blends may be considered as possible alternatives to pure PMMA in applications where partial replacement of fossil-based polymer is desired, and severe outdoor exposure is not required. Since the addition of PLA instantly improves the mechanical performance, but deformation was significantly reduced with aging.
3. PET/PLA blends may be suitable for applications where stiffness is prioritised over ductility and transparency is not a key requirement. Since the addition of PLA to PET eliminates transparency, improves Young's modulus instantly, but initially deformation is reduced. However, the performance of the blends was more constant with aging.

Acknowledgements

As I complete this work and my university degree, I realize I could not have done it alone. First, I would like to thank God, my family, and my friends, without whom I would not have reached this point. Their continued support and encouragement made this journey much more bearable. Finally, I would like to thank my supervisors and the entire All-polymer team for their help throughout this thesis and their patience.

Completando questo lavoro e il mio percorso universitario, mi rendo conto che non avrei potuto farcela da solo. Innanzitutto, vorrei ringraziare Dio, mia famiglia, e i miei amici, senza i quali non sarei mai arrivato a questo punto. Il loro costante supporto e incoraggiamento hanno reso questo percorso molto più supportabile. Infine, vorrei ringraziare i miei relatori, il mio supervisor, e tutto il team All-polymer per il loro aiuto durante questa tesi, e la loro pazienza.

Bibliography:

1. COREPLA *La sfida della Plastica - COREPLA censis - corepla*, *COREPLA Consorzio Nazionale per la Raccolta, il Riciclo e il Recupero degli Imballaggi in Plastica*. (2024) Available at: https://www.corepla.it/ricerca-corepla-censis/.
2. Plastics Europe. *Plastics the Fast Facts (2025)*. Brussels: Plastics Europe, (2025). Available at: https://plasticseurope.org/wp-content/uploads/2025/09/PE_TheFacts_25_digital-1pager-scrollable.pdf.
3. Plastics Europe. *Plastics the Fast Facts (2025)*. Plastics Europe AISBL, Brussels, Belgium, 2025. Available at: https://plasticseurope.org/wp-content/uploads/2025/09/PE_TheFacts_25_digital-1pager-scrollable.pdf.
4. Goodfellow. *PMMA Film*. Goodfellow Cambridge Ltd. Available at: https://www.goodfellow.com/eu/pmma-film-group.
5. Folien-Zentrum. *PMMA Films – Technical Films*. Folien-Zentrum GmbH. Available at: https://folien-zentrum.com/en/technical-films/pmma.html.
6. Saurabh S, Upadhyaya S, Dohare R. K, Agarwal M, Gupta A. Kinetic Study of PMMA Synthesis by Batch Emulsion Polymerization. Orient J Chem (2012);28(1). Available from: http://www.orientjchem.org/?p=24052.
7. Ni'matul Waladiya Kurniasari, Prida Novarita Trisanti, Kukuh Dwiputra Hernugrahanto, Ferdiansyah, Sumarno; Synthesis and purification process of PMMA by suspension polymerization for bone cement material. *AIP Conf. Proc.* 9 (June 2023); 2703 (1): 050004. https://doi.org/10.1063/5.0115493
8. Röhm GmbH. *PLEXIGLAS® 8N: Product Information (Technical Datasheet)*. Röhm GmbH, 2020. Available at: https://www.plexiglas-polymers.com/en/plexiglas-8n
9. Md. Tanvir Siraj, Sheikh Navid Shadab Jamil, Arnab Mustafi Arka, Sadikah Tasnim, Manoj Ghosh, Muhammad Rubayat Bin Shahadat, Md Zillur Rahman, 12.47 - Eco-friendly food packaging innovations: A review of recent progress on recyclable polymers, Editor(s): Saleem Hashmi, Comprehensive Materials Processing (Second Edition), Elsevier, (2024), Pages 693-709, ISBN 9780323960212, https://doi.org/10.1016/B978-0-323-96020-5.00077-7.
10. Ruth Amanna, Zannat Mahal, Ellen Caroline Silverio Vieira, Mahdieh Samavi, Sudip Kumar Rakshit, 26 - Plastics: Toward a Circular Bioeconomy, Editor(s): Ashok Pandey, Rajeshwar Dayal Tyagi, Sunita Varjani, Biomass, Biofuels, Biochemicals, Elsevier, (2021), Pages 781-811, ISBN 9780128218785, https://doi.org/10.1016/B978-0-12-821878-5.00027-1.
11. Firsta Group. *Features and Applications of PET Films*. Hubei Firsta Material Science and Technology Group Co., Ltd., (2021). Available at: https://www.firstagroup.com/news/features-and-applications-of-pet-films.html
12. FKuR Kunststoff GmbH. *Eastlon PET CB-602AB (Technical Data Sheet)*. FKuR Kunststoff GmbH. Available at: https://fkur.com/en/bioplastics/eastlon/eastlon-pet-cb-602ab/
13. Julia Pretula, Stanislaw Slomkowski, Stanislaw Penczek, Polylactides—Methods of synthesis and characterization, Advanced Drug Delivery Reviews, Volume 107, (2016), Pages 3-16, ISSN 0169-409X, https://doi.org/10.1016/j.addr.2016.05.002.

14. Cheng, Y., Deng, S., Chen, P. *et al.* Polylactic acid (PLA) synthesis and modifications: a review. *Front. Chem. China* 4, 259–264 (2009). https://doi.org/10.1007/s11458-009-0092-x
15. Muzamil Hussain, Shahzad Maqsood Khan, Muhammad Shafiq, Naseem Abbas, A review on PLA-based biodegradable materials for biomedical applications, Giant, Volume 18, (2024), 100261, ISSN 2666-5425, https://doi.org/10.1016/j.giant.2024.100261.
16. NatureWorks. Ingeo™ Biopolymer 4032D (Technical Data Sheet). NatureWorks. Available at: https://natureworksllc.com/getContentAsset/6797e56e-fae7-4f21-8bee-79692a1aba2c/53ffd608-340f-457b-b656-6b8cc0000bd4/TechnicalDataSheet_4032D_general.pdf?language=en
17. Chapleau, N., Favis, B.D. Droplet/fibre transitions in immiscible polymer blends generated during melt processing. *JOURNAL OF MATERIALS SCIENCE* 30, 142–150, (1995). https://doi.org/10.1007/BF00352143
18. García-Masabet, Violeta et al. "PLA/PA Bio-Blends: Induced Morphology by Extrusion." *Polymers* vol. 12,1 10. 19 Dec. (2019), doi:10.3390/polym12010010
19. Trapani, G. *Sviluppo di film a base EVA/EBA contenenti nanocariche lamellari con proprietà di ritardo alla fiamma*, *WebThesis*. (2024) Available at: https://webthesis.biblio.polito.it/32568/1/tesi.pdf.
20. Dey, D. and Joseph, M., *Screw functionality and screw profile design for extrusion processing*, *NC State Extension Publications*. Available at: https://content.ces.ncsu.edu/screw-functionality-and-screw-profile-design-for-extrusion-processing#:~:text=The%20nomenclature%20of%20the%20screw,elements%20to%20move%20melted%20material.
21. *Q-LAB, QUV Q-LAB*. Available at: https://www.q-lab.com/weathering/equipment-accessories/quv.
22. *AT3 automated film tensile testing to ASTM D882*, *INSTRON, (*2018). Available at: https://www.instron.com/en/resources/videos/2018/may/at3-automated-film-tensile-testing-to-astm-d882/.
23. Jennifer M. Lynch, Raquel N. Corniuk, Kayla C. Brignac, Melissa R. Jung, Kristine Sellona, Joelle Marchiani, Wanda Weatherford, Differential scanning calorimetry (DSC): An important tool for polymer identification and characterization of plastic marine debris, Environmental Pollution, Volume 346, (2024), 123607, ISSN 0269-7491, https://doi.org/10.1016/j.envpol.2024.123607.
24. *DSC 2910 Differential Scanning Calorimeter TA Instruments*. Available at: https://www.tainstruments.com/pdf/literature/DSC_2910.pdf.
25. *Memmert GmbH + Co.KG, Vacuum drying oven vo - gentle, powerful, energy-saving Memmert GmbH + Co.KG*. Available at: https://www.memmert.com/en/products/heating-drying-ovens/vacuum-oven#!filters=%7B%7D.
26. Nanakoudis, A. *How scanning electron microscopy works*, *Advancing Materials*. (2026) Available at: https://www.thermofisher.com/blog/materials/how-scanning-electron-microscopy-works-sem-explainer/.
27. *ZEISS, Zeiss Evo Scanning Electron Microscope ZEISS EVO Family*. Available at: https://www.zeiss.com/microscopy/en/products/sem-fib-sem/sem/evo.html.

28. Vašíček, Adam, Petr Lenfeld, and Luboš Běhálek. "Degradation of polylactic acid polymer and biocomposites exposed to controlled climatic ageing: Mechanical and thermal properties and structure." *Polymers* 15.14 (2023): 2977. https://doi.org/10.3390/polym15142977
29. Mukherji, Debashish, et al. "Thermodynamics, morphology, mechanics, and thermal transport of PMMA-PLA blends." *Physical Review Materials* 6.2 (2022): 025606. https://doi.org/10.1103/PhysRevMaterials.6.025606.
30. Mysiukiewicz, Olga, et al. "Correlation between processing parameters and degradation of different polylactide grades during twin-screw extrusion." *Polymers* 12.6 (2020): 1333. https://doi.org/10.3390/polym12061333.
31. Su Yang, Si-Ru Li, Si-Yuan Zhou, Hao-Ran Yang, Ling Xu, Gan-Ji Zhong, Jia-Zhuang Xu, Zhong-Ming Li, Xiao-Ming Tao, Yiu-Wing Mai, Cold crystallization behavior of poly(lactic acid) induced by poly(ethylene glycol)-grafted graphene oxide: Crystallization kinetics and polymorphism, Composites Science and Technology, Volume 258, (2024), 110871, ISSN 0266-3538, https://doi.org/10.1016/j.compscitech.2024.110871.
32. Fischer, E.W., Sterzel, H.J. & Wegner, G. Investigation of the structure of solution grown crystals of lactide copolymers by means of chemical reactions. *Kolloid-Z.u.Z.Polymere* 251, 980–990 (1973). https://doi.org/10.1007/BF01498927
33. M. V. Podzorova, Yu. V. Tertyshnaya, P. V. Pantyukhov, A. A. Popov, S. G. Nikolaeva; Influence of ultraviolet on polylactide degradation. *AIP Conf. Proc.* (1 December 2017); 1909 (1): 020173. https://doi.org/10.1063/1.5013854
34. Kumar, M., Shanmuga Priya, N., Kanagaraj, S., & Pugazhenthi, G. Melt rheological behavior of PMMA nanocomposites reinforced with modified nanoclay. *Nanocomposites*, (2016), *2*(3), 109–116. https://doi.org/10.1080/20550324.2016.1221876
35. Hou, Xunan, et al. "Entropy-driven ultratough blends from brittle polymers." *ACS Macro Letters* (2021), 10.4: 406-411. https://doi.org/10.1021/acsmacrolett.0c00844.
36. R.C Willemse, A Posthuma de Boer, J van Dam, A.D Gotsis, Co-continuous morphologies in polymer blends: the influence of the interfacial tension, Polymer, (1999), Volume 40, Issue 4, Pages 827-834, ISSN 0032-3861, https://doi.org/10.1016/S0032-3861(98)00307
37. Le, K. P., Lehman, R., Remmert, J., Vanness, K., Ward, P. M. L., & Idol, J. D. Multiphase blends from poly(L-lactide) and poly(methyl mathacrylate). *Journal of Biomaterials Science,* (2006), *Polymer Edition*, *17*(1–2), 121–137. https://doi.org/10.1163/156856206774879054
38. Teoh, E. L., and W. S. Chow. "Transparency, ultraviolet transmittance, and miscibility of poly (lactic acid)/poly (methyl methacrylate) blends." *Journal of Elastomers & Plastics* (2018) 50.7: 596-610. https://doi.org/10.1177/0095244317743067.
39. Matthias Balthasar Kesting, Jörg Meyer, Gunnar Seide, Assessment of polylactide as optical material, Optical Materials: X, (2024), Volume 24, 100360, ISSN 2590-1478, https://doi.org/10.1016/j.omx.2024.100360.

40. Torres-Huerta, A. M., Del Angel-López, D., Domínguez-Crespo, M. A., Palma-Ramírez, D., Perales-Castro, M. E., & Flores-Vela, A. Morphological and Mechanical Properties Dependence of PLA Amount in PET Matrix Processed by Single-Screw Extrusion. *Polymer-Plastics Technology and Engineering*, (2016), *55*(7), 672–683. https://doi.org/10.1080/03602559.2015.1132433.
41. Romain Cardinaud, Tony McNally, Localization of MWCNTs in PET/LDPE blends, European Polymer Journal, (2013), Volume 49, Issue 6, Pages 1287-1297, ISSN 0014-3057, https://doi.org/10.1016/j.eurpolymj.2013.01.007.
42. Kuru, Zehra, and Mehmet Arif Kaya. "Poly (lactic acid)/polyester blends: review of current and future applications." *The European Journal of Research and Development* (2023) 3.1: 175-199. https://doi.org/10.56038/ejrnd.v3i1.259
43. Topkanlo, H.A., Ahmadi, Z. & Taromi, F.A. An in-depth study on crystallization kinetics of PET/PLA blends. *Iran Polym J* 27, (2018) 13–22. https://doi.org/10.1007/s13726-017-0582-5.
44. Christopher W. Macosko; Extensional rheometry via flow through an abrupt contraction: A short review. *AIP Conf. Proc.* 8 (June 2023); 2997 (1): 020001. https://doi.org/10.1063/5.0159793.
45. D. Gere, T. Czigany, Future trends of plastic bottle recycling: Compatibilization of PET and PLA, Polymer Testing, (2020), Volume 81, 106160, ISSN 0142-9418, https://doi.org/10.1016/j.polymertesting.2019.106160.